Vidar Servold
Martin Dalseg
Martin Styve

Bachelor's thesis

May 2023

NTNU
Norwegian University of Science and Technology
Faculty of Engineering
Department of Energy and Process Engineering

NTNU
Norwegian University of
Science and Technology

Bachelor's thesis

2023

NTNU
Norwegian University of
Science and Technology

Vidar Servold
Martin Dalseg
Martin Styve

Bachelor's thesis
May 2023

NTNU
Norwegian University of Science and Technology
Faculty of Engineering
Department of Energy and Process Engineering

NTNU

Institutt for energi- og prosessteknikk

Bacheloroppgave

Oppgavens tittel: Elektrifisere AtB sin metrobuss på linje 1 med implementering av megawatt lade system **Project title (ENG):** Electrifying AtB's metro bus line 1 with implementation of megawatt charging system	**Gitt dato:** 21.11.2022 **Innleveringsdato:** 22.05.2023 **Antall sider rapport / sider vedlagt:** 66/16
Gruppedeltakere: Martin Dalseg, Vidar Servold og Martin Styve	**Veiledere:** Odne Stokke Burheim og Markus Solberg Wahl **Prosjektnummer:** 23
Oppdragsgiver: AtB	**Kontaktperson hos oppdragsgiver:** Pål Preede Revheim

Fritt tilgjengelig: ☒

Tilgjengelig etter avtale med oppdragsgiver: ☐

Rapporten frigitt etter:

Gruppedeltakere signaturer:

Martin Styve Vidar Servold Martin Dalseg

Preface

This thesis is the final assignment of an engineering study of renewable energy. The bachelor's thesis is the outcome of a collaboration between three students at NTNU, two supervisors, and the public transport company AtB. The students have specialization in the areas of energy storage and efficient energy consumption.

The purpose of this thesis is to present a viable solution to electrify the M1 bus route in Trondheim, with the implementation of megawatt charging.

Acknowledgments

Thanks are due to both, NTNU with Markus Solberg Wahl and Odne Stokke Burheim as our internal supervisors, and AtB with Pål Preede Revheim as our external supervisor. In addition, we would like to thank Bård Henrik Sørensen for providing the report on a similar study from Follo.

Martin Styve: Vidar Servold: Martin Dalseg:

Abstract

Due to political agreements and a common goal of sustainable development AtB aims to decarbonize their bus fleet. The underlying goal is to obtain a zero-emission state, but from the development and experience of others, electricity seems like the best option.

This thesis has aimed to perform a feasibility study regarding the development of a fully electric replacement of the "Metrolinje 1" (M1) in Trondheim, without forfeiting passenger capacity. It has also investigated the energy consumption of the bus and sizing of the needed battery pack. In addition, the thesis has evaluated options in a life cycle analysis that investigates environmental impact. On request from AtB the implementation of a megawatt charging system (MCS) has also been investigated, with 5 minute charging per end station.

An investigation into the energy consumption of the M1 has been made where several variables has been evaluated and an extensive physical model of the forces acting on the vehicle has been utilized.

The investigated energy storage system has been lithium ion batteries and different battery electrodes have been investigated in order to present a satisfactory battery pack for the M1 bus. The anode utilized in the calculations has been graphite, while the cathodes have been NMC111, NCA, and LFP.

The results found in the energy consumption calculations have been presented as two cases. A base case representing an average day for the M1 with dry asphalt, low winds and no internal heating. The other case represents a worst case scenario for the M1 with snow and ice on the road, higher winds and maximum internal heating. It is imperative to present a worst case scenario as it will be the basis of the calculations of size and capacity of the battery.

When calculation the energy consumption several sources of error has been found. The data use for calculations are average data between every stop and so inaccuracies in velocity and number of un-expected stops may occur. There are no registered acceleration and de-acceleration numbers available and so the acceleration force has been neglected from the energy calculations. For this reason a scaling number has been found by comparing the actual energy consumption number from diesel consumption with the calculated every consumption in order for the results to reflect the measured consumption.

The MCS comes with the ability to charge at very high power (3.75MW), however, the batteries have been dimensioned in a way that opens for lower power charging that also improves the cycle life.

The final results have yielded that all three evaluated battery options with the use of a mega watt charging system, would be a feasable solution to the electrification of the M1. The LFP and graphite option has shown to be the cheapest, heaviest and largest in volume. The NMC111 and graphite option has shown to be the most expensive battery pack, while also being a lot lighter and smaller in volume compared to the LFP // Gr option. The NCA and graphite option is the lightest and smallest in volume, while being cheaper than NMC111 // Gr but more expensive than LFP // Gr. Through the LCA, the LFP has shown to yield the most CO_2 equivalent emissions due to a high amount of needed energy during manufacturing, even though the Cobalt in the NMC and NCA cathode negatively impacts the environment at the end of life.

Sammendrag

På grunn av politiske avtaler og et felles mål om bærekraftig utvikling har AtB som mål å elektrifisere hele bussparken i Trondheim.

Denne oppgaven har som mål å gjennomføre et mulighetsstudie vedrørende utvikling av en helelektrisk erstatning av "Metrolinje 1" i Trondheim, uten å redusere passasjerkapasiteten. Oppgaven har også undersøkt energiforbruket til bussen og størrelsen på den nødvendige batteripakken. I tillegg har den evaluert alternativer i en livsløpsanalyse som undersøker miljøpåvirkning. På forespørsel fra Atb er det også undersøkt implementering av et megawatt ladesystem, med 5 minutters lading per endestasjon.

Det er gjort en undersøkelse av energiforbruket til M1 hvor flere variabler er evaluert og en omfattende fysisk modell av kreftene som virker på kjøretøyet er benyttet.

Det undersøkte energilagringssystemet har vært litium-ion batterier og forskjellige batterielektroder har blitt undersøkt for å kunne presentere en tilfredsstillende batteripakke for M1-bussen. Anoden som er brukt i beregningene har vært grafitt, mens katodene har vært NMC111, NCA og LFP.

Resultatene funnet i energiberegningene er presentert som to scenarier. Et scenario som representerer en gjennomsnittlig dag for M1 med tørr asfalt, lav vind og ingen intern oppvarming. Det andre scenarioet representerer et verste scenario for M1 med snø og is på veien, høyere vind og maksimal intern oppvarming. Det er viktig å presentere et worst case scenario da det vil være grunnlaget for beregningene av størrelse og kapasitet til batteriet.

Ved beregning av energiforbruk er det funnet flere feilkilder. Dataen for beregninger er gitt som gjennomsnittsdata mellom hvert stopp og dermed kan unøyaktigheter oppstå i hastighet og antall uventede stopp. Det er ingen registrerte akselerasjons- og de-akselerasjonstall tilgjengelig, og derfor har akselerasjonskraften blitt neglisjert fra energiberegningene. Av denne grunn er det funnet et skaleringstall ved å sammenligne det faktiske energiforbruket fra dieselforbruket med det beregnede forbruket for at resultatene skal reflektere det målte forbruket.

MCS kommer med mulighet til å lade med svært høy effekt (3,75MW), men batteriene er dimensjonert på en måte som åpner for lavere ladeeffekt som også forbedrer levetiden til batteriet.

De endelige resultatene har vist at alle de tre evaluerte batterialternativene, med bruk av et megawatt-ladesystem, vil være mulige løsninger på elektrifiseringen av M1. Alternativet LFP og grafitt har vist seg å være det billigste, tyngste og størst i volum. NMC111 og grafitt-alternativet har vist seg å være den dyreste batteripakken, samtidig som det er mye lettere og mindre i volum sammenlignet med LFP // Gr-alternativet. Alternativet NCA og grafitt er det letteste og minste i volum. Det er billigere enn NMC111 // Gr, men dyrere enn LFP // Gr. Gjennom livsløpsanalysen har LFP vist å gi mest CO_2-ekvivalente utslipp på grunn av en høy mengde nødvendig energi under produksjon, selv om kobolten i NMC- og NCA-katoden påvirker miljøet negativt ved slutten av batteriets levetid.

Contents

List of terms

Okstadbakken	The steepest slope of the M1 route
Ranheim	An end station for the M1 bus route
SimaPro	A software with several databases used to perform life cycle analysis´
Slope angle	Slope angle (degree) is defined as the angle measured between a horizontal plane at a given point on the land surface.
Østre Lund	An end station for the M1 bus route
MATLAB	A programming platform used by engineers, and students at NTNU.

List of abbreviations

Al	Aluminum
Co	Cobalt
COP	Coefficient of performance
Cu	Copper
ERS	Energy recovery system
ESS	Energy storage system
EV	Electrical vehicle
KERS	Kinetic energy recovery system
LCO	A cathode material with formula $LiCoO_2$
LFP	A cathode material with formula $LiFePO_4$
LFP // Gr	A battery utilizing an LFP cathode and a graphite anode
LIB	Lithium ion battery
LMO	A cathode material with formula $LiMn_2O_4$
LNO	A cathode material with formula $Li_4Ti_5O_12$
LTO	A anode material with formula $Li_4Ti_5O_{12}$
M1	Metro line number 1
MW	Mega watt

MCS	Megawatt charging system
Mn	Manganese
NCA	A cathode material with formula $LiNi_{0.8}Co_{0.15}Al_{0.05}O_2$
NCA // Gr	A battery utilizing an NCA cathode and a graphite anode
NMC	A cathode material with formula $LiNi_{0.33}Co_{0.33}Mn_{0.33}O_2$
NMC // Gr	A battery utilizing an NMC cathode and a graphite anode
NMO	A cathode material with formula $LiNi_{0.5}Mn_{0.5}O_2$
PCM	Phase change material
RBS	Regenerative braking system
rj	r is resistance and j is current density, utilized in battery cell calculations
SoC	State of charge of a battery, between 0-100%
UNFCCC	United Nations Framework Convention on Climate Change
Wh	Watt-hour, a unit of energy
COP	Coefficient of performance for a heat pump

List of symbols

η	The symbol for efficiency
J	Joule, ampere per second
ρ	Fluid density, for this thesis fluid represents air.
A	Area
a	Acceleration
C_d	Drag coefficient, a dimensionless coefficient used to describe the resistance of an object trough a fluid.
C_{rr}	Rolling resistance coefficient, the value of the rolling resistance force divided by the wheel load
α	Slope angle

List of Figures

List of Tables

1 Introduction

The transition from fossil-fuel based public transportation to a sustainable zero emissions alternative are vital in order for Norway to meet the emission goals pledged in the Paris agreement. The availability of charging stations as well as sufficient battery solutions are factors affecting the possibility of transitioning into a viable zero emissions public transportation alternative. This thesis aims to perform a feasibility study regarding the development of a fully electric replacement of the "Metrolinje 1" (M1) in Trondheim, without forfeiting passenger capacity as the Metro buses are liable for the biggest portion of people traveling with AtB. This thesis will investigate the energy consumption of the bus and sizing of the needed battery pack. It will also evaluate options in a life cycle analysis that investigates environmental impact, and the benefits of a megawatt charging system. Line one has a total distance of 21,7km in each direction, and the route is driven every ten minutes.

1.1 Motivation

Fossil powered transportation are increasingly being replaced by electric vehicles (EVs) in Norway and the western world. In 2021, 65% of the 176 000 newly registered passenger cars in Norway were fully electric. There are several positive economical and environmental reasons to switch from fossil fuels to batteries. A political initiative towards a sustainable development will likely result in laws and regulations that benefits EVs in the future. An example is the Norwegian government's implementation of a discount for electric vehicles in tolls. Previously, the maximum toll for an EV was 50% of a petrol powered vehicle, and from 2023 it has increased to 70% due to the increased share of EVs [11]. The price of batteries has decreased while the gas price has increased the last decades. From 1991 to 2018 the price per kWh of lithium batteries fell by 97%, due to an increase in efficiency per cell, and a decrease in price per cell [38]. On the other hand, the price of gas and diesel per liter has increased a lot in the same period of time [1]. Also, the efficiency of an electric engine is exceptionally higher than the diesel engine resulting in a more advantageous use of the energy pr. kWh. In addition, the economic and environmental benefit of an EV depends on the electricity price, the utilized power production source and the emissions connected to the production of the battery. If the electricity used to charge an EV originates from a renewable energy source this leaves no emissions related to the charging. But if the electricity is obtained from a gas power plant this yields emissions related to the charging process. The reduction of petroleum driven vehicles also benefits human health, as there are no exhaust emissions from EVs to increase air toxicity.

The transition to battery-powered transportation in society is an important milestone regarding the goal of the Paris Agreement, to reduce the total emissions of greenhouse gasses by 50-55% from year 1990 to 2030 [30]. In Oslo, Ruter AS has implemented electric buses and they aim to electrify all public transport in the city by the end of 2023 [40]. There are regulations in place from the Norwegian government setting parameters for the emissions requirements for public transportation and with a goal of ensuring that public acquisition of vehicles contributes to zero emissions solutions [24]. However, implementing electrical buses in Trondheim is a different challenge due to variations in conditions such as the landscape, weather, speed limits and passenger patterns.

2 Background

Trøndelag, previously North- and South-Trøndelag, is a county located in the middle of Norway. The county includes several towns and smaller communities, with Trondheim as the biggest city. Trøndelag has about half a million inhabitants, whereas 60% are located in the area around Trondheim.

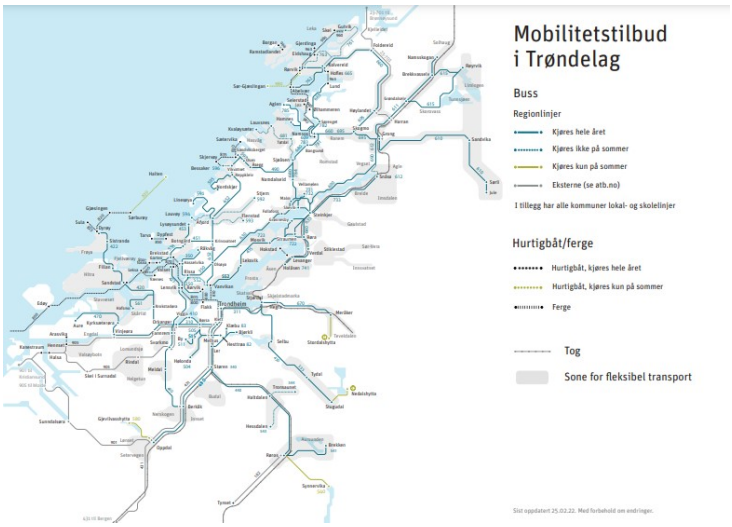

Figure 2.1: Map of lines both land-based and at sea.[9]

AtB, founded in 2009, is the sole proprietor of public transportation in Trøndelag excluding trains, and is owned in full by Trøndelag county. At first, AtB only managed the bus transport in Trondheim. In 2011 AtB took over the responsibility for both the tram at Gråkallbanen, in addition to the remaining bus traffic in the south of Trøndelag. Over the years, most of public transport in the region was transferred to AtB. After the merge of counties in 2018 all of the public transport in Trøndelag was transferred to AtB except of trains, but including buses, trams, boats and ferries. Although the public transport is under the responsibility of AtB, all the driving are conducted by other companies contracted through AtB. As an example, the bus traffic in Trondheim are conducted by both Vy Buss and Tide buss, while the ferry and boat traffic is conducted by Fjord1, Fosenlinjen and Torghatten Midt.[6]

2.1 AtB and metro line

The M1 runs from Ranheim to Østre Lund and back, through the city centre of Trondheim and is one of the most used public transportation offers at AtB. The route is approximately 21.5km long each way and includes a difference of 150 meters in height. As the world continues to look towards the implementation of EV-public transportation it is important to find a satisfactory solution to manage the M1, where the passenger capacity is minimally affected. The most energy consuming part of the route is Okstadbakken, which is a steep hill southbound on the E6. Since it is a highway there is a minimum speed limit of 40 km/h, and therefore it is essential to ensure that the new electric metro buses are able to overcome the physical challenges on the route.

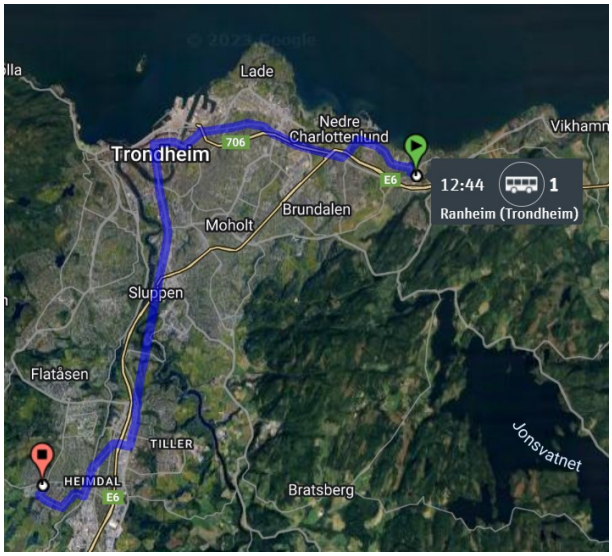

Figure 2.2: Route for M1.[9]

Today the M1 is a hybrid bus with a diesel engine. By using data provided by AtB it is possible to calculate the current energy usage with the diesel engine. It is listed with a usage of 0.56 l/km, on a regular day, and 0.7 l/km for worst case, and that diesel has an energy density of 10.1 kWh/l[7]. The efficiency of the diesel engine,η_{diesel}, is in the range of 0.3 - 0.4 [4]. This gives a specific energy consumption of (1.7 - 2.26) kWh/km for a regular day, and (2.1-2.83) kwh/km for a worst case scenario based on the efficiency of a diesel motor. These values represent the actual measured values for the energy consumption of the M1, and can later be compared with the calculated energy consumption. [7]

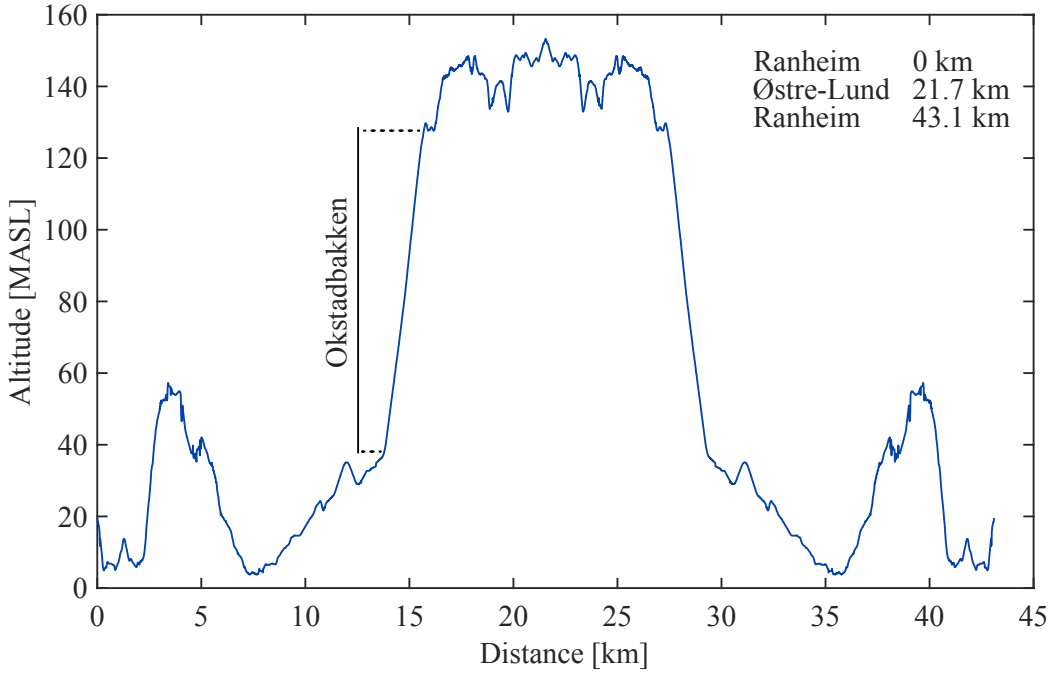

Figure 2.3: Elevation profile for the M1 route.[25]

The height differences of the M1 route is essential to the calculations of the total energy consumption between the end stations, figure 2.3 shows an elevation profile of the route with the most energy consuming part of the route marked as "Okstadbakken". The entire route is made up of asphalt roads and consists of 32 stops, each way, in addition to several traffic light stops throughout the route. As a result of the fact that Trondheim is located on the coast, it is affected by harsh weather, heavy winds and rain throughout the year, combined with ice and snow in the winter.

2.2 ATB's electrical buses today

From August 2019 the first fully electric buses were implemented into the bus fleet of AtB, and utilized in Trondheim. The metrobuses were presented at the same time and were revolutionary for their high load capability as well as the ability to run on higher speeds. In addition to this, a large part of the fleet of buses were already running on bio-fuel.[7]

2.2.1 Pantograph charging

The electric bus fleet of Trondheim is currently charged with the use of a pantograph while being in use, and charged in a charging depot at night typically at low power. The pantograph

charging solution utilizes an extender from either the pantograph charging station or from the bus, to connect the bus to the charging station by a current collector.

Figure 2.4: Pantograph charging[36]

The advantages of the pantograph charging solution vs the plug in solution is that the pantograph charging does not require an extensive action from the driver of the vehicle. When the bus is underneath the pantograph, the driver presses a button to connect the extender to either the vehicle or the charging station. It is an easy accessible charging method that can charge at high powers. This solution is best for "topping off" buses that can recharge frequently for a short duration of time. However a big disadvantage of the pantograph solution is that it is more maintenance dependent as it has moving mechanical parts.

2.3 Sustainable development

In 2021 CO_2 emissions from traffic were responsible for 18% of the the total emissions in Norway [27]. It is AtB's belief that this number can be reduced significantly, and one of the major factors is public transportation. AtB is currently operating collective transport vehicles running on bio-fuel, diesel, batteries and hybrids, and are constantly looking for ways to reduce the CO_2 emissions of their fleet.

In total 36 fully electric buses were implemented in 2019, driving 4 different fully electric routes. It was the claim of AtB that this would save approximately 1955 tons of CO_2 equivalents pr year compared to their then existing offer. [8]

2.3.1 International climate negotiations

The issue of climate change has been a major topic of concern and debate in recent years. There has been several gatherings between nations where the topic was global warming, and although

there is no definite solution in sight, several nations are looking for ways to reduce their global warming potential.

In 1992, 152 nations signed the United Nations Framework Convention on Climate Change (UNFCCC), a treaty designed to combat humans dangerous interference with the climate. The treaty stated that the signing countries would participate in scientific research, future meetings and negotiations. From the United Nations point of view it was obvious that wealthier countries have more potential to contribute towards sustainable development, compared to less developed countries, and were therefore given a greater responsibility within the agreement. [42]

An extension of the UNFCCC was signed in Kyoto in 1997 and implemented in 2005. Since the Kyoto protocol was an extension of the UNFCCC, the goals remained the same, to reduce greenhouse gas concentrations in the atmosphere. Although 192 parties committed to the protocol, global emissions were increased by 32% from 1990 - 2010. [42]

The Paris agreement, signed in 2016, is the latest treaty signed and is a legally binding international treaty on climate change. This treaty is more aggressive in it's goals than the first two as greater measures is now required to combat climate change. The treaty contains three main aspects:

- *"Holding the increase in the global average temperature to well below 2 °C above pre-industrial levels and to pursue efforts to limit the temperature increase to 1.5 °C above pre-industrial levels, recognizing that this would significantly reduce the risks and impacts of climate change"*[32]
- *"Increasing the ability to adapt to the adverse impacts of climate change and foster climate resilience and low greenhouse gas emissions development, in a manner that does not threaten food production"*[32]
- *"Making finance flows consistent with a pathway towards low greenhouse gas emissions and climate resilient development"*[32]

The Paris agreement works in cycles of 5 years, where it is each nations responsibility to submit a national climate action plan and long term plans on how to keep their emissions on a steady decline. For Norway the goal is to reduce the CO_2 emissions of 1990 by 40%, and one way to achieve this is to find sustainable solutions to problems such as public transportation.

3 Theory

The theory section of this thesis will cover the background information on preliminary calculations. These calculations aim to determine the required battery size and charging specifications to drive the M1 through the route while meeting the load (number of passengers) and speed requirements. In addition, it will include background on lithium ion batteries, their usage in EVs, and how different types of lithium ion batteries differ in performance based on the utilized electrode materials. It will also cover the technology behind mega watt charging systems.

3.1 Preliminary energy calculations

In order to determine the size and the required power of the battery solution, calculations regarding the energy consumption of M1 are conducted. When considering the total energy consumption of a bus there are several factors that affect the outcome. The number of passengers and number of stops and starts are a few of the variables that need to be taken into account in order to give a precise evaluation of the bus' energy consumption.

There are different ways to calculate the energy consumption of a bus, where some are more advanced than others. The most elementary way is to calculate the potential energy of the bus in different places of its course. Appendix A shows the height difference between every stop the bus makes along the route, and by using these numbers it is possible to calculate the energy consumption, and the energy gained from regenerative braking for the bus throughout the route.

$$E_{pot} = m * g * h \tag{3.1}$$

Equation 3.1, where m is the mass, g is the gravitational constant and h is height, presents the most elementary way of calculating the energy needed in order to take the bus through the route. Negative values of the height difference indicates that the bus is going downhill and regenerative braking will recharge the battery with a specified efficiency. By multiplying the efficiency of regenerative braking in the cases where the potential energy values are negative it will simulate the total energy loss for the bus. However using only this formula negates a lot of the key factors for the energy consumption, and does not give an accurate description of the overall energy needed for a round trip.

It is possible to expand on 3.1, and obtain a more advanced physics-based model of the predicted energy consumption of the bus.

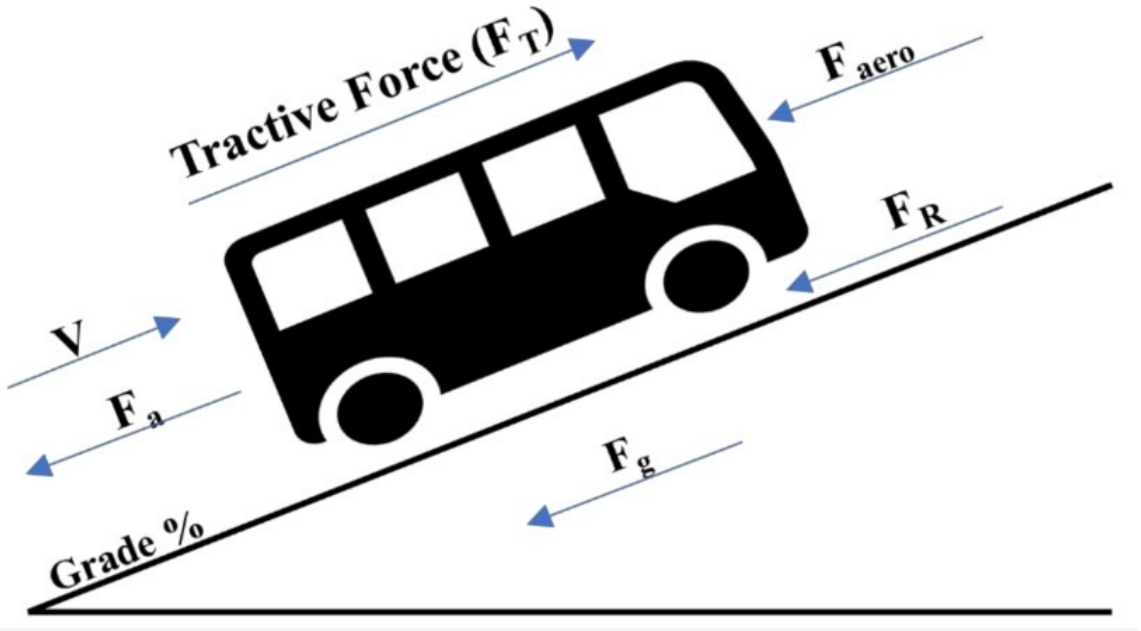

Figure 3.1: Forces acting on a moving bus [2]

The tractive force (FT) should be equal or more than the summation of the four resistance forces (Equations (3.5)–(3.6)) that face the bus during the movement.[2] [37]

$$F_{tot} = F_{aero} + F_s + F_r + F_a \tag{3.2}$$

In equation 3.2 F_{aero} is the air resistance force, F_s is the inclination force, F_r is the rolling resistance force, and F_a is the acceleration resistance force. The total energy consumption of the bus is given by adding all the forces working on the bus, and therefore the equation 3.2 represents the required traction force, F_{tot} , needed to propel the bus with a specified, V, velocity.[37]

3.1.1 Inclination resistances

One major force when calculating forces that impede the vehicle's acceleration is the inclination force. Both the upwards inclination and downwards impacts the overall energy consumption as the upwards inclination helps to de-accelerate the vehicle and the downwards contributes to the acceleration.

$$F_s = m \cdot g \cdot sin(\alpha) \tag{3.3}$$

Equation 3.3 is the mathematical expression for the slope resistance imposed on the vehicle and is directly affected by the inclination of the slope, where α is the angle of the slope. [37]

3.1.2 Rolling resistances

The rolling resistance or rolling friction is the resistance when a body (the wheels) is rolling on a surface. Hysteresis losses from the continued deformation and reformation of the tyres under the pressure of the vehicle, and losses from slippage between the surface and the tires.

$$F_r = m \cdot g \cdot C_{rr} \cdot cos(\alpha) \tag{3.4}$$

The rolling resistance coefficientC_{rr} can be described as the value of the rolling resistance force divided by the wheel load.

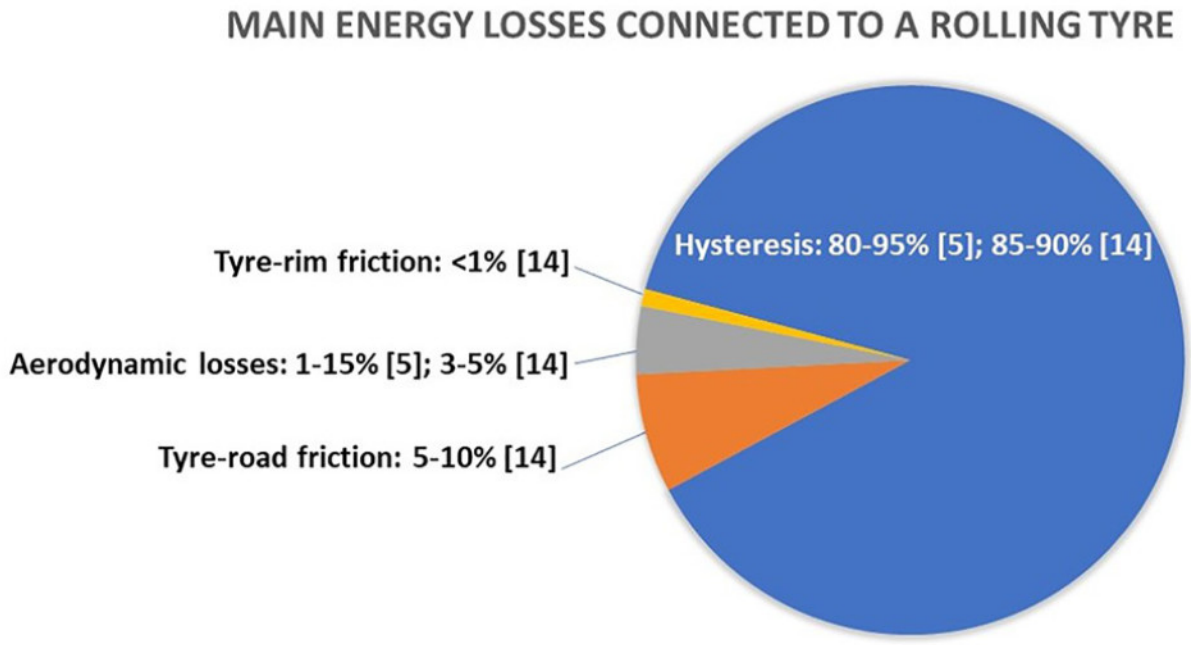

Figure 3.2: Main energy losses connected to a rolling tyre, related to C_{rr} [45]

There are different factors affecting the rolling resistance coefficient, and therefore the numerical value may differ from vehicle to vehicle and trip to trip. A higher inflation pressure of the tires causes lower rolling resistance as the inflation pressure works against the deformation of the wheels during rolling. The inflation pressure will typically increase while driving as the mechanical energy converts to heat and the inflation gas heats up and expands. The outside temperature may also contribute to the increasing or decreasing of the inflation pressure. [26]

An increase to the wheel load will also increase the overall rolling resistance. When considering the M1, the wheel load will variate with the number of passengers on the bus, and rolling resistance coefficient alike variate with a change of load. [26][45]

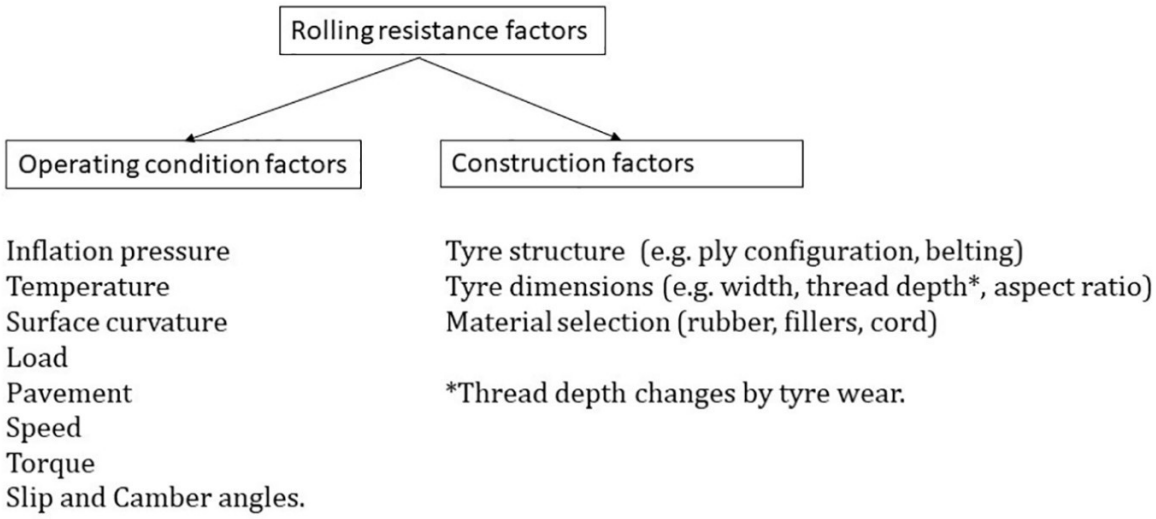

Figure 3.3: Factors affecting the rolling resistance coefficient.[45]

Other main factors contributing to the rolling resistance coefficient are the speed of the vehicle, the surface conditions (weather and road deformation), and the slip angle of the wheels. Some of these factors are seasonally dependent or may change on a daily basis. Therefore it is difficult to determine an overall rolling resistance coefficient that is set for the entire year. An extensive sensitivity analysis has to be made to ensure that the values utilized are within an acceptable level of accuracy. [26][45]

3.1.3 Aerodynamic resistances

Aerodynamic drag is one of the most relevant topics in the automobile industry and has been a motivating factor for innovation in the topic of car design since the automobile was invented. The aerodynamic forces affecting the vehicle can be described in equation 3.5.

$$F_{aero} = \frac{1}{2} \cdot \rho \cdot C_d \cdot A \cdot V^2 \tag{3.5}$$

In equation 3.5, C_D is the drag coefficient, ρ is the density of the fluid which the object is moving through, A is the front area of the moving object and V is the relative velocity of the object to the fluid. In this case, V is the relative velocity between the vehicle and the air. [37]

3.1.4 Acceleration resistances

The acceleration force is the force required to accelerate or de-accelerate the vehicle, or in other terms, the vehicle's resistance to velocity changes. When de-accelerating the energy can be re-gained by using a energy recovery system, but this type of technology can only recover about 50-70% of the energy effectively, the rest is lost in the braking system mostly as heat.

$$F_a = m \cdot a = m \cdot \frac{dV}{dt} \tag{3.6}$$

The force required to accelerate a vehicle is determined by the mass and the acceleration rates, where negative values indicates a de-acceleration. [2] [37]

3.1.5 Energy recovery systems

In a traditional braking system, the kinetic energy of the vehicle is converted into thermal energy through friction. This energy is just dissipated and is a major source of energy loss. With the use of energy recovery systems, (ERS), the wasted energy can be converted back into the vehicle's energy storage system (ESS). One of the main limitations of the ERS is the ability to store all of the recuperated energy and therefore the ESS is one of the main components of the ERS. There are several different methods of energy storage such as flywheel, pneumatic/hydraulic, electrochemical, Rankine, and thermic storage. As almost all vehicles, whether internal combustion, electric, or both (hybrid), rely on batteries to store energy. The best economic solution to the ESS is to store the recuperated energy in the batteries. [5]

There are different types of ERS but the most applied in electric vehicles are regenerative braking systems, (RBS), or kinetic energy recovery systems (KERS). The KERS operate by recuperating part of the vehicle's kinetic energy mainly during braking operations. When driving normally the electric motor applies force to the wheels resulting in vehicle speed. But when the accelerator is not applied the wheels drive the motor causing it to act as a generator. This will happen both when the brakes are applied or when the driver releases the accelerator and the vehicle is coasting.[44][5]

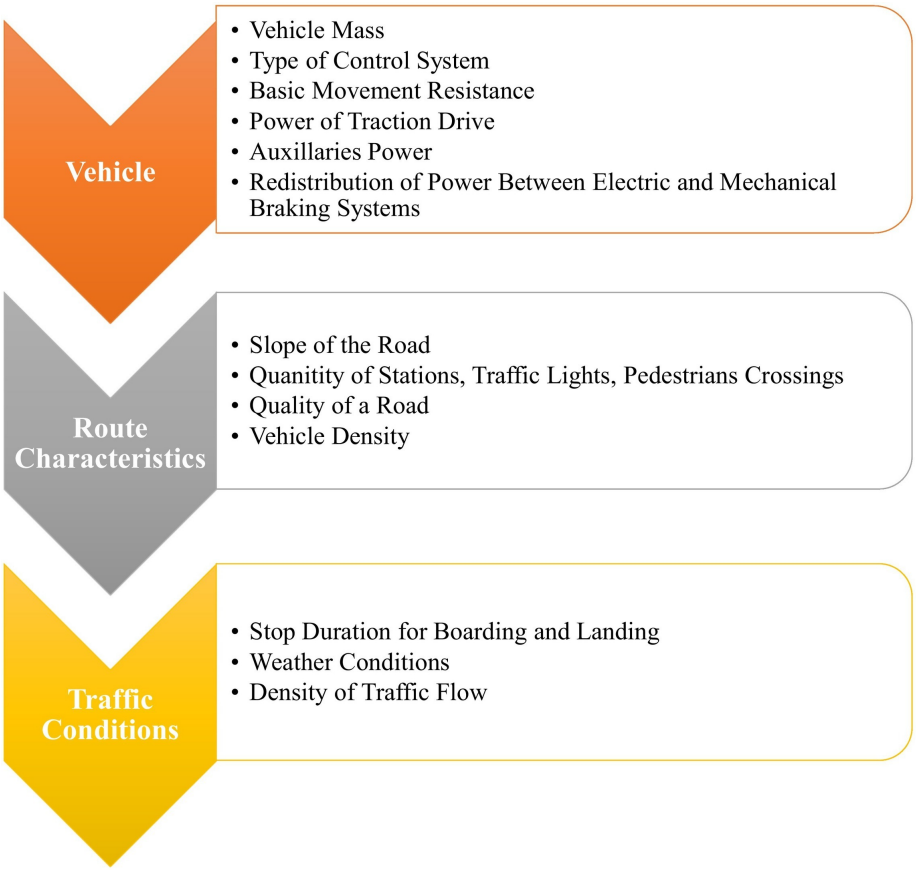

Figure 3.4: Classification of factors impacting brake energy consumption and generation [5]

Figure 3.4 shows some of the factors affecting brake energy recovery and therefore the efficiency of a regenerative braking system. The average (RBS) provides up to 70% recovery for the kinetic energy. For this project, the RBS efficiency is set to a fixed value of 50%. The reason is that

these calculations are preliminary, while real-time simulations are unavailable. For the battery calculations, it is better to overestimate the energy needed by the battery pack which is why the RBS efficiency is set to 50% and not 70%. A thorough sensitivity analysis will be performed to show the effect of different values for the efficiency of the RBS.[5]

3.1.6 Energy consumption of the interior

The energy consumption of a vehicle can be divided into two groups:

- Exterior energy consumption - Driving of the vehicle
- Interior energy consumption - clean traction, auxiliary drives, heating, air conditioning, energy for 24 V appliances.

The most extensive energy consumption in the cabin of the bus is the heating and air conditioning. With the variations of climate in Trondheim, air temperatures may be in the range of -20℃ to +30℃. A study conducted by the Industrial University of Tyumen explored the impact of natural and climatic conditions on energy consumption by an electric city bus. Their study showed that the highest value for energy consumption was at -20℃ where a *"regular heater"* and battery heater were utilized. The lowest values of energy consumption was established at 14℃ where no heater and AC were used. At 20℃ the AC was applied and the energy consumption increased significantly. [15]

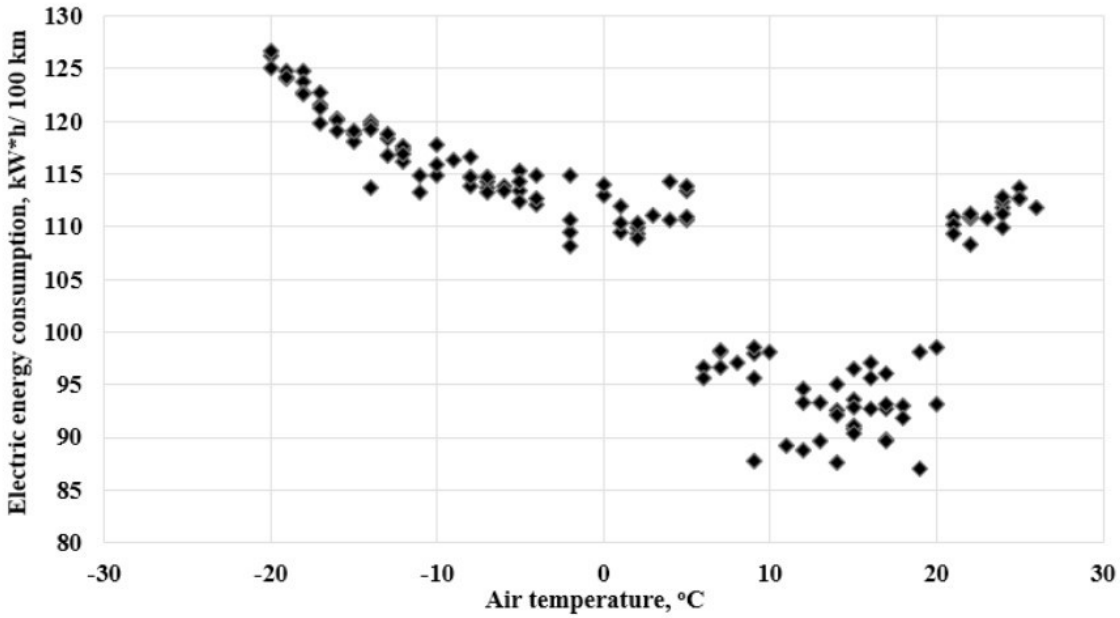

Figure 3.5: Energy consumption of a bus shown with ambient air temperature as a factor. [15]

For this thesis a base case with no cooling or heating will be investigated. Currently the M1 has two heaters pulling 11W each. However it is likely to implement a single heat pump with a efficiency (COP factor) of 2.

3.1.7 Total energy

When all forces that impact the vehicle has been calculated, it is possible to convert that into energy.

$$E_{force} = \frac{1}{3600}\frac{1}{\eta_{motor}} \cdot \Sigma_{i=0}^{43,1km}((F_{tot} > 0) \cdot i) + \frac{1}{3600} \cdot \Sigma_{i=0}^{43,1km}((F_{tot} < 0) \cdot regen \cdot i) \tag{3.7}$$

Equation 3.7 describes how to convert the forces to energy, where η_{motor} is the motor efficiency, i is the intervals used to calculate the sum of forces, and *regen* is the efficiency of regenerative braking. If the sum of the forces is positive they perform a negative work on the bus and the accelerator is required to counter it. This implies that motor efficiency has to be considered. Multiplying the sum of the forces with a distance identifies the work applied to the bus, N·m = J. Furthermore, multiplying the work with $\frac{1Wh}{3600J}$ converts the energy from J to Wh. Equation 3.7 shows how to compute the energy in the two cases that can occur. Either the sum of the forces within the specified distance is greater than 0, $F_{tot} > 0$, and the accelerator is applied thus factoring in the efficiency of the motor. The other case applies if the sum of the forces and distance is less than 0, $F_{tot} < 0$. In this case, the accelerator is not used and the forces acting on the bus are performing a positive work on the bus. Here the ESR is applied and therefore factoring in the efficiency of the ESR, (*regen*). In this thesis the sum of forces is calculated every 10m therefore i = 10.

When the sum of the forces has been converted to energy, it can be added to the rest of the variables affecting the energy consumption of the bus.

$$E_{tot} = (E_{force} + E_{heating} + E_{regen} + E_{aux}) \tag{3.8}$$

In equation 3.8, E_{force} is the energy when all forces act on the bus, $E_{heating}$ is the energy consumption related to heating and cooling, E_{regen} is the regenerated energy from the ESR and E_{aux} is the remaining energy utilized to charge devices and lighting.

3.2 Batteries

This section will include the theory of lithium ion batteries and different lithium ion battery electrodes and how they impact the performance of a LIB.

3.2.1 General technology behind LIBs

Lithium ion battery technologies are based on oxidation of lithium atoms during discharge, and reduction of the positively charged lithium ions during charging. During oxidation, electrons are released and travel through an external circuit where load can be applied. Similar to all electrochemical batteries the LIB consists of an anode, a cathode, and an electrolyte. The anode typically consists of a current collector with high electrical conductivity, for example Al or Cu, and a chemical structure that facilitates for storage of lithium atoms. The cathode also consists of a conductive current collector, and a layer structure for storage of the lithium ions. Between the anode and cathode, the electrolyte secures passage for the lithium ions through its solvent molecules. The chemistry of the cathode varies between different types of LIBs, while

the anode preferably consists of a graphite structure, though alternative anode materials are being frequently researched.

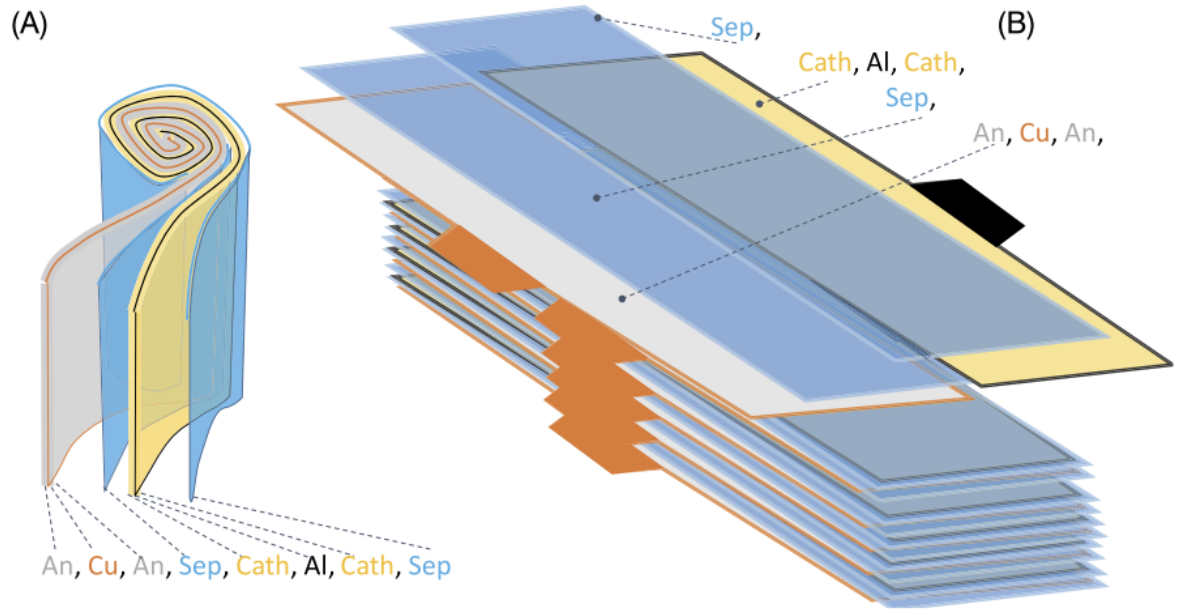

Figure 3.6: Assembly of a cylindrical (A) and a pouch (B) cell of lithium ion battery [12]

During discharging the lithium in the anode release an electron, while the lithium ion migrates to the cathode, the reaction is triggered by the potential difference between the two electrodes. The electron is picked up by the anode current collector and travels through an external circuit and the applied load that could be anything from a light bulb to an electric motor. In the cathode, the lithium ion is stored as a lithium metal oxide. During charging, the process is reversed. The charger forces the lithium ions back into the anode, while the electrons are picked up by the cathode current collector and travel through the circuit assembled by the charger with minimal load. However, not all of the lithium is removed from the cathode during charging, as this could lead to atomic crystal structure collapse in the cathode material. [12]

The following half cell reaction equations includes anode, cathode and total reaction of an operating lithium ion battery where "M" stands for transition metal, which varies depending on the cathode chemistry. The half cell voltages and the open cell voltage mentioned is correct for a lithium ion battery with an LCO cathode and a graphite anode. [12]

$$Anode : Li_xC \rightarrow C + xLi^+ + xe^- \qquad E^0 = -3.0V \qquad (3.9)$$

$$Cathode : Li_{1-x}MO_2 + xLi^+ + xe^- \rightarrow LiMO_2 \qquad E^0 = 1.0V \qquad (3.10)$$

$$Total : Li_xC + Li_{1-x}MO_2 \rightarrow LiMO_2 + C \qquad E^0 = 1.0V - (-3.0V) = 4V \qquad (3.11)$$

Lithium is the lightest metal there is, and it has the lowest reduction potential of all elements resulting in a high possible cell potential. These qualities of lithium contribute to the LIB's high capacity and power density. Lithium is also a very common element in the world, resulting in a low risk of lithium shortage in the near future. However, it is possible that a shortage of

transition metals currently used in LIBs may become an issue. An example of a transition metal used in lithium ion batteries with a risk of future shortage is cobalt.

3.2.2 Comparison of LIBs in EVs

LIBs in general have many properties that beneficially contribute to it's usage in electric vehicles. As shown in figure 3.7 they yield a relatively high specific energy and specific power which is important in order to keep the total weight of the EV satisfactory. Fast recharge with high C-rates and a relatively low self-discharge rate, together with long cycle life also benefits vehicles as it improves the max range between charges and reduces charge time. In addition, LIBs are reliable and able to operate at the necessary variety of temperatures.[47]

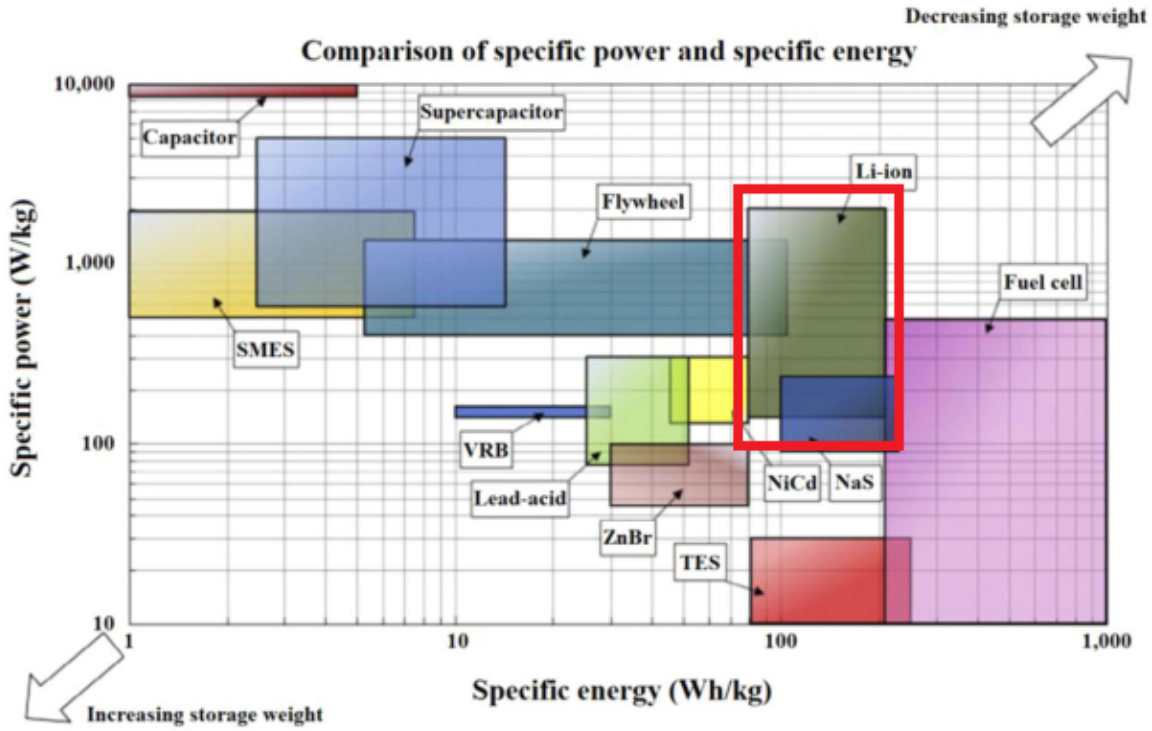

Figure 3.7: Specific power and specific energy of different energy storage systems [47]

On the other hand, LIBs have a relatively high cost and some concerns regarding safety. If the battery is not assembled accurately, maintained properly, or charged responsibly this could lead to gas development, thermal runaway, and explosions. The risk increases if the battery is exposed to heat. If the battery cell is not fabricated properly, this could cause short-circuiting, heat development and fire due to undesirable contact between electrically conductive components. An example of this issue was registered in Samsung's Galaxy Note 7 smartphone, where the short-circuiting was a result of a weakening of the separator layers between electrodes in the battery cells. [31]

3.2.3 Different LIB electrodes

Buses have unique requirements regarding batteries, as they need to be able to handle the demands of frequent stop-and-go traffic and long daily routes. Lithium-ion batteries are becoming the standard for electric vehicles and there are several variations of the lithium ion battery that are used in buses. Each has variations in chemical structures, properties, and exploited materials. Many scientific breakthroughs regarding LIBs in the previous years have been in relation to the development of new electrodes utilizing a variety of materials. Specifically, there are different chemistries that can be utilized in both the battery cathode, and anode, which yield higher rate capability, charge capacity and voltage. The electrode chemistry can impact energy and power density while varying in price. For example, cathodes made with cobalt (Co) are more expensive than cathodes made with manganese (Mn) due to the fact that Co is a less common metal than Mn on the earth. The prices may also depend on supply and demand, in addition to rarity. [33]

An intercalation cathode contains a crystal structure fit for storing positively charged Li-ions. Mainly four different crystal structures are used in LIB cathodes, including layered, spinel, olivine and tavorite, as shown in figure 3.8. Intercalation cathodes are the most relevant technology for today's applications, even though conversion cathodes can be mentioned as technology for the future. Conversion cathodes will not be covered in this report as it has yet to be utilized in modern electric vehicles. [33]

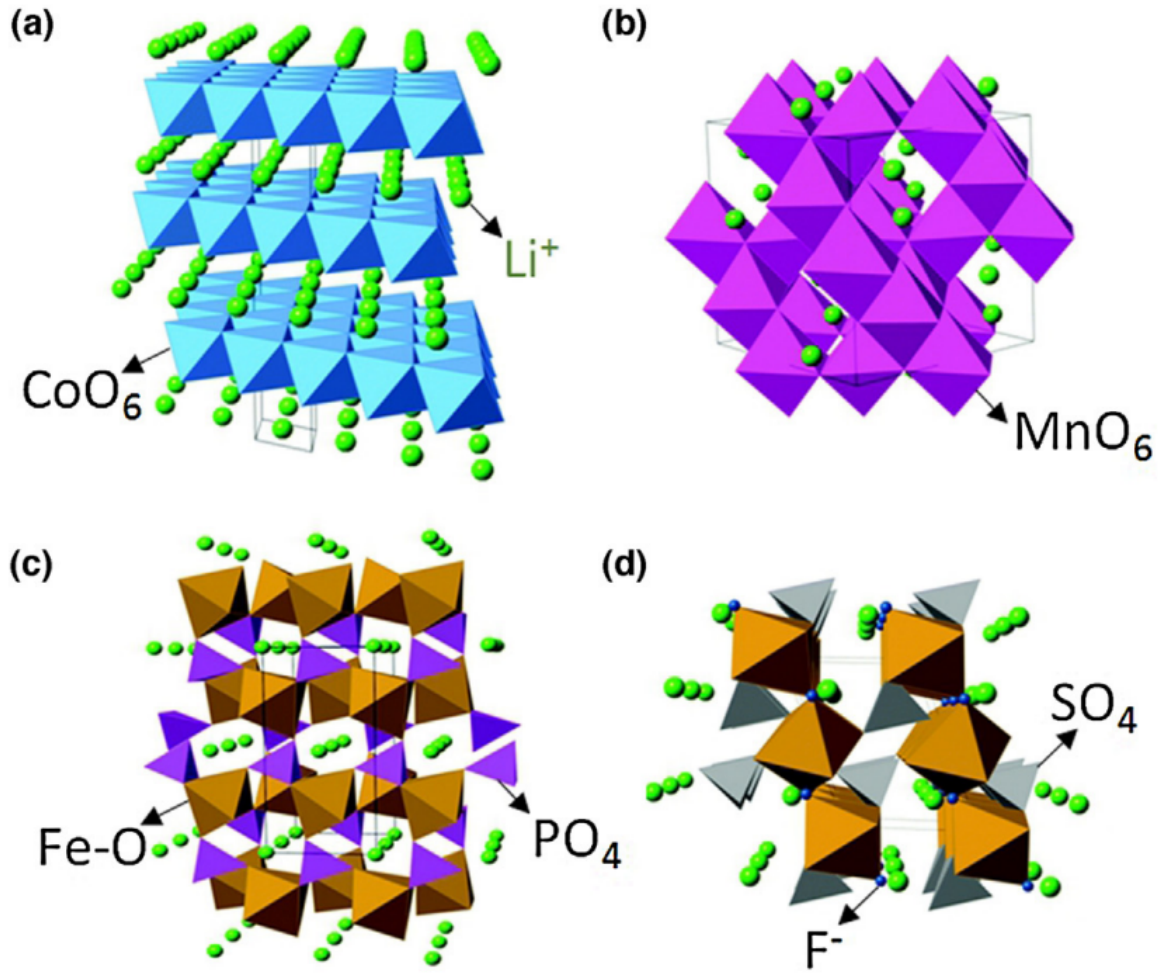

Figure 3.8: Crystal structures of LIB cathodes storing Li ions, Layered (a), spinel (b), olivine (c), tavorite (d) [33]

Crystal structure	Compound	Specific capacity (mAh g^{-1}) (theoretical/experimental/typical in commercial cells)	Volumetric capacity (mAh cm^{-3}) (theoretical/ typical in commercial cells)	Average voltage (V) [34]	Level of development
Layered	$LiTiS_2$	225/210 [35]	697	1.9	Commercialized
	$LiCoO_2$	274/148 [36]/145	1363/550	3.8	Commercialized
	$LiNiO_2$	275/150 [37]	1280	3.8	Research
	$LiMnO_2$	285/140 [38]	1148	3.3	Research
	$LiNi_{0.33}Mn_{0.33}Co_{0.33}O_2$	280/160 [32]/170	1333/600	3.7	Commercialized
	$LiNi_{0.8}Co_{0.15}Al_{0.05}O_2$	279/199 [33]/200	1284/700	3.7	Commercialized
	Li_2MnO_3	458/180 [39]	1708	3.8	Research
Spinel	$LiMn_2O_4$	148/120 [40]	596	4.1	Commercialized
	$LiCo_2O_4$	142/84 [41]	704	4.0	Research
Olivine	$LiFePO_4$	170/165 [42]	589	3.4	Commercialized
	$LiMnPO_4$	171/168 [43]	567	3.8	Research
	$LiCoPO_4$	167/125 [44]	510	4.2	Research
Tavorite	$LiFeSO_4F$	151/120 [30]	487	3.7	Research
	$LiVPO_4F$	156/129 [45]	484	4.2	Research

Figure 3.9: Characteristics of a variety of intercalation cathode compounds [33]

$LiCoO_2$ (LCO) was the first commercialized layered transition metal oxide utilized in LIB cathodes as it yields a relatively high specific capacity as well as a high theoretical volumetric capacity as shown in figure 3.9. However, due to the price of cobalt, these cathodes are expensive. They also have low thermal stability increasing the risk of exothermic release of oxygen

(thermal runaway). Substituting Co with Ni $LiNiO_2$ has been attempted with the purpose of reducing cost and improving thermal stability, but Ni-ions may block Li diffusion pathways, making pure LNO cathodes a bad choice. Further research has resulted in development of $LiNi_{0.8}Co_{0.15}Al_{0.05}O_2$ (NCA) cathodes. These are popular in today's market for electric vehicles and are used in Tesla EVs among others. The reduced amount of cobalt compared to LCO results in a reduced cost, the reduction of Ni compared to LNO makes the battery reliable and the addition of aluminum improves both thermal stability and electrical conductivity. [33]

The $LiNi_{0.33}Co_{0.33}Mn_{0.33}O_2$ (NMC) cathode was invented by adding cobalt into an $LiNi_{0.5}Mn_{0.5}O_2$ (NMO) layered structure. The cobalt was found to enhance the NMO structure stability. Despite the high cost of cobalt, the $LiNi_{0.33}Co_{0.33}Mn_{0.33}O_2$ (NMC-111) and the $LiNi_{0.8}Co_{0.1}Mn_{0.1}O_2$ (NMC-811) cathode is widely used in the battery market. For usage such as in electric vehicles, that demands higher energy/power density, the NMC-811 is the preferred option. In theory you can apply the preferred amount of nickel, cobalt and manganese in the $LiNi_xCo_yMn_zO_2$ chemical structure where Ni enhances capacity, Co enhances C-rate and Mn improves stability and safety. [33]

Commercialized LMO cathodes, $LiMn_2O_4$, have a spinel crystal structure as shown in 3.8. The absence of cobalt makes this cathode cheaper and more environmentally friendly compared to NMC and NCA and it has a higher average voltage of 4.1V, compared to 3.7V for NMC and NCA. However, LMO cathodes have an insufficient long-term cycle life due to the frequent formation of a solid electrolyte interface (SEI) blocking the transfer of ions through the electrolyte. This problem increases in relevance at high C-rates such as for megawatt charging systems. [33]

LFP cathodes, $LiFePO_4$, are also frequently utilized in the battery market and it has an olivine structure for storing of Li-ions as shown in figure 3.8. The LFP cathodes are known for their thermal stability together with a high power capability in addition to a low cost. They have a long cycle life, making them a reliable choice for electric vehicles. A low average potential is the main weakness of the LFP cathode as shown in figure 3.10. It also has low electrical conductivity, but this property can be improved by adding conductive material coating, usually carbon black. [33]

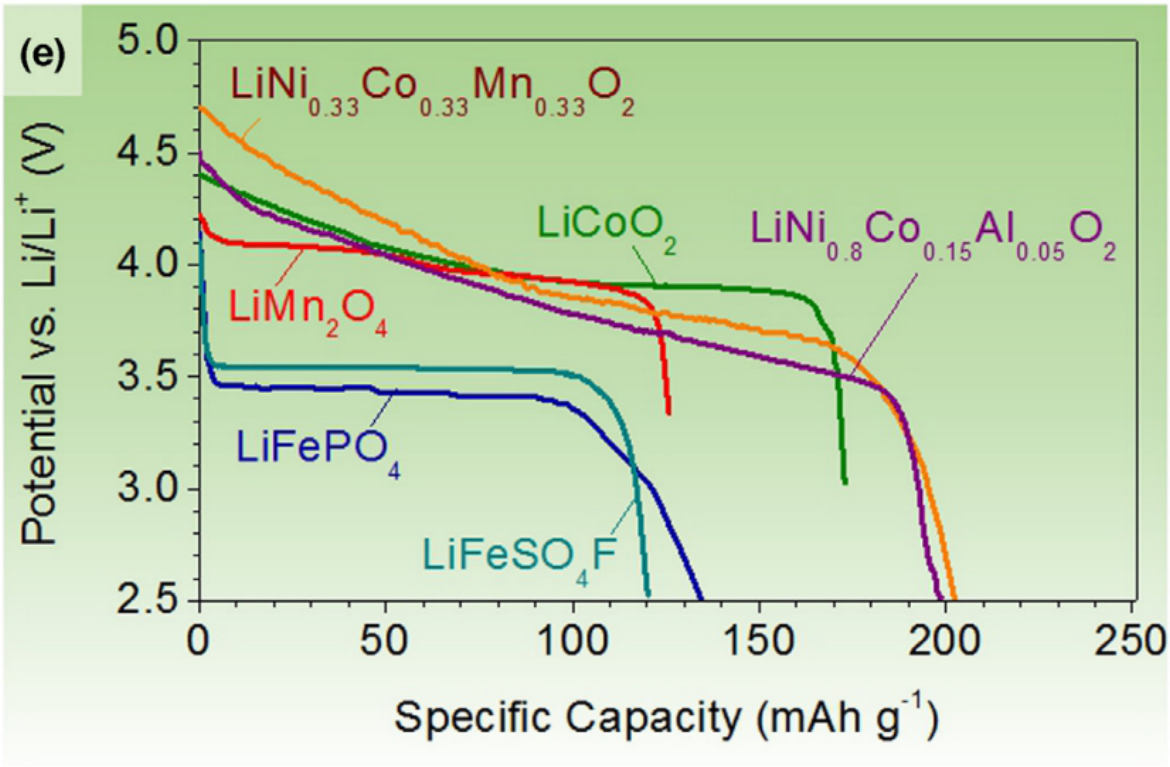

Figure 3.10: Discharge profiles of some intercalation cathodes (from 2014) [33]

The battery's anode stores stable lithium atoms while charging, and for the anode, graphite is the most commercialized option. With its hexagonal structure, it can store up to 1 Li-atom per 6 C-atoms as shown in figure 3.11. Carbon electrodes are cheap and materially easily obtained. They also have high electrical conductivity with good Li-transport. In addition, the structure has high mechanical stability leading to a minimal volume change of 10% during charging/discharging as listed in 3.12. Figure 3.13 shows that graphite cathodes have low potential vs. Li/Li+. In addition, conversion type anodes such as graphite have a high gravimetric capacity, but a small volumetric capacity (330-430 mAh/cm^{-3})[33].

The solid electrolyte interface layer is purposely formed on all graphite anodes during the process of formation in the LIB manufacturing process. Formation of the solid layer on the anode surface improves the battery cycle life, while also decreasing its efficiency and capacity. It allows passage for Li-ions but not for electrons. This contributes to the desired emigration of electrons through the external circuit and load, benefiting battery life. But the layer also consumes lithium, reducing the capacity of the battery cell during cycling.

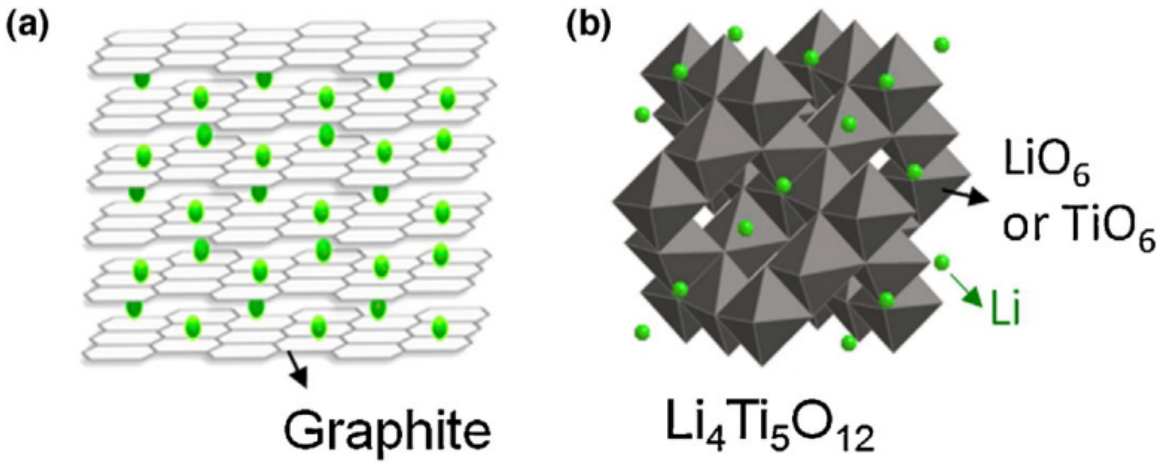

Figure 3.11: Chemical structure and storing of Li in graphite and LTO anodes [33]

$Li_4Ti_5O_{12}$ (LTO) is another good anode option for electrical vehicles regarding its performance. It has a high cycle life and low degradation rate because the high voltage above 1V as shown in figure 3.13 prevents the formation of anode SEI. This makes the LTO anode the most long-lasting option on the market for high power applications, and greatly improves fast charging performance. High voltage in the cathode also contributes to the battery's very high safety, due to the minimal lithium dendrite formation. In addition, LTO anodes have a close to negligible volume change during charging/discharging of 0.20% 3.12 further increasing safety. LTO anodes can be used in combination with NMC cathodes. [33]

Compared to the graphite option, The LTO anode is much more expensive while also being heavier than the graphite anode due to their gravimetric capacities of 175mAh g^{-1} and 350mAh g^{-1} respectively [33]. This shows in 3.13 for graphite and LTO on the x-axis. On the other hand, the LTO anode is smaller in volume compared to graphite with volumetric capacities of 600mAh cm^{-3} and 330-430mAh cm^{-3} respectively [33].

Properties of some commonly studied anode materials.

Material	Lithiation potential (V)	Delithiation potential (V)	D ($cm^2\ s^{-1}$)	Volume change
Graphite [182,193–198]	0.07, 0.10, 0.19	0.1, 0.14, 0.23	10^{-11}–10^{-7}	10%
LTO [199–203]	1.55	1.58	10^{-12}–10^{-11}	0.20%
Si [34,191,204–209]	0.05, 0.21	0.31, 0.47	10^{-13}–10^{-11}	270%
Ge [34,209–212]	0.2, 0.3, 0.5	0.5, 0.62	10^{-12}–10^{-10}	240%
Sn [34,209,213–215]	0.4, 0.57, 0.69	0.58, 0.7, 0.78	10^{-16}–10^{-13}	255%
Li_2O [216] **(amorphous)**	N/A	N/A	5×10^{-12}–5×10^{-10}	N/A

Figure 3.12: "Properties of some commonly studied anode materials"[33]

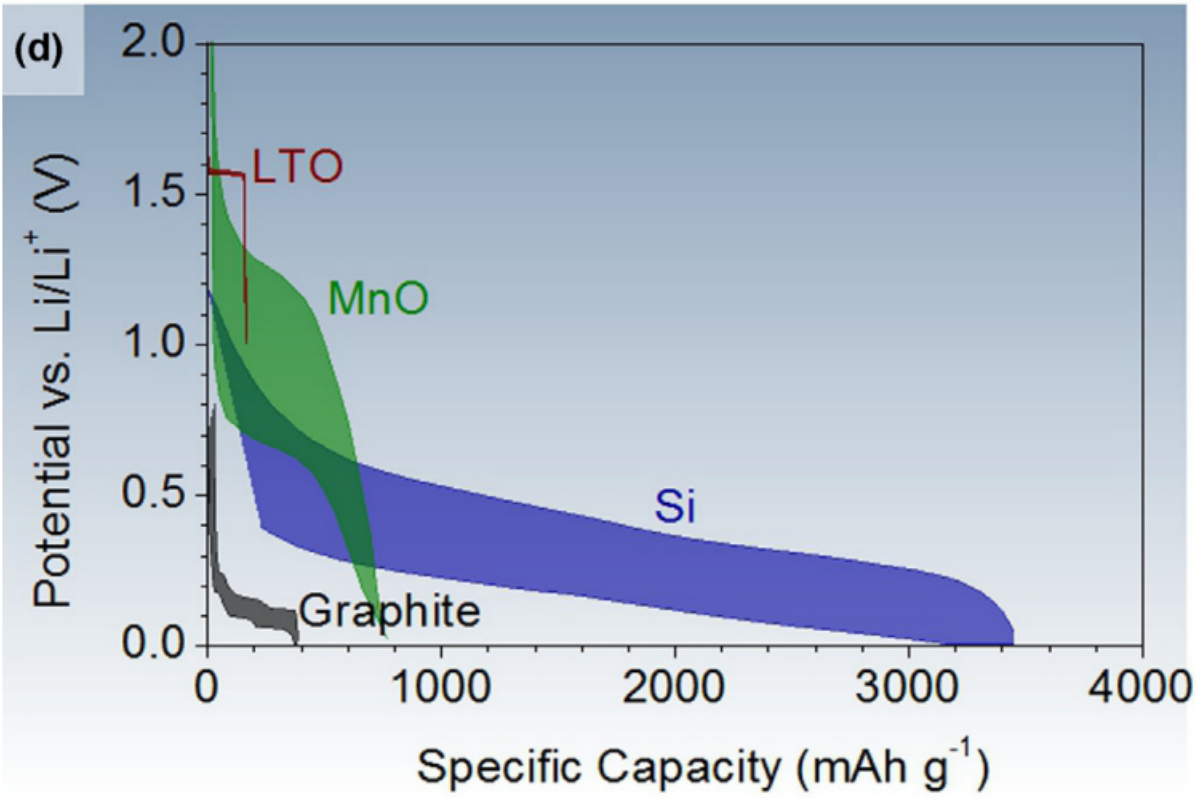

Figure 3.13: Potential vs. Li and specific capacity of some LIB conversion type anode materials during charging/discharging [33]

Another anode worth mentioning is the silicon anode which is included in figure 3.13. It has an extremely high capacity both volumetric and gravimetric. The extreme volume change during charging/discharging of 270% as shown in table 3.12, makes the pure silicon anode mechanically unstable and a bad choice for an electric vehicle due to the hazard that follows a potential loss of electrical contact and protective layers. It also tends to yield a low electric conductivity. However, adding silicon to a graphite anode has shown to enhance the performance while maintaining stability and conductivity. [34]

3.2.4 Investigation of electrode performance

This part will cover the theory behind the calculations and evaluations regarding potential battery solutions for the M1 bus. The graphite anode has been decided to be the best option for investigation because of its wide usage in the battery market, and good general performance specifications with a high specific energy capacity and low cost. The LTO anode could be a reliable option with respect to its performance and safety, but will be ignored further in this report due to the extremely high cost and high weight yielding a low specific energy. Henceforth the NMC111, the NCA, and the LFP chemistries will be the cathodes of investigation.

In order to calculate the theoretical electrochemical capacity of cell electrodes, equation 3.12 has been used.

$$Q_{theoretical} = \frac{nF}{3600 \cdot M} \tag{3.12}$$

In equation 3.12, n is the number of charge carriers (Li+), equal to the number of electrons from the half cell reaction, F is the Faraday's constant in sA/mol and M is the molecular weight of the electrode active material in g/mol. Further, this formula has been utilized to determine the theoretical specific capacity of an NMC111, NCA, and an LFP cathode.

$$LiNi_{0.33}Co_{0.33}Mn_{0.33}O_2 \rightarrow Ni_{0.33}Co_{0.33}Mn_{0.33}O_2 + Li^+ + e^- \tag{3.13}$$

$$Q_{theoretical\ NMC_{111}} = \frac{1 \cdot 96485[\frac{As}{mol}]}{3600[\frac{s}{h}] \cdot 96.46[\frac{g}{mol}]} = 0.278[\frac{Ah}{g}] = 278[\frac{mAh}{g}] \tag{3.14}$$

$$LiNi_{0.8}Co_{0.15}Al0.05O_2 \rightarrow Ni_{0.8}Co_{0.15}Al_{0.05}O_2 + Li^+ + e^- \tag{3.15}$$

$$Q_{theoretical\ NCA} = \frac{1 \cdot 96485[\frac{As}{mol}]}{3600[\frac{s}{h}] \cdot 96.08[\frac{g}{mol}]} = 0.279[\frac{Ah}{g}] = 279[\frac{mAh}{g}] \tag{3.16}$$

$$LiFePO_4 \rightarrow FePO_4 + Li^+ + e^- \tag{3.17}$$

$$Q_{theoretical\ LFP} = \frac{1 \cdot 96485[\frac{As}{mol}]}{3600[\frac{s}{h}] \cdot 157.7[\frac{g}{mol}]} = 0.170[\frac{Ah}{g}] = 170[\frac{mAh}{g}] \tag{3.18}$$

For the anode, the theoretical capacity of graphite has been calculated, given that you can store 1 Li-atom per 6 C-atoms[12]. With carbon's molecular weight of 12 g/mol this yields the molecular weight of graphite that is 72 g/mol (6*12), and a theoretical capacity of graphite of 372mAh/g 3.19.

$$Q_{theoretical\ Graphite} = \frac{96485[\frac{As}{mol}]}{3600[\frac{s}{h}] \cdot 72[\frac{g}{mol}]} = 0.372[\frac{Ah}{g}] = 372[\frac{mAh}{g}] \tag{3.19}$$

However, the theoretical electrochemical calculated capacity will be higher than the experimental capacity in lithium ion battery electrodes. The capacity that is delivered from the battery will depend on several factors as mentioned in section 3.2.4, as well as the voltage range at which the battery cell operates, see 3.10. In addition, the theoretical capacity value assumes that all the lithium in the cathode is utilized. This is not true for a lithium ion battery as lithium is only depleted and not entirely removed from the cathode. Entirely removing the lithium would damage the cathode mechanical structure and prevent lithium from reacting back into the structure again. [12]

For the battery's overall gravimetric capacity, the capacity of the anodes has to match that of the cathode, while also taking the rest of the battery components into account. If we for example consider an NCA cathode with an experimental capacity of 200 mAh/g as shown in figure 3.9 and a graphite anode with an experimental capacity of 360mAh/g, this yields a cathode/anode weight ratio of 1.8 (360/200). This means that 1.8 times as many grams of cathode material compared to anode material is needed for max performance per gram. In theory, you would then have an overall battery cell capacity of 360mAh by utilizing 1.8g of cathode material and

1g of anode material. The overall gravimetric capacity of the battery cell would then be almost 129mAh/g (360/2.8). However, this only considers the battery electrodes. In addition, all other components in the battery such as separator layers, electrolytes, conductive material and current collectors will have an impact on the gravimetric and volumetric capacity. This is because they affect both the weight and the volume of the battery pack. If you assume that these components take up about 40% weight [13] of the battery pack you are left with the following expression given these exemplifying values for an NCA cathode and a graphite anode as shown in equation 3.20. (The 40% weight share has been included by multiplying the weight of the electrodes by 5/3).

$$Battery\ gravimetric\ capacity_{NCA//Gr} = \frac{360[mAh]}{(2.8 \cdot \frac{5}{3})[g]} = 77.14 \left[\frac{mAh}{g}\right] \tag{3.20}$$

In order to determine the specific energy in Wh/kg, this value is multiplied by the average operating cell voltage of an NCA cell, 3.6V, determined by the potential difference between the average voltage of the NCA cathode of 3.7V and graphite (about 0.10V) [33].

$$77.1 \left[\frac{mAh}{g}\right] \cdot 3.6[V] = 278 \left[\frac{Wh}{kg}\right] \tag{3.21}$$

For an NMC111 cathode with 170 mAh/g together with a graphite anode that operates on an average voltage of 3.6V, this yields 250.8Wh/kg as calculated in equation 3.23 by utilizing values from figure 3.9.

$$Battery\ gravimetric\ capacity_{NMC111//Gr} = \frac{360[mAh]}{(3.1 \cdot \frac{5}{3})[g]} = 69.7 \left[\frac{mAh}{g}\right] \tag{3.22}$$

$$69.7 \left[\frac{mAh}{g}\right] \cdot 3.6[V] = 251 \left[\frac{Wh}{kg}\right] \tag{3.23}$$

And for an LFP cathode with 165 mAh/g with a graphite anode operating at an average voltage of 3.3V.

$$Battery\ gravimetric\ capacity_{LFP//Gr} = \frac{360[mAh]}{(3.2 \cdot \frac{5}{3})[g]} = 67.5 \left[\frac{mAh}{g}\right] \tag{3.24}$$

$$67.5 \left[\frac{mAh}{g}\right] \cdot 3.3[V] = 223 \left[\frac{Wh}{kg}\right] \tag{3.25}$$

However, the value from equations 3.21, 3.25, 3.23 is not always accurate as the capacity of a battery pack is impacted by several factors. The following points mention factors that contribute to the overall battery capacity.

- *"Area and the physical size of the plates in contact with the electrolyte"*[34]
- *"Weight and the amount of material in plates."*[34]
- *"Number of plates and the type of separator between them."*[34]

- *"Quantity and specific gravity of the electrolyte"*[34]
- *"The age of the battery; the older the battery the less capacity it has."*[34]
- *"Cell conditions: sulfation, sediments reduce the cell voltage."*[34]
- *"Temperature: the higher the temperature the higher the capacity"*[34]
- *"Discharge rate: the higher the discharge rate, the lower the capacity"*[34]

Adding more electrode material to a battery cell, increasing its thickness, will increase the specific energy capacity of the battery as it lowers the weight share of the other components. This process will also increase the current density on the electrodes, regardless of the C-rate. Increased current density will lead to increased internal heating, potentially risking thermal runaway in addition to accelerating battery aging. Equations 3.26 and 3.27, show how an increase in current density (j) contributes to increased irreversible voltage loss. A lower electrode thickness would contribute to higher power output from the battery as the decrease in current density lowers the voltage loss and increases the discharge/charge efficiency, see 3.29 and 3.28. Figure 3.14 shows an example of how the reversible cell potential increases, while the cell resistance decreases when a lithium ion battery is charged. [12]

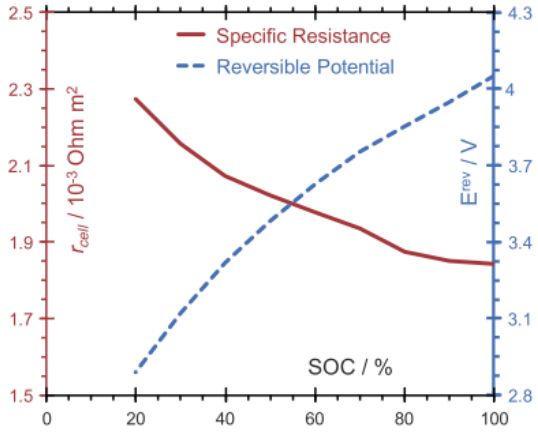

Figure 3.14: Reversible cell potential and cell resistance in relation to the state of charge (SoC) [12]

Due to the many factors deciding the battery capacity and power outputs, battery testing in labs is an important process in order to investigate and improve battery performance. The discharge rate relates closely to the operating voltage which changes continuously through a charge/discharge cycle as shown in 3.13 and 3.10.

3.3 Charging and discharging a battery

During discharging of a battery, the potential available in the cell is determined by the reversible cell potential minus the potential losses in the battery. When the battery is charging, the required voltage has to overcome the irreversible voltage losses while maintaining the reversible potential. The reversible voltage refers to the equilibrium state of the battery electrodes where it is practically fully discharged. The irreversible potential losses in a lithium ion battery are the friction loss of transferring charged Li+ through the battery regions (rj), the friction loss of component diffusion on the electrode surface $\eta_{Conc.}$, and the friction of electron transfer between

reacting compounds η_{tafel}[12]. This yields the following expressions for the obtained voltage of the cell during charging and discharging.

$$E^{Cell}_{Discharge} = E^{reversible} - rj - \eta_{tafel} - \eta_{Conc.} \tag{3.26}$$

$$E^{Cell}_{Charge} = E^{reversible} + rj + \eta_{tafel} + \eta_{Conc.} \tag{3.27}$$

The efficiency of the battery's discharge process can be determined by taking the discharge potential of the battery divided by the reversible cell potential. This is because the discharge potential accounts for the total applied voltage, while the reversible potential includes the irreversible potential losses. During charging the efficiency of the charging process is determined by the reversible cell potential divided by the applied charging voltage, as the voltage applied in the charging process has to overcome the irreversible potential losses.[12]

$$\epsilon_{discharge} = \frac{E^{Cell}_{Discharge}}{E^{Rev}} \tag{3.28}$$

$$\epsilon_{charge} = \frac{E^{Rev}}{E^{Cell}_{Charge}} \tag{3.29}$$

The rate of charging of a battery is usually referred to as the C-rate. The C-rate relates to the speed of the charging process and is calculated by the charging current in A divided by the battery capacity in mAh, or by dividing the power of the charging in W by the capacity in Wh as in equation 3.30. For example a battery with the capacity of 10kWh charged with a power of 20kW yields a C-rate of 2. Practically, this means that the charger has the required power of charging the battery from 0-100% SoC in 30 minutes.

$$C - rate = \frac{Charging\ power\ [W]}{Battery\ capacity\ [Wh]} \tag{3.30}$$

The electrical efficiency of a lithium ion battery may vary depending on several factors. This efficiency will for example decrease with temperature and with rising discharge currents as some of the energy is lost to heat and higher currents increase current density and voltage loss. Also, the battery's electrical efficiency decreases over time when the battery degrades, due to an increase in internal resistance [43]. The electrical efficiency is given as follows:

$$\epsilon_{electrical} = \frac{Useful\ power\ output}{Total\ electrical\ power\ consumed} \tag{3.31}$$

3.3.1 Megawatt Charging System (MCS)

Climate-friendly mobility has previously been limited to passenger cars as a result of limitations on battery capacity and high power charging. To satisfy the market demand of heavy duty vehicles such as buses, a charging solution for high power charging to reduce charging time is essential.

In 2018 a charging interface initiative, CharIN, was formed by industry actors to "define a new commercial vehicle high power charging standard to maximize customer flexibility."[14]. After the CharIN board approved a set of requirements for the charging plug and socket in 2018 the five companies, Tesla, Electrify America, ABB, paXos, and Stäubli submitted candidate designs. In 2019 a design of charging plug and socket was selected for High Power Charging for Commercial Vehicles, HPCCV, later known as MCS. Version 1.0 HPCCV connector had a triangular shape and round power pins but required development to further improve the design. In 2020 several vehicle inlets and connectors went through a series of tests conducted by the US National Renewable Energy Laboratory, NREL. The results led to version 3.2 of the MCS which is shaped triangular with the addition of larger pins and longer protective sheaths as safety measures. Prototype connectors were tested at power up to 3.75 megawatts in August 2021, and in December the MCS version 3.2 was endorsed. The aim for CharIN is to have the specification document completed by 2024 so that it is ready to be included by ISO and IEC as a global standard.

3.3.2 MCS Specifications

The connector consists of 7 pins, where two are primary power pins, DC, as illustrated in figure 3.15. The four pins surrounded by a white area are the communications and detection pins and the last pin, PE, is the protective earth pin. One connector can deliver a maximum of 3000 amperes and 1250 volts which is equal to 3.75 megawatts as mentioned above.

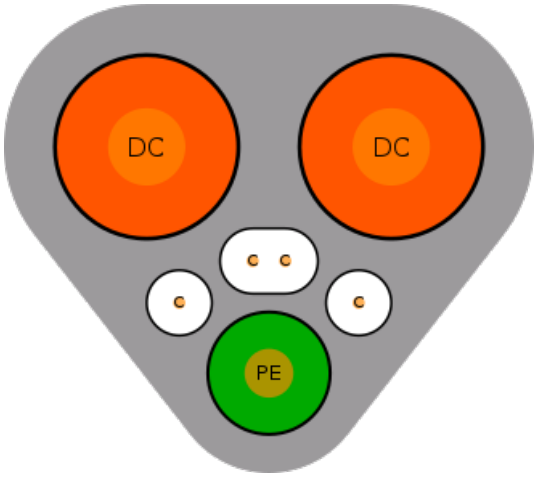

Figure 3.15: The MCS charging output [29]

Today's chargers are able to deliver power in the range of a few hundred kW. Due to the increased power required for MCS integration the energy supply to charging stations requires an upgrade. Electrical interconnections to the distribution systems for MCS through a direct voltage AC connection could benefit the power demand. Two alternatives for MCS, one, include AC system with series connected AC/DC and DC/DC converters or, two, DC system with DC/DC converters tied to a front-end AC/DC converter. The most beneficial alternative is the second option as it supports integration of resources like photovoltaics (PV) and energy storage (ES) systems. To optimize the charging station, a reduction of load swings could be achieved by a constant power pull from the electric grid. This is a possibility with the implementation of PV's and ES that may decrease potential impacts on the grid.

4 Life Cycle Analysis of Battery Chemistries

Electric vehicles charged with the use of renewable energy have no tailpipe emissions, however the production, transportation and disposal of the batteries inflicts environmental burdens. To present these impacts and compare the differences in emissions of NMC, NCA and LFP batteries, a life cycle analysis (LCA), has been conducted by the use of the SimaPro software. An LCA is used to evaluate the environmental impact of a product encompassing extraction and processing of the raw materials in addition to manufacturing, distribution, use, possible recycling, and final disposal.

There is two main methods of impact assessment. The first is the cradle to grave method, which includes the whole life span of a product as mentioned above. The other alternative is a cradle to gate method, which includes only the part of the life cycle up until the product leaves the factory.

4.1 System boundaries

This LCA study is a cradle to gate assessment of a single battery cell of each battery type and not a complete battery. A battery pack can be divided into four main components which is illustrated in fig 4.1. The other three components not considered in the LCA, is assumed to have an equal impact in combination with all of the battery cells. They are therefore neglected in the LCA to further differentiate the battery types. All three of the battery cells have an energy capacity of 0.168 kWh and so the functional unit is a battery cell with a capacity of 0.168 kWh. The purpose of the LCA is to identify the emissions of the different battery cells to further compare the different battery chemistries besides performance and cost.

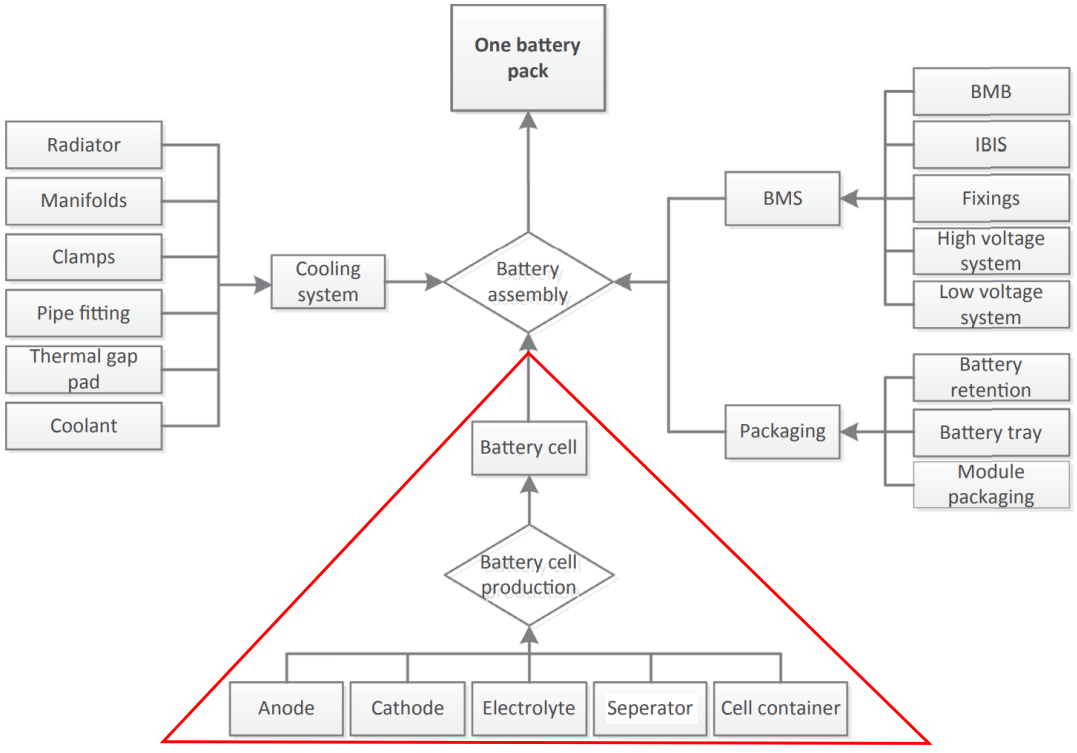

Figure 4.1: Composition of a battery, where the red triangle limits the chosen system boundary. BMS = battery management system; BMB = battery management board; IBIS = Integrated Battery Interface System. [22]

4.2 Life cycle inventory

An inventory list is required to perform an LCA. The weight distribution of the considered battery cell is presented in table 4.1. For the production of the battery cell an energy of 13 kWh is necessary per kg of produced battery.

	NMC (111)	NCA	LFP
Active cathode material	34.7%	35.3%	32.7%
Graphite (anode material)	19.4%	22.1%	16.8%
Carbon black	2.3%	2.1%	2.2%
Polyvinylidene Fluoride (binder)	3.0%	2.9%	2.7%
Copper	15.7%	16.7%	13.9%
Aluminum	8.2%	8.6%	7.5%
LiPF6 (Electrolyte)	2.2%	2.3%	3.4%
Ethylene carbonate (Electrolyte)	6.2%	6.3%	9.4%
Dimethyl carbonate (Electrolyte)	6.2%	6.3%	9.4%
Polypropylene (Plastic)	1.5%	1.6%	1.3%
Polyethylene (Plastic)	0.3%	0.4%	0.3%
Polyethylene terpephthalate (Plastic)	0.3%	0.3%	0.3%
Cell mass	0.856 kg	0.750 kg	1.054 kg
Energy	11.128 kWh	9.75 kWh	13.702 kWh

Table 4.1: The materials and energy required for one battery cell equivalent to 0.168 kWh of capacity. [16]

The materials are all available in the Ecoinvent 3 database on the SimaPro software, except the cathode material for the LFP battery. In order to acquire the necessary data to perform the LCA of a LFP battery cell, a new process was made for the LFP cathode in SimaPro.

4.2.1 Production of Lithium-iron-phosphate

The active cathode material for an LFP//Gr battery cell is lithium iron phosphate, $LiFePO_4$. $LiCO_3$, lithium carbonate is utilized in the production of $LiFePO_4$. Following a molar calculation, equation 4.1 shows the required materials to produce the LFP cathode material.

$$73.8[g]Li_2CO_3 + 159.6[g]Fe_2O_3 + 133[g](NH_4)_2HPO_4 \rightarrow 158[g]LiFePO_4 \tag{4.1}$$

Lithium carbonate, ferric oxide and diammonium phosphate are all found in the Ecoinvent 3 database. In addition, 2% graphite is used in the manufacturing process. The process requires energy for two temperature increases. Firstly, an increase up to 500 °Celsius, where the grinded graphite is added. Secondly a temperature rise to 800 °Celsius. If a heat capacity of 0.9 $\frac{kJ}{kg*K}$ is assumed, then the two temperature increases have an energy demand of $0.9*400+0.9*800 = 1080\frac{J}{g}$. Furthermore there is a small energy demand by the reaction while heat losses has to be accounted for. Therefore a total of 3kJ of electricity per gram $LiFePO_4$ is utilized in SimaPro. [46]

4.3 Life Cycle Impact Assessment

In this section the results of the LCA's is presented for each battery cell type. The impact categories of focus is abiotic depletion (fossil fuels), which represents the energy of non-renewable

resources, and global warming potential(GWP100a) which represents the gradient increase in global temperature, measured in kg CO_2.

4.3.1 Results of LFP

In figure 4.2 the CO_2 emissions is presented as 22.5kg CO_2eq, along with the network of the LFP battery cell. All the impact categories in the baseline method is presented in Appendix C, along with the distribution of the different processes in each category. The biggest part of the CO_2 emissions is the production energy given as electricity.

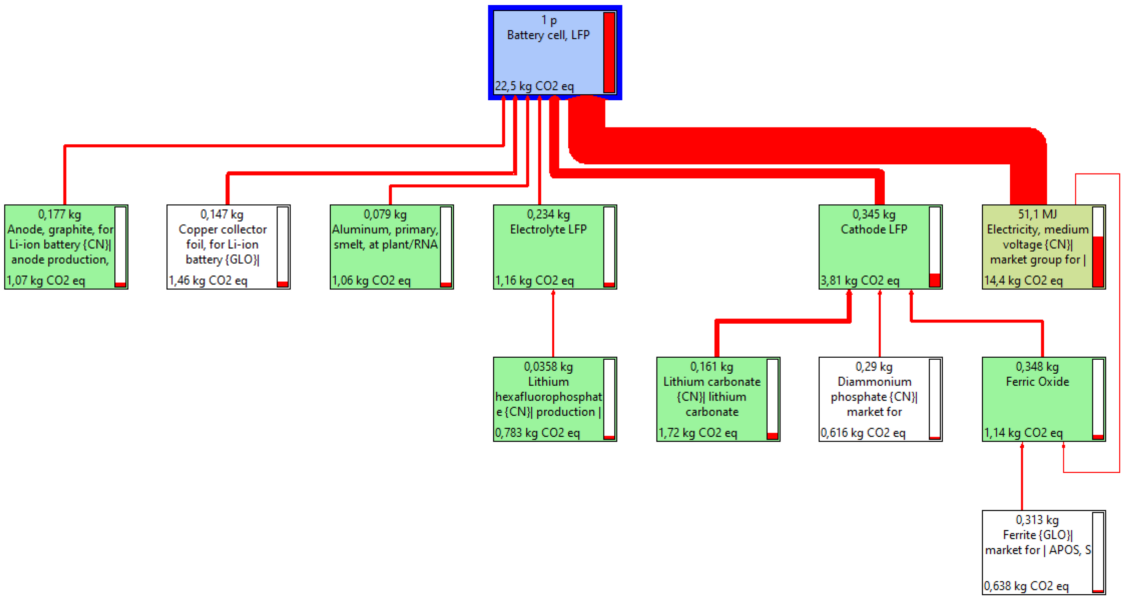

Figure 4.2: The network of one LFP cell.

4.3.2 Results of NMC(111)

The results for the NMC(111) calculations is presented in the same manner, with a total emission of 23.8kgCO_2eq per cell and with the electricity still being the biggest factor as shown in figure 4.3.

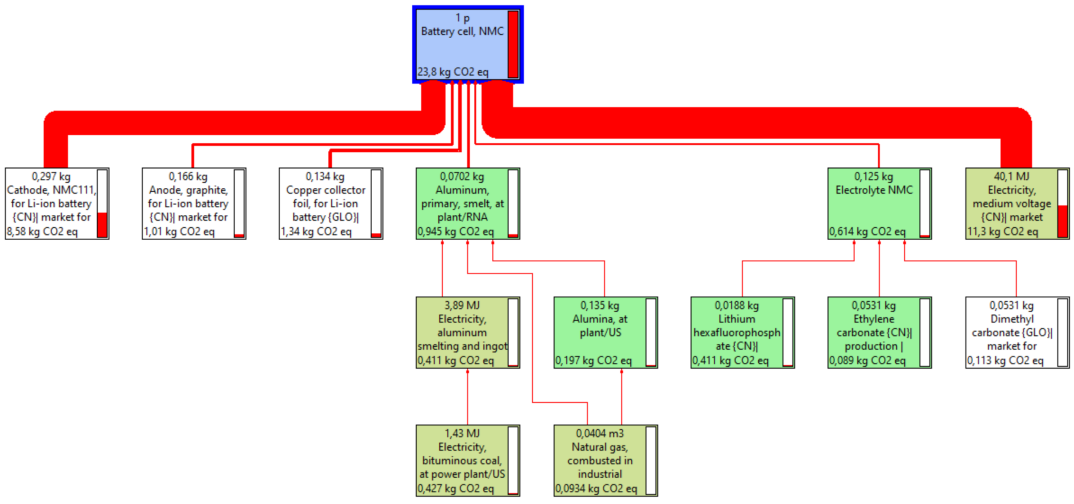

Figure 4.3: The network of one NMC(111) cell.

4.3.3 Results of NCA

The results of the calculations for the NCA battery shows a reduction in emissions compared to the LFP//Gr and NMC111//Gr with a total emission of 20.3kgCO_2eq per cell. Similarly to the LFP and NMC, the biggest part of the emissions is due to the utilized electricity as shown in figure 4.4.

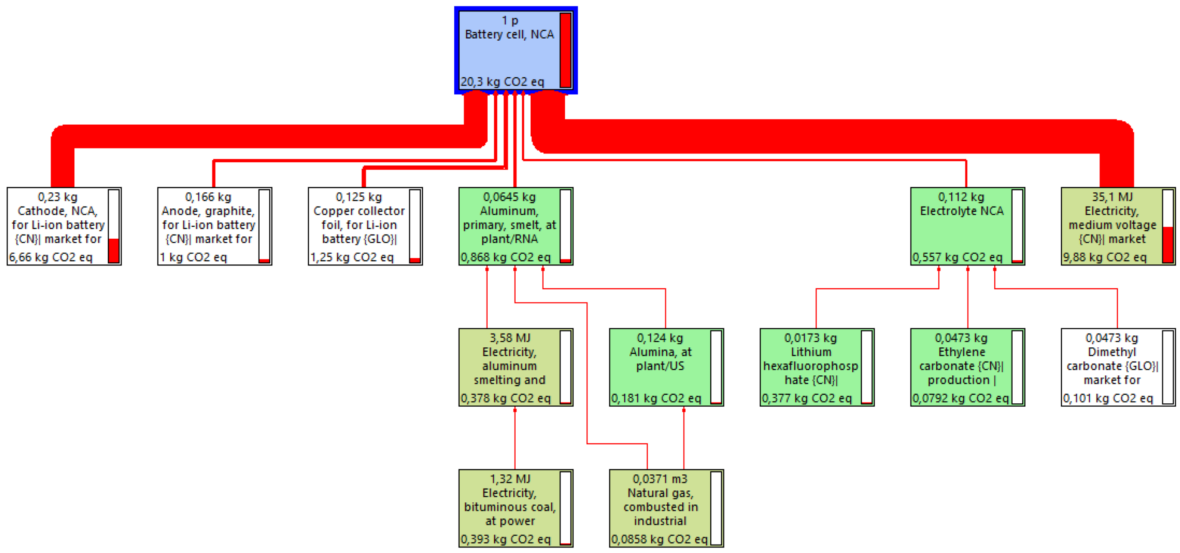

Figure 4.4: The network of one NCA cell.

In table 4.2 the impact categories of focus, GWP100a and abiotic depletion, is presented in combination with all of the battery cells. The total impact is compared in addition to comparing the electricity, anode and cathode impacts.

		Global Warming (GWP100a)	Abiotic depletion (fossil fuels)
	Unit	kg CO_2	MJ
Total	LFP	22.5	228
	NMC(111)	23.8	263
	NCA	20.3	223
Electricity	LFP	13.9	124
	NMC(111)	11.3	100
	NCA	9.88	88
Anode	LFP	1.07	19.3
	NMC(111)	1.01	18.1
	NCA	1	18.1
Cathode	LFP	3.81	38.4
	NMC(111)	8.58	1.08
	NCA	6.66	83.9

Table 4.2: GWP and AD values of all the battery cell types with the contribution of electricity, anodes and cathodes.

4.4 Interpretation

By analyzing the production of three different battery cells this LCA has revealed that the differences in emissions are mainly because of the cathodes and the energy demand of the manufacturing processes. The LFP cathode cause an emission of 3.81kg of carbon dioxide equivalents, while the NCA and the NMC emits 6.66kg and 8.58kg respectively. The reason for the increased emissions from the NCA and the NMC is because of the utilized cobalt. Cobalt extraction has a bigger impact on the environment compared to the other materials used in cathodes[23]. The electricity demand of the manufacturing is dependent on the weight of the cell. Therefore the LFP cell requires more energy as it is less energy dense, as shown in 3.10, than both the NMC(111) and NCA battery cells. The other processes are approximately the same when it comes to the CO_2 equivalent emissions.

From the tables above the reduction of fossil fuels is measured in MJ for each battery cell type. They all require between 220-270MJ of fossil fuels per battery cell manufactured, which includes the whole life cycle aspect with material extraction, transportation and manufacturing. This is mainly because the production is based in China. Today, 78% of the EV batteries produced are manufactured in China [28]. Therefore it is assumed that the batteries are produced with electricity from a Chinese power mix. China is still heavily dependent on coal contrary to many western countries [19]. In figure 4.5 the difference between a fossil fuel dependent power mix and a renewable power mix is presented in the production part of the graph. If the battery production were moved to for example Norway instead of China, the CO_2 emissions from the energy would be approximately cut in half. The negative side of moving the production is the increased costs as China is considered the cheapest option.

Based on the results from the LCA's the battery cells are fairly equal when it comes to emissions, but the NCA battery cell has a slight advantage over the other two as its total CO_2 emission is about three kilograms less per cell. Ideally, the production should be based on renewable energy, but as economic profit is important for the lithium ion battery manufacturers, this is prioritized over environmental impact in today's market.

A possible source of error in this LCA could be the production process of the LFP cathode. The steps are presented above, but there may be a difference in the theoretical numbers and the actual production process. Nonetheless, the process is evaluated as realistic as the LFP cathode emissions is better than the other two cathodes, as expected due to the absence of cobalt. [23]

4.5 CO_2 equivalent emissions of EVs vs. fossil fuelled vehicles

In addition to the environmental impact of battery production, there is also an environmental footprint from the production of the electricity used to charge the batteries. In the report *The size and range effect: lifecycle greenhouse gas emissions of electric vehicles* [21], the CO_2-equivalent emissions in tons have been evaluated for different electric car sizes through their lifetime. A-segment refers to mini-EVs, C-segment refers to medium EVs, D-segment includes large EVs and F-segment includes large luxury electric cars. In figure 4.5a and 4.5b the gray area refers to the CO_2 equivalent emissions from petroleum driven cars of the four segments (A, C, D and F), where the total CO_2 equivalent emissions ranges from 27-48 tons at the end of life when the car is scrapped. This report has been done with respect to electric cars, but the results are relevant for all electric driving vehicles including buses and heavy transport, as it compares fossil fuelled vehicles with electric vehicles.

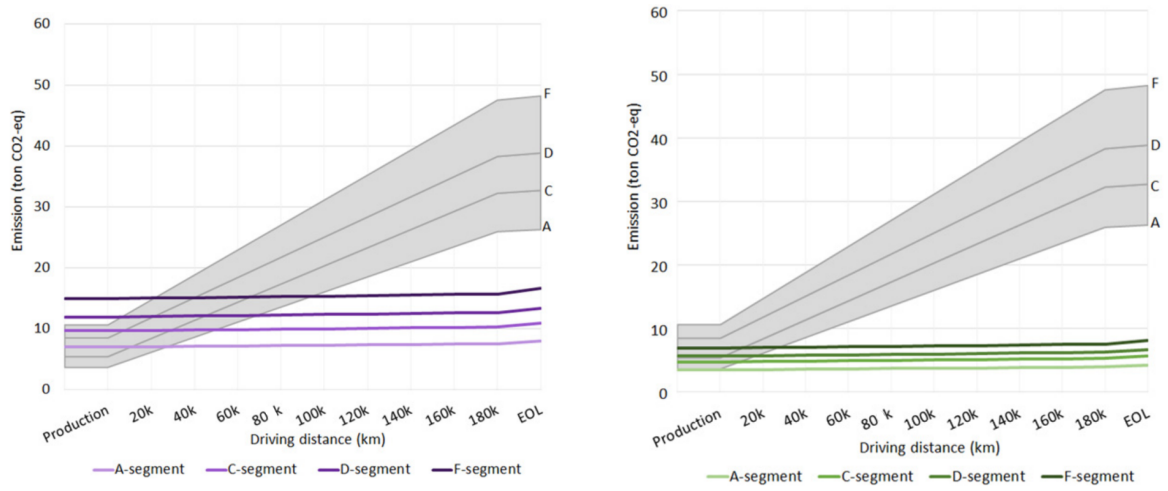

Figure 4.5: Life time CO_2-equivalent emissions [tons] of electric cars with fossil fuelled production (a), wind powered production (b), and wind powered charging (a, b) [21]

Figure 4.5a shows the emissions of the electric car segments where the production has been powered by fossil fuels which is common in Chinese factories, but during its lifetime the battery has been charged by renewable wind power. It can be seen that the environmental impact of vehicle production is higher for electric cars compared to fossil fuelled vehicles. However, the A-segment mini electric and the C-segment small electric cars have a lower total emission overall after it has driven about 30 000km. The D-segment and F-segment electric cars obtain a lower overall emission after about 23 000km range driven. Assuming that the electric cars have a driving range of 180 000km before being scrapped, all the electric cars have less than half of the total emissions compared to the fossil fuel alternatives. The graph 4.5a is a good indication of the emissions related to electric cars in Norway today. The batteries in today's electric cars usually originate from manufacturers that utilize fossil energy sources in their factories in China, while the energy used to charge cars in Norway originates mostly from wind and hydro.

Figure 4.5b shows a situation where the production process is also driven completely by renewable wind energy. This lowers the emissions related to the production of electric cars by a lot, and therefore also the lifetime emissions. The production emissions of the vehicles are lowered by about 50% for all the investigated car sizes. Producing lithium ion batteries by utilizing renewable energy, for then to charge the batteries with renewable energy would be the ideal situation in a future with green lithium ion batteries.

Figure 4.5b could be the situation if the production of the batteries and electric vehicles were moved to Norway and powered by renewable energy. This would accelerate sustainable development even further, but would also increase the production cost and the energy demand in Norway. However, Norway has over time experienced excess power and cheap electricity, especially in the northern parts of the country. This has inspired companies such as Freyr to develop battery factories producing green lithium ion batteries from renewable energy. [17]

5 Methods

The methods part of the report will give insight into the performed calculations regarding the energy consumption and the battery.

5.1 Energy calculation assumptions and limitations

When calculating the energy consumption of an EV there are a lot of assumptions and limitations that affect the overall result, but in order for the calculations to be reliable these have to be addressed.

The energy calculations are limited by the average data between stops in appendix A. This means that no real-time data from the route is available such as acceleration and de-acceleration numbers, and the number of unplanned stops the bus encounters in a day. This means that it is hard to accurately calculate the acceleration and de-acceleration forces and therefore it is not included in the energy calculations. An average speed between each stop has been used in the calculations provided by AtB and is listed in appendix A. Extending the velocity array so that it covers the entire route is possible as the Excel file in appendix A has listed total meters pr stop.

Another assumption is that every passenger weighs 80 kg. This is the assumption made as the average weight of a person.

There are two cases that will be investigated and presented, one base case representing a regular day for the M1, and a worst case designed to represent the highest capacity the battery of the bus will need.

5.2 Energy calculation methods

Appendix B shows the MATLAB script used to calculate the energy consumption of the M1. By using the elevation profile found at *høydedata.no*[25], it is possible to calculate the slope angle at any given point in the route. For every 10m of the route the MATLAB script checks if the next 10m are higher or lower than the measuring point by subtracting the height at the measuring point from the height at 10m ahead. By that point, a right triangle is formed with 10m and the height difference as the adjacent and opposite. The slope angle is then given by equation 5.1.

$$\Theta^\circ = tan^{-1}(\frac{opposite}{adjacent}) \tag{5.1}$$

When the slope angle is derived the rest of the variables can be put into equations (3.5)–(3.6) as shown in appendix B. The velocity vector has been inserted into the script from appendix A. The rest of the values has been found from research.

5.3 Battery calculation assumptions

In the following results regarding the battery calculations, some assumptions have been made in relation to the specifications of the battery pack for the M1.

The electrical efficiency 3.31 of the battery has been assumed to be 100%, which includes both charge and discharge efficiency. [43]

Table 5.1 is assumed to be the practical capacities of the different considered lithium ion battery chemistries [3]. These values are typical in commercial cells even though technological innovations are frequent in the lithium ion battery industry.

There are differences between a battery pack and a battery system, where the system weight among many factors includes cooling systems, safety systems, and a possible reinforced framework for the battery pack. This thesis bases its calculations on the battery pack and neglects the other parts of the battery system as a simplification.

Battery chemistry	Practical specific energy [Wh/kg]	Practical energy density [Wh/L]
NMC // Graphite	210	530
NCA // Graphite	265	690
LFP // Graphite	126	325

Table 5.1: Typical practical specific energy and energy density for the evaluated electrode chemistries

When deciding the required capacity for the bus' battery package, the calculated energy consumption has been set as the required end of life capacity. Therefore, due to an assumed degradation rate of 20% over 10 years, where 10 years is the required battery life time, the energy consumption is divided by 0.8 in order to account for the degradation and the end of life capacity. [12]

Lithium ion batteries should also be operated in the range of 20%-90% state of charge (SoC) [12]. This means that the battery should not be charged beyond 90% or discharged beyond 20% in order to maintain the battery performance in the best way possible. Due to this preferred SoC of operation, the battery package should only operate within 70% of its maximum energy storage capacity. Because of this, the calculated energy demand for the bus will also be divided by 0.7 to account for the SoC limitation.

$$Battery\ capacity = \frac{Calculated\ energy\ consumption}{0.7 \cdot 0.8} \tag{5.2}$$

According to Trondheim municipality [20], today's electrical buses are dimensioned for 5 hour drive time in order to prevent delays if charging issues occur. In the case of this report regarding the M1 bus, the battery pack has been dimensioned to be able to drive the round trip (Ranheim to Østre lund + Østre lund to ranheim) 3 times without charging. This corresponds to about 5.25 hours of drive time given that the round trip takes 1 hour and 45 minutes.

5.4 Battery calculation methods

Overall the assumptions 5.3 yield the following equations for calculating the battery's required capacity, weight, and volume:

$$Battery\ capacity\ [kWh] = \frac{Calculated\ energy\ consumption\ of\ a\ round\ trip[kWh] \cdot 3}{0.7 \cdot 0.8} \tag{5.3}$$

$$Battery\ weight\ [kg] = \frac{Battery\ capacity[kWh]}{Practical\ specific\ energy[\frac{kWh}{kg}]} \tag{5.4}$$

$$Battery\ volume\ [L] = \frac{Battery\ capacity[kWh]}{Practical\ energy\ density[\frac{kWh}{L}]} \tag{5.5}$$

When calculating the weight and capacity of the necessary battery package, the fact that the battery weight affects energy consumption has to be taken into account. The implementation of a battery increases the overall weight of the bus, further increasing the need for battery capacity. The battery weight calculation has therefore been done in 4-6 steps, as shown in figures 6.8a, 6.8b, 6.8c, in order to obtain a value at which the need for battery capacity no longer increases compared to the weight of the added battery. In step 1, the required battery weight to power a fully loaded M1 bus has been determined based on the calculated worst-case energy consumption listed in table 6.2. In step 2 the weight of the battery pack determined in step 1 is added to the weight of the fully loaded bus, yielding an increased energy consumption, and an increased battery capacity demand. The process has been repeated until the required battery weight and capacity no longer increases due to a minimal increase in energy consumption, as shown in table 6.7.

For the NMC111 and NCA cathode chemistries, this required 4 calculation steps without scale-up. The LFP cathode calculation required 5 steps due to the low specific energy yielding a high required battery weight heavily impacting the energy consumption.

When deciding the capacity and weight of the battery, given the scaled up energy consumption, the NMC111 and NCA cathode chemistries required 5 calculation steps before the energy consumption increase yielded close to 0 as shown in figures 6.10a, 6.10b and 6.10c. The LFP cathode battery required a 6-step calculation after the energy consumption was scaled up by the determined factor of 1.27 from table 6.2.1.

An aspect of the feasibility study is the finances of the studied batteries. The price of lithium-ion cells has been reduced by as much as 85% from 2010-2019 [35]. An unpublished article made by PhD associates at NTNU presents a bottom-up model of lithium-ion production costs from 2010 to 2030 in order to accurately predict the prices of different Li-ion batteries[35].

The price of the battery pack has been determined by multiplying the price for each battery chemistry per kWh by the scaled up battery capacity:

$$Price_{Battery} = Price\ \left[\frac{USD}{kWh}\right] \cdot Scaled\ up\ battery\ capacity\ [kWh] \tag{5.6}$$

The battery's C-rate has been determined by dividing the charging power by the total battery capacity 3.30. Given a charging power of 1MW this yields the following equation for the C-rate.

$$C - Rate_{battery} = \frac{1000\ [kW]}{Battery\ capacity\ [kWh]} \tag{5.7}$$

Regarding table 6.5, the determined values for the required charging power is utilized in equation 5.7 as the charging power.

6 Results

In this section the results of the energy consumption calculations and subsequently the needed size and capacity of the batteries are presented.

6.1 Energy consumption

By using the equations in 3.1, the size and maximum power of the battery can be determined. This chapter will introduce two cases of energy consumption of the M1 bus, a worst case scenario and a base case scenario, in order to accurately present the results. Due to the inconsistency of the variables facing a moving vehicle, a comprehensive sensitivity analysis of all affectable variables will also be included in this chapter. For this study, it is intended that there will be a charging station at each of the end stations. It is therefore not only relevant to look at the round trip values but also the end station to end station energy consumption.

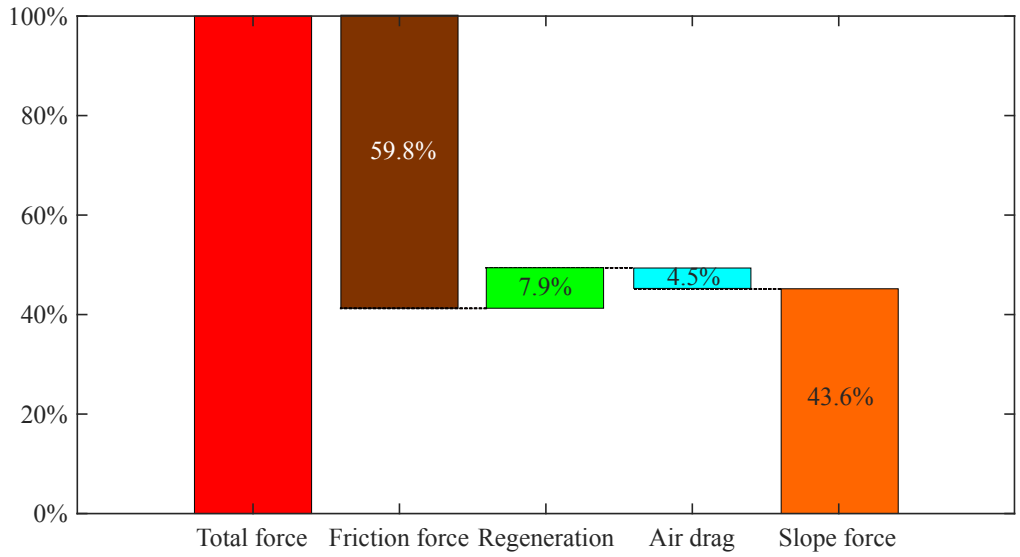

Figure 6.1: Bar chart showing all the forces and how much each force contributes to the total amount.

Figure 6.1 shows the impact of the different forces and how much of the total amount each force is responsible for. The regenerative contributes positively as it provides energy back to the battery.

6.1.1 Base case

For the base case study, variables have been selected regarding a normal sunny day in Trondheim, with dry asphalt and no particular winds. There is assumed no interior heating and no battery heating. The numerical values given in this base case are either given by AtB or found as measured values.

- Rolling resistance coefficient: 0.01 [10]
- Front area: 8.5 m^2
- ERS: 0.5 efficiency

- Weight: 0, 50, 100, and 159 passengers weighing 80kg each
- Drag coefficient: 0.633 [18]
- Velocity is set to measured values
- No heating

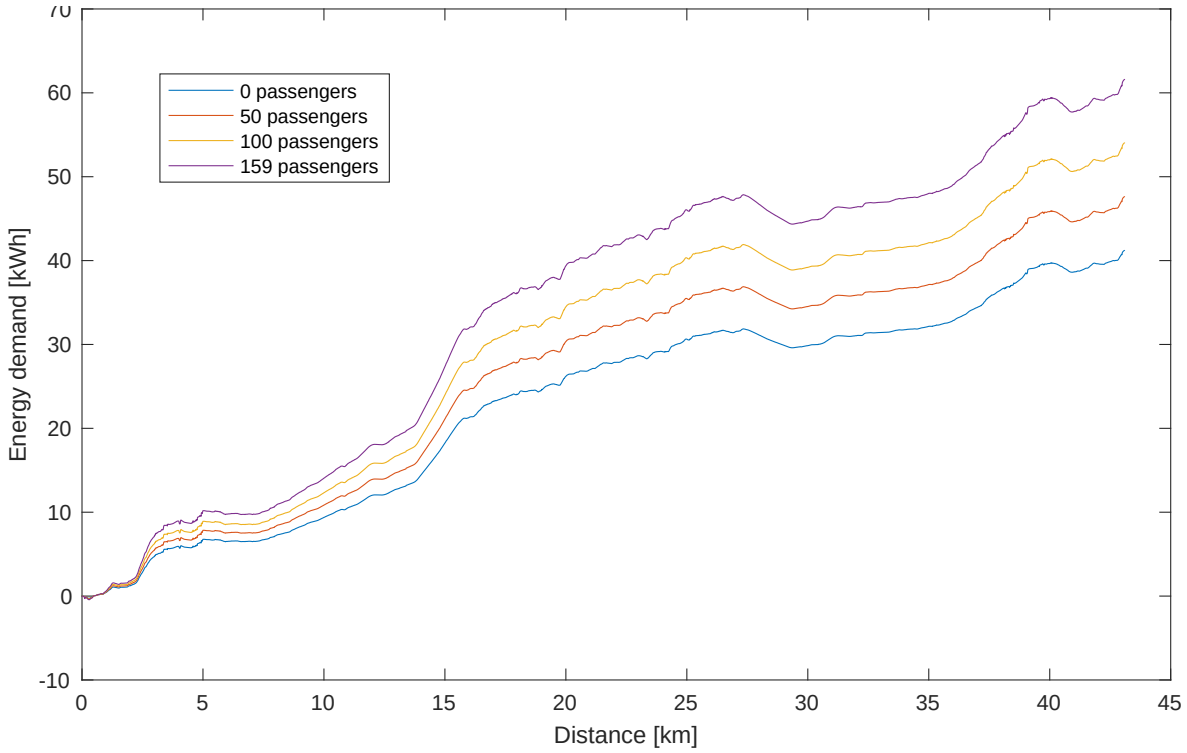

Figure 6.2: Energy consumption for M1 base case.

A more in-depth display of the round trip is presented in figure 6.3.

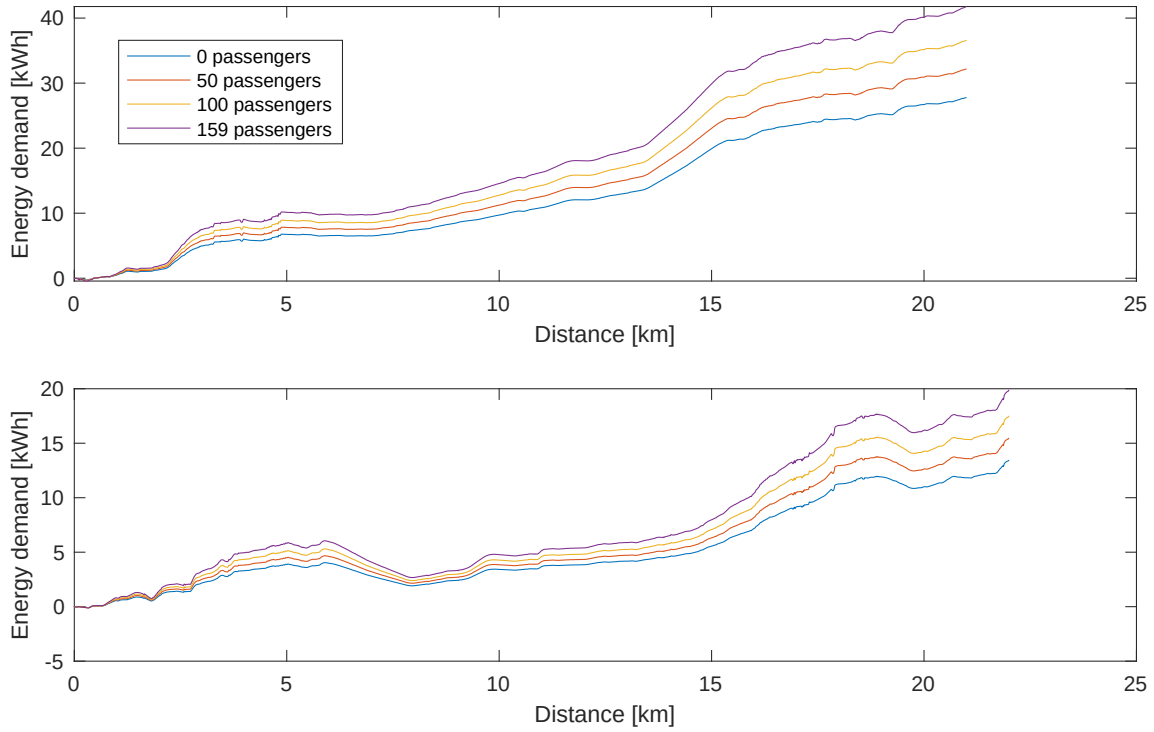

Figure 6.3: Energy consumption for M1 base case for Ranheim-Østre Lund (above) and Østre Lund-Ranheim (beneath).

Figure 6.2 presents the results for the base case energy consumption for a round trip (Ranheim - Østre Lund - Ranheim).

These results represent the base case study for the energy consumption of the M1. As shown, the values will vary with passenger load. However, it gives an accurate representation of the energy consumption on any given day.

6.1.2 Worst case

For the worst case study, the calculation variables have been altered to accumulate an energy demand corresponding to a day with rough weather and challenging road conditions. In addition, the front area is increased to adjust for the possibility that the front area is designed larger than today's buses. The energy recovery system is the same, as it is considered a constant. The variables utilized in this scenario are listed below:

- Rolling resistance coefficient: 0.015
- Front area: 10 m^2
- 50% RBS
- A load of 0, 50, 100, and 159 passengers with a weight of 80kg per passenger
- Drag coefficient: 0.7
- Velocity is set to 40 % higher than measured values
- Maximum heating, equivalent to two 11kW heat pumps with COP 2

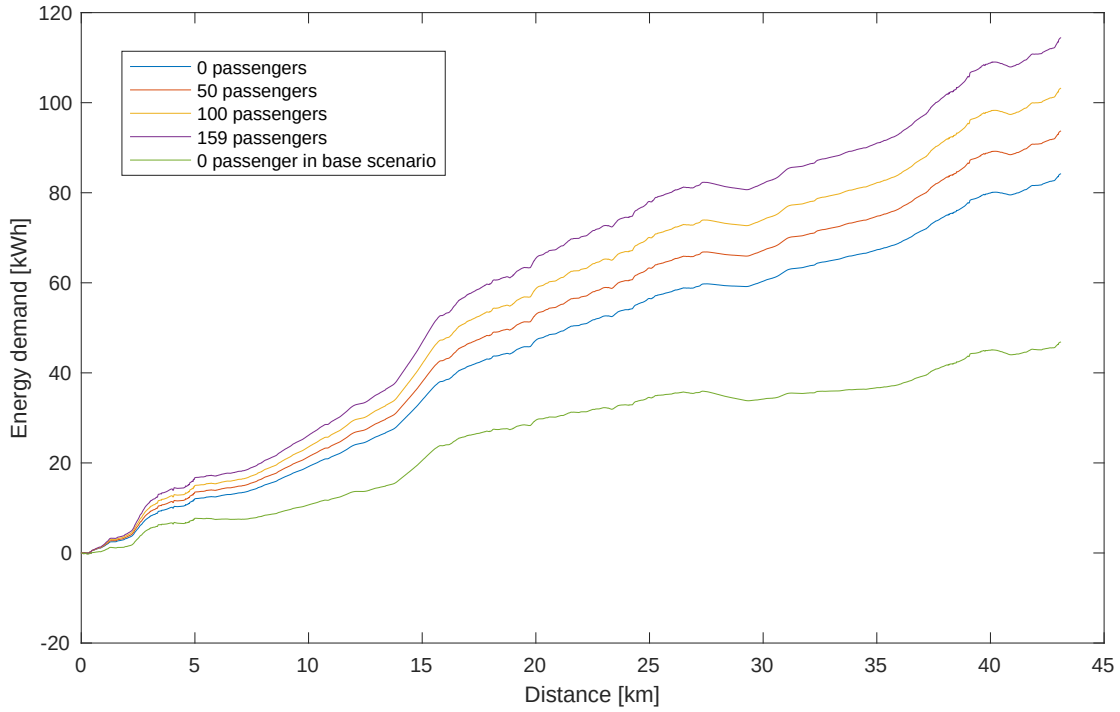

Figure 6.4: Energy consumption for M1 worst case.

A more in-depth display of the round trip is presented in figure 6.5.

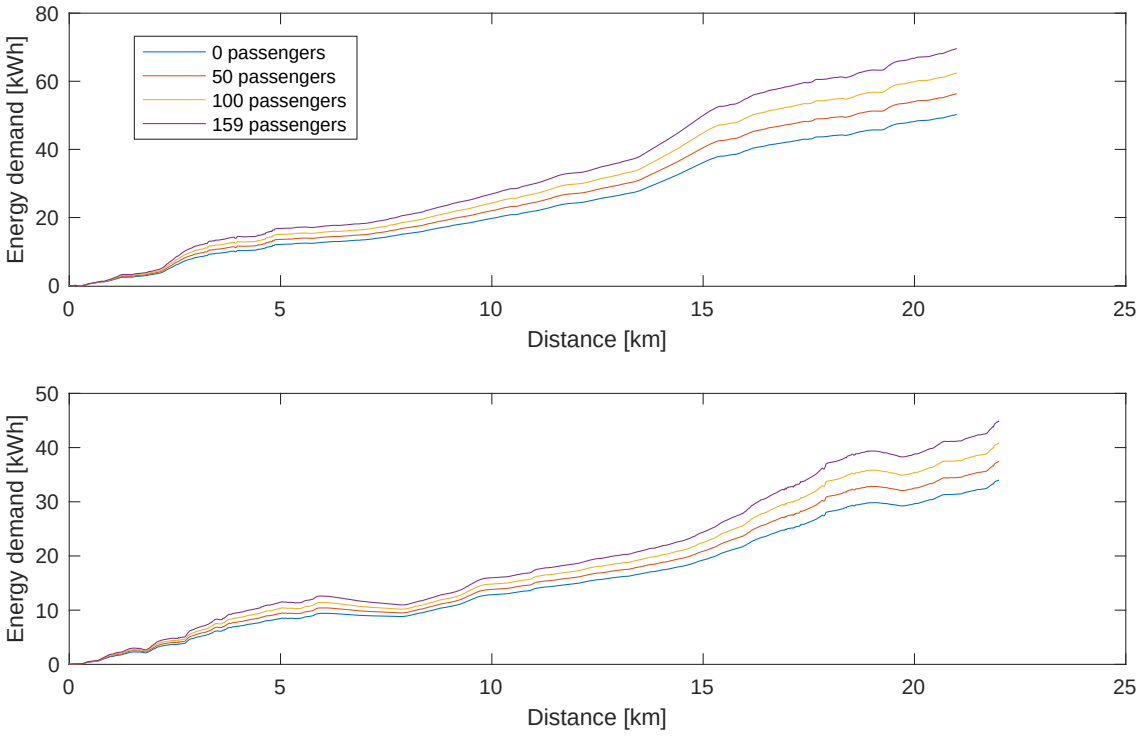

Figure 6.5: Energy consumption for M1 worst case shown for both ways. Ranheim-Østre Lund (above) and Østre Lund-Ranheim (Beneath)

A worst case study is used to obtain values for the worst possible scenario which can be realistic in specific conditions. In 6.4 the accumulated energy demand is presented for four different loads. At the greatest load, the M1 bus would consume 95 kWh on the 43 km long route in the worst possible conditions. This is an increase of about 30% in comparison to the base scenario shown in 6.2.

6.2 Sensitivity analysis

There are variables in the energy consumption calculations which may vary, and who is easily affected by uncontrollable factors such as ambient temperature, winds, surface conditions and loads. In order to be able to present a credible result it is important to look at how much these variables affect the overall energy consumption.

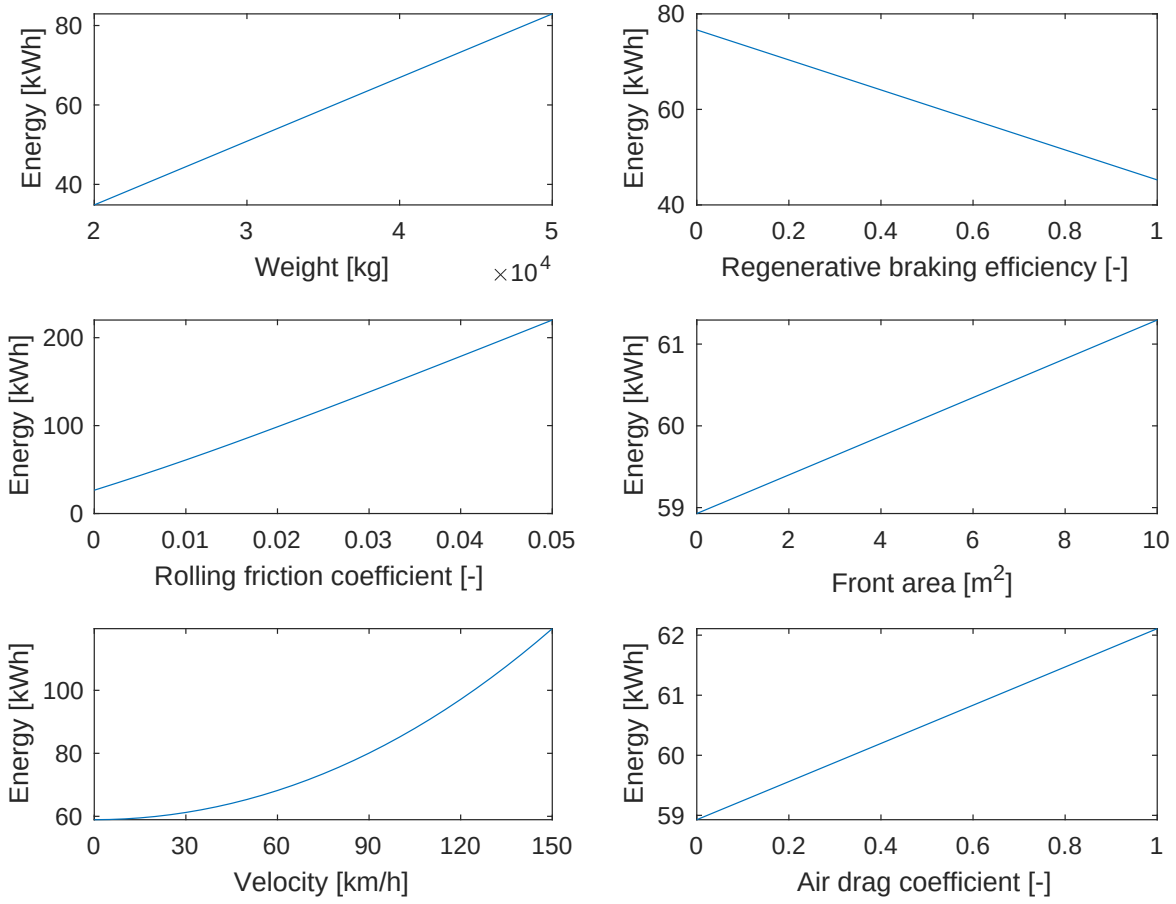

Figure 6.6: Sensitivity analysis.

From the plots shown in figure 6.6, a table of all variable and the difference between their minimum and maximum values can be presented.

	Unit	Utilized value	Sensitivity range	Min energy consumption	Max energy consumption	Variance
Air drag coefficient	[-]	0.633	[0 - 1]	58.9276 kWh	62.1082 kWh	3.1806 kWh
Front area	mˆ2	8.5	[0 - 17]	58.9276 kWh	62.9581 kWh	4.0305 kWh
Weight	kg	36720	[20000-50000]	40.4428 kWh	82.9322 kWh	42.4894 kWh
Regenerative braking efficiency	[-]	0.5	[0 - 1]	45.2357 kWh	76.6412 kWh	31.4055 kWh
Rolling friction coefficient	[-]	0.01	[0 - 0.02]	26.5265 kWh	98.6305 kWh	72.104 kWh
Mean velocity	km/h	28.06	[0 - 60]	58.9276 kWh	68.2011 kWh	9.2735 kWh

Table 6.1: Comprehensive sensitivity analysis.

Figure 6.6 and table 6.1 shows how the different calculation variables impact the overall energy consumption. Both the rolling friction coefficient and the passenger load heavily affect the calculated energy consumption. The weight is effected by the number of passengers and will mostly vary by the time of day where it will be higher during rush hours. Figure 3.3 shows the factors affecting the rolling resistance coefficient.

6.2.1 Energy consumption comparison

The total energy consumption for both the base case and the worst case scenario is presented in table 6.2.

	Load	Total	Ranheim-Østre lund	Østre lund-Ranheim	Specific
Base Case	0%	46.91 kWh	31.25 kWh	15.66 kWh	1.09 kWh/km
	50%	58.63 kWh	39.17 kWh	19.46 kWh	1.36 kWh/km
	100%	70.20 kWh	46.98 kWh	23.22 kWh	1.63 kWh/km
Worst Case	0%	84.26 kWh	50.23 kWh	34.03 kWh	1.95 kWh/km
	50%	99.48 kWh	59.97 kWh	39.51 kWh	2.31 kWh/km
	100%	114.51 kWh	69.59 kWh	44.92 kWh	2.66 kWh/km

Table 6.2: Calculated energy consumption of the M1 presented with base case and worst case.

Section 2.1 describes the measured energy consumption of the M1 today by comparing the diesel consumption and looking at the energy density of diesel. The calculated energy consumption done in section 3.1 for the M1 is considerably less than the measured consumption of diesel.

	Engine efficiency	Passenger load	Specific energy consumption	$\frac{mech}{el}$
Diesel base case	35%	0%	1.98 kWh/km	
Diesel worst case	35%	0%	2.47kWh/km	
Electric base case	90%	0%	1.09kWh/km	1.81
Electric worst care	90%	0%	1.95kWh/km	1.27

Table 6.3: Measured energy consumption and calculated energy consumption.

By dividing the measured energy consumption by the calculated energy consumption the ratio or scaling number can be derived as shown in table 6.3. It is also possible to look at how much the base case calculated energy consumption has to be scaled up in order to match the worst case measured energy consumption. This is relevant when a worst case energy consumption calculation is made. This scaling factor becomes 1.27.

6.3 Battery calculations

This part of the report will include the results from the calculations regarding the evaluated M1-battery, and battery charging solutions.

6.3.1 Battery capacity, weight and volume results

The following table 6.7 includes the results regarding the weight of the bus, the battery weight, and the energy consumption increase originating from the extra weight applied by the battery. The final step for each battery chemistry yields the final result of the required battery weight and the overall weight of the bus.

Battery weight evaluation with respect to energy consumption increase from the battery					
	step 1	step 2	step 3	step 4	step 5
Total weight bus including battery [kg]	36720	39641	39820	39831	
Necessary weight of NMC // Gr battery [kg]	2921	3100	3111	3111	
Energy consumption increase per step [kWh]	0	6,921	0,426	0,026	
Total weight bus including battery [kg]	36720	39035	39147	39153	
Necessary weight of NCA // Gr battery [kg]	2315	2427	2433	2433	
Energy consumption increase per step [kWh]	0	5,480	0,266	0,014	
Total weight of bus including battery [kg]	36720	41589	42084	42134	42139
Necessary weight of LFP // Gr battery [kg]	4869	5364	5414	5419	5419
Energy consumption increase per step [kWh]	0	11,553	1,177	0,119	0,012

Figure 6.7: Calculation results from battery weight and energy consumption investigation without scale up

The diagrams 6.8a, 6.8b and 6.8c shows the calculation steps for the NMC111, NCA and LFP electrode chemistries, while including the overall weight of the M1 and the weight of the battery pack.

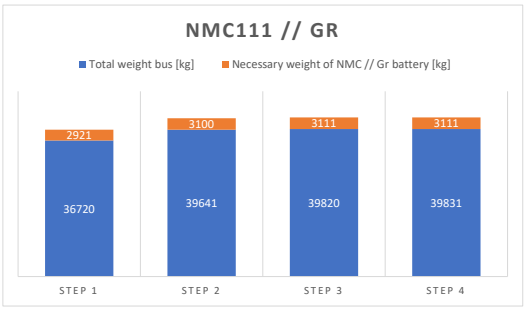

(a) NMC battery and vehicle weight.

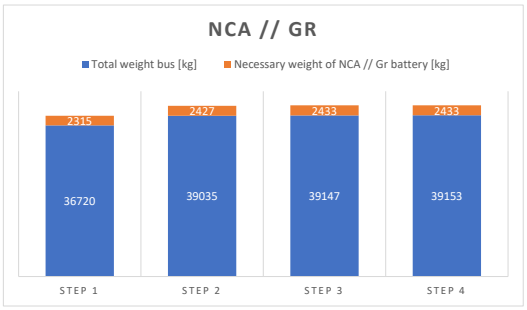

(b) NCA battery and vehicle weight.

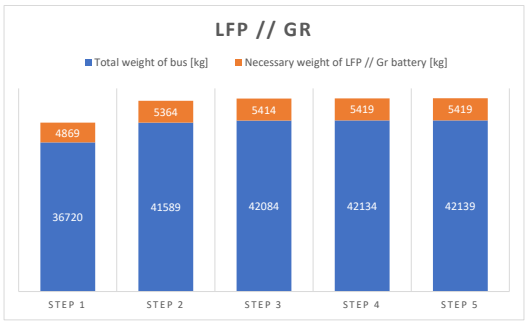

(c) LFP battery and vehicle weight.

Figure 6.8: Total weight of M1 and necessary battery weight for NMC cathode cells. Worst case, 100% load, 4-step calculation (no scale up)

Table 6.9 shows how this method is affected by increased energy consumption, obtained by scaling up the determined worst case, 100% load consumption by the factor of 1.27 determined in section 6.2.1.

Battery weight evaluation with respect to energy consumption increase (scale up factor: 1.27) from the battery						
	step 1	step 2	step 3	step 4	step 5	step 6
Total weight bus [kg]	36720	40430	40718	40740	40742	
Necessary weight of NMC // Gr battery [kg]	3710	3998	4020	4022	4022	
Energy consumption increase per step [kWh]	0	11,298	0,870	0,067	0,006	
Total weight bus [kg]	36720	39660	39841	39852	39853	
Necessary weight of NCA // Gr battery [kg]	2940	3121	3132	3133	3133	
Energy consumption increase per step [kWh]	0	8,971	0,547	0,033	0,002	
Total weight of bus [kg]	36720	42902	43698	43803	43816	43818
Necessary weight of LFP // Gr battery [kg]	6182	6978	7083	7096	7098	7098
Energy consumption increase per step [kWh]	0	18,710	2,466	0,318	0,039	0,006

Figure 6.9: Calculation results from battery weight and energy consumption investigation with a scale up factor of 1.27

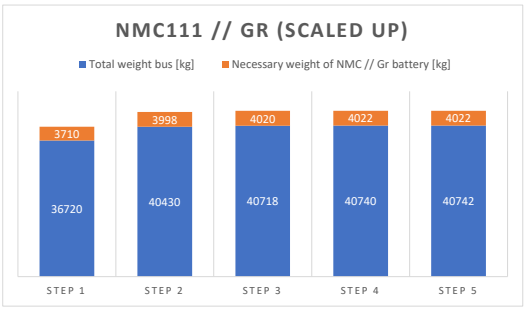

(a) NMC battery weight.

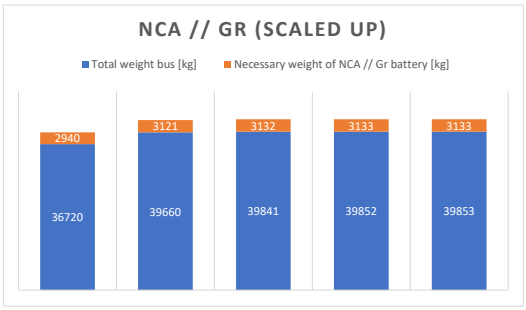

(b) NCA battery weight.

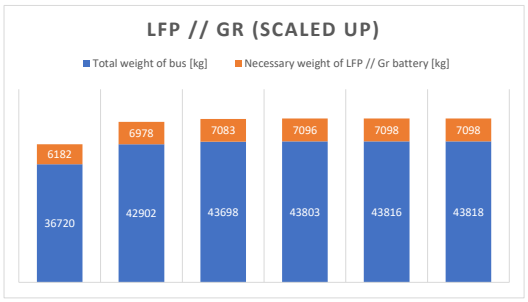

(c) LFP battery weight.

Figure 6.10: Total weight and necessary battery weight for NMC, NCA and LFP cathode cells. Worst case, 100% load, scaled up

Step 5 in figure 6.10a shows how a battery weight of 4022kg with the NMC111 cathode chemistry together with a graphite anode would be sufficient in order to carry the bus with an overall weight of 40 742kg. 3133kg of the NCA cathode chemistry, with graphite anode, would be a sufficient option for an overall M1 weight of 39 853kg as shown in figure 6.10b. With the LFP cathode and graphite anode, 7098kg of battery is needed as illustrated in figure 6.10c. The overall weight of the bus becomes 43 818kg.

The energy consumption obtained from the previous battery calculations yields values for the battery capacity, weight and volume in table 6.11 by utilizing equation 5.3, 5.4 and 5.5 respectively.

Scaled up energy consumption (factor of 1.27) and determined battery capacity, weight and volume				
Electrode chemistry	Energy consumption 1 round trip [kWh]	Battery capacity [kWh]	Battery weight [kg]	Battery volume [L]
NMC111 // Gr	157,65	844,55	4021,7	1593,5
NCA // Gr	154,96	830,14	3132,6	1203,1
LFP // Gr	166,95	894,37	7098,2	2751,9

Figure 6.11: Final evaluated energy consumption with battery capacity, weight and volume

Figure 6.12a compares the required capacity for the three different evaluated battery chemistries. Figure 6.12b compares the needed weight for the different battery chemistries while figure 6.12c

compares the needed battery volume for the different battery chemistries.

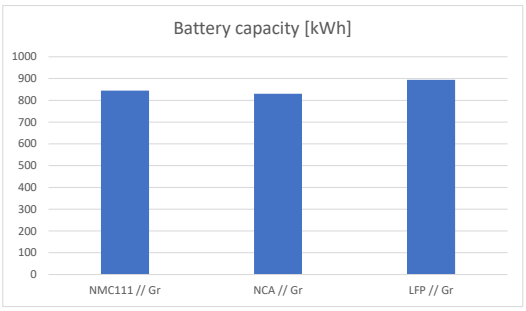

(a) Battery capacity.

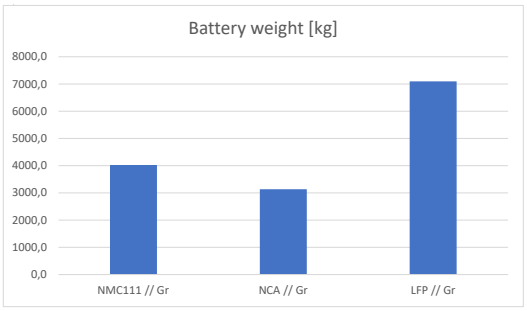

(b) Battery weight.

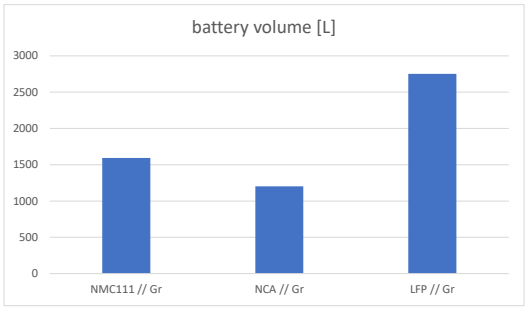

(c) Battery volume

Figure 6.12: Total weight and necessary battery weight for NMC, NCA and LFP cathode cells. Worst case, 100% load, scaled up

6.3.2 Battery charging results

In table 6.4 the C-rate for each battery chemistry with 1MW charging power has been calculated using equation 5.7, and the battery capacity from table 6.9.

	Charging power [MW]	Charging per 5min stop [kWh]	C-rate
NMC // Gr	1	83.33	1.18
NCA // Gr	1	83.33	1.20
LFP // Gr	1	83.33	1.12

Table 6.4: Charging power, charging per 5 min stop and C-rate for the evaluated battery chemistries

The figures below shows two cases of charging. Figure 6.13 represent a case where the charging power is high enough so that 5 minutes of charging at both end stations result in 90% SoC after each round trip. Figure 6.14 represents a case where the battery is at 20% SoC after eight round trips.

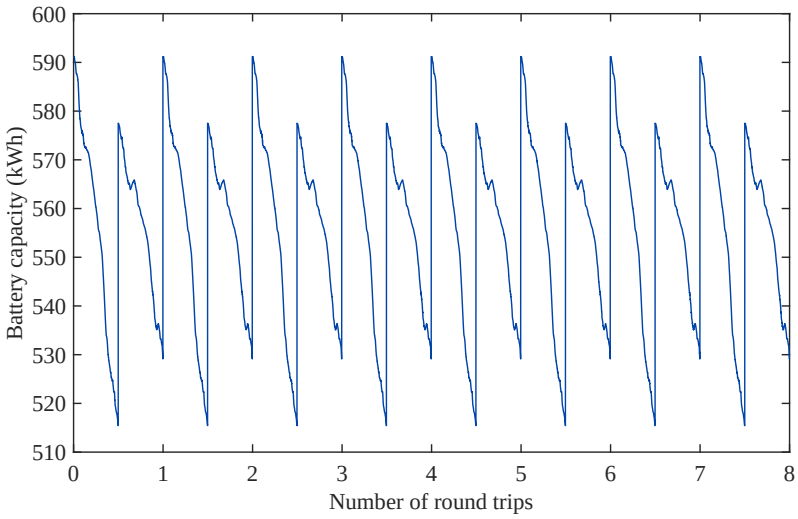

Figure 6.13: Charging cycle where the battery is at 90% at every round trip

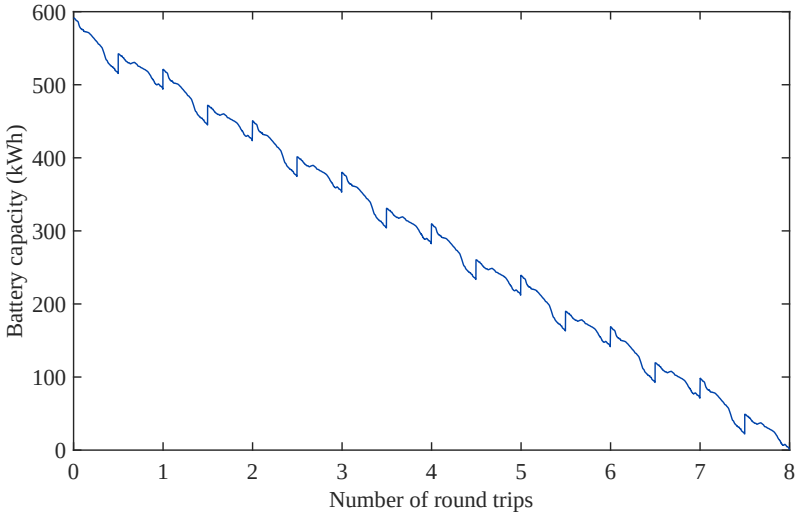

Figure 6.14: Charging cycle where the battery is at 20% after 8 round trips.

	20% SoC	90% SoC	$C-rate_{20\%SoC}$	$C-rate_{90\%SoC}$
NMC	325kW	745kW	0.38	0.88
NCA	316kW	732kW	0.38	0.88
LFP	340kW	790kW	0.38	0.88

Table 6.5: The required charge power to maintain a 20% and 90% state of charge throughout the day for all three battery cells

The table above shows the exact charging power necessary for the two cases. It is important to note that the battery only will be charged up to a maximum of 90% SoC, and never below 20% SoC. This means that a completely discharged state in figure 6.14 is the equivalent of 20% SoC for the actual battery, and the maximum SoC shown in figure 6.13 is the equivalent of 90% SoC. The C-rates for the different charging powers are also calculated by equation 5.7 and presented in table 6.5.

6.3.3 Economic battery results

	(USD/kWh)	Scaled up battery capacity	Total price
NMC_{111}//Gr	110	844.55kWh	92900,5$
NCA//Gr	100	830.14kWh	83014,0$
LFP//Gr	85	894.37kWh	76021,5$

Table 6.6: Estimated battery prices.

Table 6.6 shows an estimated price for the scaled-up battery sizes in USD. This estimation is the result of an unreleased report which investigates the prices of batteries. Further on, the prices will be used relative to the NCA battery. This is to avoid confusion about the differences in battery cell prices and battery system prices, in addition to the uncertainty of the market prices in general. The battery system includes the likes of a cooling system and safety systems opposite to only the battery cells. This means the LFP is the cheapest option, while the NMC is more expensive than the NCA batteries.

7 Discussion

The goal of this thesis is to explore the feasibility of replacing the M1 with a fully electric bus without forfeiting passenger capacity or durability. The vehicle will be exposed to megawatt charging at each end station, and slow charging charging during the night. This section will discuss sources of error in energy and battery calculations made, as well as look into different battery packages and every factor affecting the decision of which package is most suitable for this specific case.

7.1 Sources of error in energy calculations

There are several factors that may affect the energy consumption calculations when only using the physical model without any onboard data.

The biggest source of error in the energy calculations is the acceleration and de-acceleration numbers. In order to accurately measure the number of stops, and number of major accelerations and de-accelerations an onboard sensor needs to be applied. This is possible to implement in the M1 bus but in order for the data to be relevant it needs to be gathering data for an extended period of time, exceeding the available time for this project. An average acceleration/de-acceleration number for buses in Norway can be gathered from Statens Vegvesen[41], but it is difficult to implement when the data regarding the vehicle's driving patterns is unavailable. For the energy calculations made in this thesis, the acceleration forces have been disregarded and are likely to be one of the bigger sources of error in the calculations. Another related factor is the driving pattern including traffic lights, queues, and the individual driver's ability to perform economic driving. In addition, there is no data on the energy consumption of the auxiliary systems in the bus. It is believed that these numbers are minuscule compared to the sum of forces so they were excluded from the energy calculations.

Appendix A shows data from the M1 obtained from Atb. This data represents the average data from stop to stop on the route of M1. This limits the accuracy of the calculations to the stop-to-stop data and not in real-time data. When calculating the energy consumption the forces have been calculated every 10m and not from stop to stop. This means that the data obtained from Atb have been interpolated to fit the array of the route divided into 10m segments. The most affected value from this is the velocity vector, as it gives the average velocity between the different stops and does not take into account disturbances during driving. Even though the average velocity between stops gives an accurate description of the driving habits, it still leaves room for bigger variations from trip to trip.

The elevation profile retrieved from høydedata.no[25] gives a relatively accurate description of the route the M1 follows. However, it is hard to be fully accurate when making the profile, and it may therefore be susceptible to noise. Upon retrieving the elevation profile it became apparent that the data were riddled with noise as it would sometimes spike from one meter to the next. This meant that the data had to be smoothed and that the elevation profile may include minor errors. Although this is a source of error, it is estimated that the elevation profile noise will affect the calculated energy consumption minimally.

7.2 Sources of error in battery calculations

There are several factors that heavily impact the battery calculations presented in 6.3.1. This section will cover how some of the sources of error might change the results practically.

In the calculations where the bus' weight has been included, the weight of the bus of 36 720kg includes today's hybrid diesel/battery machinery in addition to the weight of 159 people with an average weight of 80kg. In reality, the weight of the bus machinery will change with respect to the transition to an electric engine and the removal of some components such as the diesel tank. This would yield a lower weight of the vehicle excluding the battery [39]. However, a reduction in the specific weight of the bus would decrease the energy consumption and would therefore not critically impact the performance of the vehicle. Considering that the weight contribution from the battery has been accounted for. Here, it is also important to note that the implementation of a battery system, excluding the battery pack itself, comes with several components adding weight to the M1 which has not been taken into account. Further, the average weight of the passengers could lead to an increased energy consumption if it exceeds 80kg and the bus is full. An increase in energy consumption leads to an increased demand for battery capacity as shown in 6.3.1. The average weight of the passengers is difficult to predict, but the fact that the energy consumption utilized in the battery calculations considers a worst case scenario in addition to being scaled up by the factor of 1.27, lowers the probability of performance failures.

Changes in the values for specific energy of the batteries from table 5.1 would impact the required battery capacity, weight, and volume heavily. These values depend on several factors, some of them listed in section 3.2.4, where the specific energy is the most important specification regarding an electric vehicle. This is due to the fact that the battery has to provide the energy to transport its own weight together with the remaining machinery and passengers. An increase in these values could be the result of future research and would lead to a decrease in battery weight that also decreases the overall energy consumption. If the values, in reality, are lower than the utilized values given in table 5.1, this would lead to a heavier battery package with higher volume.

The electrical efficiency 3.31 for the batteries during charging and discharging has been set to 100% in the calculations. Lithium ion batteries are known for their high electrical efficiency, however this value could decrease below 90% due to low temperatures and battery degradation (which has been taken into account) [43]. The impact of this source of error is reduced by multiplying the energy consumption by 1.27, as this considers a worst case scenario with low temperatures, tough road surface conditions and a full bus.

The battery pack has been dimensioned assuming a battery degradation of 20% over 10 years, where an increased degradation rate increases the need for battery capacity. Some of the factors that could effect the battery degradation are given in the list 7.2.

- High power output in steep hills such as Okstadbakken (accelerates SEI development)
- High power charging (accelerates SEI development)
- Inaccuracies during manufacturing of the battery and cell stacking
- Extreme temperatures
- External force leading to mechanical damage (crashes, dents, etc.)
- The type of electrolyte utilized in the battery

Furthermore the calculations of costs in table 6.6 contain a degree of insecurity. The price of USD per kWh is obtained through an unpublished article[35], but the numbers were published in a graph. This means that the prices of the batteries do have a factor of uncertainty, but

the possible differences are considered unsubstantial. In addition, the progressive research on batteries results in a regular price reduction as the technologies are further developed along with the discovery of new technologies. However, unforeseen events such as a pandemic, could lead to an increase in battery prices if it affects mineral extraction, manufacturing or transport.

7.3 Battery and battery charging discussion

The battery has been dimensioned with energy being the limiting factor, "When considering power versus energy, energy is usually the limiting factor, and thus a battery package usually offers sufficient power." [12]. This means that the values for the max power output of the battery have been neglected when the weight, volume and storage capacity has been determined. In general, high power batteries usually has a lower electrode thickness, while high energy batteries have thicker electrodes as mentioned in the investigation of electrode performance in section 3.2.4. If the power demand were to be the limiting factor of the M1 bus battery, this would yield a larger battery pack as an increase in specific power in the battery cells requires thinner electrodes, decreasing the specific energy.

When comparing the environmental impact of the different battery cells, the battery cell with the NCA cathode is the cell with the least amount of CO_2 emissions. This would not be the case if the production were to be moved to a country with more sustainable energy. The greatest part of the emissions is a consequence of the energy mix as mentioned in the interpretation in section4. In fact, the LFP cathode is the most environmentally friendly cathode of these three because of the cobalt used in the other two cathodes. Nonetheless, with the data obtained through SimaPro with the assumptions made for the three battery cells, the battery cell with the least impact on the environment is the one with the NCA cathode.

Several electrodes that have been mentioned in the part about different LIB electrodes in section 3.2.3, may be good options for the M1 bus even though they have not been included in the battery calculations. For the cathode, variations of the NMC chemistry could be good options, as the NMC cathode is fairly easy to customize in regard to the share of utilized nickel, manganese and cobalt. For example, NMC811 enhances the specific energy and power, resulting in a reduced required battery weight for the M1 bus. It also lowers the amount of cobalt which may reduce the material cost of the M1 battery. However, the reduced amount of cobalt also negatively affects the battery's ability to perform at higher C-rates. NMC532 is also a good option that yields a more balanced performance and safety while also increasing the specific energy and power compared to the NMC111. However, the reduction in cobalt compared to NMC111 again reduces the ability to perform at high C-rates. For the anode of the M1 battery, the LTO could be a good option in combination with an NCA cathode. The LTO anode is the safest and most stable on the market which is important for a bus carrying a valuable load. The LTO anode also offers good fast charging performance which is beneficial with the implementation of MCS, even though it is heavier (lower specific energy). After analysing how an increase in battery weight on the M1 bus affects the overall energy consumption, the weight increase might not be critical. However, the LTO anode is very expensive and will probably impact the material cost of the M1 battery pack heavily. [33]

In order to maintain the safety and stability of the M1 battery package, battery temperature and volume monitoring in addition to battery cooling is important. Because thermal runaway in lithium ion batteries in a worst case may lead to an explosion, a monitoring device should be installed in order to communicate with the driver regarding extreme volume and temperature

changes. Cooling of the battery will be necessary in the form of liquid or air coolant, or by the use of a phase change material (PCM). PCMs such as paraffin wax may store some of the heat developed in the M1 battery in the phase change from solid to liquid, and therefore maintaining a safe temperature. The implementation of a cooling system may further increase the energy consumption of the bus. Here, the increase is determined by the amount of heat released from the three evaluated battery technologies. The cooling systems will be a part of the battery system, hence increasing both weight and volume.

In chapter 6.3.1 the battery dimensions are calculated based on the energy calculations from the worst case. Furthermore, the battery is dimensioned to be able to drive the M1 route three times without charging. It is conducted in this way to ensure that the battery has the capacity to endure the most challenging days. In addition to being able to withstand challenging conditions, another factor in the increased capacity of the battery is unforeseen circumstances. An important criteria for AtB is the fact that the electric buses should not be implemented at the expense of the passengers/customers. With the bus able to drive the route three times on one full charge (90% SoC), problems like a defective charger can be avoided by constructing a form of flexibility in the charging structure of the buses. A consequence is that the battery capacity is excessive on a regular day, and that the full capacity of the battery will rarely be required.

Charging of the battery is a critical part of maintaining the energy capacity. The SoC of the battery is chosen to be between 20-90% to extend the number of cycles the battery can provide. In chapter 6.3.2 the results of the charging calculations are presented. To avoid charging or discharging the battery outside those limitations, two charge powers were determined where one power ensures that the battery never discharges below 20% and one that keeps the battery at 90% SoC. It is worth mentioning that all charging powers between the two situations mentioned in table 6.5 can be utilized. However, these numbers are calculated with a full health battery. With the degradation of the battery over time, the capacity of the battery between 20-90% SoC also decrease. As a consequence of this, the charging power should be reduced in a later stage to keep the battery in the same SoC range. Furthermore, the MCS can provide charging with greater power, but to prevent unnecessary wear and tear on the battery a reduced charging power is desirable. This means that in order to create the optimal environment for the battery, the C-rate should be as low as possible, as lower C-rates improve the number of cycles the battery can provide.

If the bus' battery is charged at high power quickly after it has delivered high power to the electric engine this could contribute to increased battery degradation. This situation is relevant for the M1 bus as it charges at high power at Østre Lund quickly after the high power output through Okstadbakken 2.3. From Østre Lund to Ranheim the energy consumption and the power requirement is comparably a lot smaller, meaning that the battery may "rest" on the way to Ranheim. Due to the difference in performance requirements of the two trips, charging at higher power at Ranheim and lower power at Østre Lund might be beneficial to the M1 battery pack with respect to battery degradation and cycle life. In theory, the charging power at each station can be modified, yielding variations in C-rate from the MCS at Østre Lund and Ranheim.

7.4 Battery presentation

The weight as well as the volume of the batteries has to be taken into account when deciding which of the battery packages is best suited for the M1. The added energy demand from a heavy battery has been taken into account and it is possible to directly see the effects from a higher mass in equations ((3.5)–(3.6)). The energy consumption calculations do not include the acceleration and de-acceleration force, which are also directly affected by the mass. This means that the higher the mass of the bus the higher the ratio between the calculated energy demand and the measured energy demand will be. It is not only the added energy demand that affects the M1 when it comes to battery weight. A bigger mass leads to higher degradation rates for mechanical components in the buss such as tires, springs and brakes. Seeing as the mechanical wear is directly correlated to weight, it would be most optimal to have as light of a battery as possible. The heaviest of the battery packages, (LFP), weighs 7.098 tonnes, which is 226.59 % more than the NCA battery package which is the lightest. The NMC weighs approximately 4 tonnes, 900kg more than the NCA option.

It has been found that the required overall capacity with respect to the weight of the battery of the NMC111, NCA and LFP cathode batteries are 845kWh, 830kWh and 894kWh respectively. Yielding a volume of 1593.5L for NMC111, 1203.1L for NCA and 2751.9L for LFP. The challenge related to storing the batteries in the bus will therefore be easiest for the NCA cathode battery, and most difficult for the LFP cathode battery.

The price for NMC111 // Gr, NCA // Gr and LFP // Gr has been investigated to 92 900.5 USD, 83 014.0USD and 76 021,5USD respectively as shown in 6.6. This means that the cheapest option is the LFP // Gr battery chemistry. The price of the LFP cathode battery option is about 82% of the NMC111 // Gr price, and 92% of the NCA // Gr option. These price estimations accounts for the scaled up battery capacity and the fact that the LFP // Gr battery pack is the the heaviest and the largest in volume.

8 Conclusion

All the evaluated lithium ion battery solutions together with high power charging (MCS) provide a feasible solution to the electrification of the M1 bus. However, they differ in weight, volume, price and environmental impact.

The LFP and Graphite battery option for the M1 has shown to be the heaviest and largest in volume, while inflicting a large environmental impact in production, but it is also the cheapest option. This means that if you have sufficient space (volume) for storing the battery pack, the LFP // Gr battery would be the preferred solution from an economic point of view regarding the initial investment in the battery pack. However, the added weight contributes to higher energy consumption and degradation of mechanical components, increasing the expenses of electricity and maintenance. The large environmental impact of the LFP originates mainly from the energy used in the production of the battery cell. This means that the LFP could become the most environmentally friendly option if the production were to be utilizing renewable energy in the future.

The NMC111 // Gr battery has been evaluated as the most expensive option (+17 000 USD compared to LFP), while being substantially lighter and smaller in volume compared to the LFP // Gr option with a smaller negative impact on the environment. The fact that the NMC cathode can be customized to meet the requirements of the specific situation opens possibilities of increasing the specific energy (reducing weight), or improving high power charging and stability (safety).

The NCA and Graphite battery solution has yielded the smallest volume, while also being the lightest and overall most environmentally friendly with today's manufacturing situation. It is slightly more expensive compared to the LFP solution (+7000 USD), but the reduction in weight compared to the LFP // Gr and NMC111 // Gr will result in cheaper maintenance and electricity costs during its lifetime. The small volume makes the challenge of storing the battery in the bus easier compared to the other evaluated options.

Megawatt charging systems provide the potential to charge batteries at up to 3.75MW power. The calculations made in this thesis show that it is not necessary to charge the M1 bus at maximum power. Charging on lower C-rates is also beneficial as it ensures a healthy operation of the battery.

The calculations performed in this report imply that it could be possible to electrify the M1 with a smaller battery package than calculated. This would however demand higher charge power and reliable chargers while also increasing the degradation rate and reducing the safety of the battery solution. Therefore, a larger battery pack evaluated by scaling up the energy consumption and the possible drive time without charging enhance the performance, safety, and cycle life of the battery.

9 Future work

Even though several aspects of the M1 electrification have been considered in this report, there are many things that can be done in order to obtain more information and improved results.

Collecting more data by monitoring and registering driving patterns would give useful information regarding energy consumption. This would provide insight into driver tendencies and could be used to improve economical driving. The acceleration numbers have been neglected in this report but could be included if there existed reasonable estimates.

Obtaining data for the temperature of the bus given different outside temperatures could be useful in order to evaluate energy consumption in relation to heating and cooling during the seasons. This would be dependent on the heat loss through doors (opened/closed), windows, walls, floor, and roof of the bus.

Battery testing could give more information about the effects over time of high-power (MW) charging. This could contribute to an accurate estimation of the degradation rate and cycle life of the evaluated battery chemistries, improving the accuracy of the results. This could be covered by utilizing a battery laboratory, or previous research on the subject.

Estimating the power output of the battery in different parts of the M1 route could be useful when dimensioning the battery weight and volume. This has not been done in this report but could be a useful investigation for future work. This could be done by measuring the energy in relation to real-time and acceleration numbers.

References

[1] *09654: Priser på drivstoff (kroner per liter), etter petroleumsprodukt, måned og statistikkvariabel. Statistikkbanken*. no. URL: https://www.ssb.no/system/ (visited on 03/27/2023).

[2] Hatem Abdelaty and Moataz Mohamed. "A Prediction Model for Battery Electric Bus Energy Consumption in Transit". In: *Energies* 14.10 (Jan. 2021). Number: 10 Publisher: Multidisciplinary Digital Publishing Institute, p. 2824. ISSN: 1996-1073. DOI: 10.3390/en14102824. URL: https://www.mdpi.com/1996-1073/14/10/2824 (visited on 03/27/2023).

[3] K. M. Abraham. "Prospects and Limits of Energy Storage in Batteries". en. In: *The Journal of Physical Chemistry Letters* 6.5 (Mar. 2015), pp. 830–844. ISSN: 1948-7185, 1948-7185. DOI: 10.1021/jz5026273. URL: https://pubs.acs.org/doi/10.1021/jz5026273 (visited on 05/13/2023).

[4] Aiman Albatayneh et al. "Comparison of the Overall Energy Efficiency for Internal Combustion Engine Vehicles and Electric Vehicles". In: *Environmental and Climate Technologies* 24.1 (Jan. 1, 2020), pp. 669–680. ISSN: 2255-8837. DOI: 10.2478/rtuect-2020-0041. URL: https://www.sciendo.com/article/10.2478/rtuect-2020-0041 (visited on 05/12/2023).

[5] *An overview of regenerative braking systems — Elsevier Enhanced Reader*. DOI: 10.1016/j.est.2022.105033. URL: https://reader.elsevier.com/reader/sd/pii/S2352152X22010350?token=5A9F3C4CE105987082F6B51EC47F059391593E3ADDC5AF7F7B30C12E7E0E2F5A7720EC771646D23DC2B12632E705B181&originRegion=eu-west-1&originCreation=20230418100240 (visited on 04/18/2023).

[6] *AtB*. nb. Page Version ID: 23466691. Apr. 2023. URL: https://no.wikipedia.org/w/index.php?title=AtB&oldid=23466691 (visited on 05/16/2023).

[7] AtB.

[8] AtB. *Første elbusstur med passasjerer i Trondheim*. June 13, 2019. URL: https://www.atb.no/getfile.php/1341470-1560522168/Pressemelding/190613-F%C3%B8rste%20elbusstur%20med%20passasjerer%20i%20Trondheim.pdf (visited on 05/20/2023).

[9] *AtB - Forside*. URL: https://www.atb.no/ (visited on 03/30/2023).

[10] Camiel Beckers et al. "Energy Consumption Prediction for Electric City Buses". In: June 4, 2019. URL: https://www.researchgate.net/profile/Camiel-Beckers/publication/335542182_Energy_Consumption_Prediction_for_Electric_City_Buses/links/5d6cb5394585150886066091/Energy-Consumption-Prediction-for-Electric-City-Buses.pdf.

[11] *Bompenger*. nb-NO. URL: https://elbil.no/elbil-fordeler/bompenger/ (visited on 03/27/2023).

[12] Odne Stokke Burheim. *ENGINEERING ENERGY STORAGE*. Academic Press Inc, 2017. ISBN: 978-0-12-814100-7. (Visited on 03/09/2023).

[13] Felipe Cerdas et al. "Exploring the Effect of Increased Energy Density on the Environmental Impacts of Traction Batteries: A Comparison of Energy Optimized Lithium-Ion and Lithium-Sulfur Batteries for Mobility Applications". In: *Energies* 11.1 (2018). ISSN: 1996-1073. DOI: 10.3390/en11010150. URL: https://www.mdpi.com/1996-1073/11/1/150.

[14] *CharIN HPCCV Task Force - High Power Plug Update*. English. July 2020. (Visited on 04/20/2023).

[15] Evgeniy Chikishev. "Impact of natural and climatic conditions on electric energy consumption by an electric city bus". In: *Transportation Research Procedia* 57 (2021), pp. 113–121. ISSN: 2352-1465. DOI: https://doi.org/10.1016/j.trpro.2021.09.032. URL: https://www.sciencedirect.com/science/article/pii/S2352146521006608.

[16] Qiang Dai et al. *EverBatt: A closed-loop battery recycling cost and environmental impacts model*. Tech. rep. Argonne National Lab.(ANL), Argonne, IL (United States), 2019.

[17] *Decarbonizing transportation and energy systems...* en. URL: https://www.freyrbattery.com/ (visited on 05/20/2023).

[18] *Drag Coefficient*. URL: https://www.engineeringtoolbox.com/drag-coefficient-d_627.html (visited on 05/15/2023).

[19] *Electricity sector in China*. en. Page Version ID: 1152618144. May 2023. URL: https://en.wikipedia.org/w/index.php?title=Electricity_sector_in_China&oldid=1152618144 (visited on 05/15/2023).

[20] *Elektrisk buss i Trondheim*. nb-NO. Section: Bli med. Mar. 2019. URL: https://trondheim2030.no/2019/03/27/elektrisk-buss-i-trondheim/ (visited on 05/13/2023).

[21] Linda Ager-Wick Ellingsen, Bhawna Singh, and Anders Hammer Strømman. "The size and range effect: lifecycle greenhouse gas emissions of electric vehicles". In: *Environmental Research Letters* 11.5 (May 2016), p. 054010. DOI: 10.1088/1748-9326/11/5/054010. URL: https://dx.doi.org/10.1088/1748-9326/11/5/054010.

[22] Linda Ager-Wick Ellingsen et al. "Life Cycle Assessment of a Lithium-Ion Battery Vehicle Pack". In: *Journal of Industrial Ecology* 18.1 (), pp. 113–124. DOI: https://doi.org/10.1111/jiec.12072. eprint: https://onlinelibrary.wiley.com/doi/pdf/10.1111/jiec.12072. URL: https://onlinelibrary.wiley.com/doi/abs/10.1111/jiec.12072.

[23] Shahjadi Hisan Farjana, Nazmul Huda, and M. A. Parvez Mahmud. "Life cycle assessment of cobalt extraction process". In: *Journal of Sustainable Mining* 18.3 (2019), pp. 150–161. ISSN: 2300-3960. DOI: https://doi.org/10.1016/j.jsm.2019.03.002. URL: https://www.sciencedirect.com/science/article/pii/S2300396018301836.

[24] *Forskrift om utslippskrav til kjøretøy ved offentlig anskaffelse til veitransport - Lovdata*. URL: https://lovdata.no/dokument/SF/forskrift/2022-12-20-2384?fbclid=IwAR0v41Up8lpa0cwp8FFh9SjmQyVqJql54orkW6j540ahrBCWBoCFP3DSrkA (visited on 05/20/2023).

[25] *Høydedata*. URL: https://hoydedata.no/LaserInnsyn2/ (visited on 03/30/2023).

[26] Viktoria Jansson. "A LITERATURE STUDY OF ROLLING RESISTANCE AND ITS AFFECTING FACTORS". In: *vehicle dynamics.* (). URL: https://www.diva-portal.org/smash/get/diva2:1678831/FULLTEXT01.pdf.

[27] *Klimagassutslipp fra transport i Norge*. Miljøstatus. Nov. 16, 2022. URL: https://miljostatus.miljodirektoratet.no/tema/klima/norske-utslipp-av-klimagasser/klimagassutslipp-fra-transport/ (visited on 05/20/2023).

[28] *Mapped: EV Battery Manufacturing Capacity, by Region*. en-US. Feb. 2022. URL: https://www.visualcapitalist.com/sp/mapped-ev-battery-manufacturing-capacity-by-region/ (visited on 05/15/2023).

[29] *Megawatt Charging System*. en. Page Version ID: 1150149244. Apr. 2023. URL: https://en.wikipedia.org/w/index.php?title=Megawatt_Charging_System&oldid=1150149244 (visited on 04/20/2023).

[30] Klima-og miljødepartementet. *Klimaendringer og norsk klimapolitikk*. no. Redaksjonellartikkel. Publisher: regjeringen.no. Oct. 2021. URL: https://www.reg

jeringen.no/no/tema/klima-og-miljo/innsiktsartikler-klima-miljo/klimaendringer-og-norsk-klimapolitikk/id2636812/ (visited on 03/23/2023).

[31] Tim Moynihan. "Samsung Finally Reveals Why the Note 7 Kept Exploding". en-US. In: *Wired* (). Section: tags. ISSN: 1059-1028. URL: https://www.wired.com/2017/01/why-the-samsung-galaxy-note-7-kept-exploding/ (visited on 03/09/2023).

[32] UNITED NATIONS. *PARIS AGREEMENT*. URL: https://unfccc.int/sites/default/files/english_paris_agreement.pdf.

[33] Naoki Nitta et al. "Li-ion battery materials: present and future". In: *Materials Today* 18.5 (2015), pp. 252–264. ISSN: 1369-7021. DOI: https://doi.org/10.1016/j.mattod.2014.10.040. URL: https://www.sciencedirect.com/science/article/pii/S1369702114004118.

[34] Ziyad Salameh. "Chapter 4 - Energy Storage". In: *Renewable Energy System Design*. Ed. by Ziyad Salameh. Boston: Academic Press, 2014, pp. 201–298. ISBN: 978-0-12-374991-8. DOI: https://doi.org/10.1016/B978-0-12-374991-8.00004-0. URL: https://www.sciencedirect.com/science/article/pii/B9780123749918000040.

[35] Orangi Sina et al. *Bottom-up Modeling of Lithium-Ion Production Cost from 2010 to 2030(Unpubliched)*.

[36] Ole-Petter Spaun. *Skal teste trådløs lading av elbusser*. Norsk elbilforening. Mar. 10, 2023. URL: https://elbil.no/skal-teste-tradlos-lading-av-elbusser/ (visited on 05/04/2023).

[37] Nader A. El-Taweel, Aboelsood Zidan, and Hany E. Z. Farag. "Novel Electric Bus Energy Consumption Model Based on Probabilistic Synthetic Speed Profile Integrated With HVAC". In: *IEEE Transactions on Intelligent Transportation Systems* 22.3 (2021), pp. 1517–1531. DOI: 10.1109/TITS.2020.2971686.

[38] *The price of batteries has declined by 97% in the last three decades*. URL: https://ourworldindata.org/battery-price-decline (visited on 03/27/2023).

[39] *The Switch from Gas and Diesel Engines to Electrical Motors*. en-US. Aug. 2019. URL: https://www.whitehorncapital.com/whitehorn-blog/2019/8/29/nb6ubz9n4gj8oqx725a51j3nzxmkrk (visited on 05/15/2023).

[40] Martin Thronsen. *Stadig mer elektriske Oslo*. nb-NO. Dec. 2021. URL: https://elbil.no/stadig-mer-elektriske-oslo/ (visited on 03/27/2023).

[41] *Tilrettelegging for Kollektivtransport på veg*. URL: https://vegvesen.brage.unit.no/vegvesen-xmlui/bitstream/handle/11250/196092/Hb-232-2008-08.pdf?sequence=5&isAllowed=y (visited on 05/18/2023).

[42] *UNFCCC*. URL: https://unfccc.int/ (visited on 05/20/2023).

[43] *Voltage Efficiency - an overview — ScienceDirect Topics*. URL: https://www.sciencedirect.com/topics/engineering/voltage-efficiency (visited on 05/11/2023).

[44] *What is Regenerative Braking?* J.D. Power. URL: https://www.jdpower.com/cars/shopping-guides/what-is-regenerative-braking (visited on 04/13/2023).

[45] Lisa Ydrefors et al. "Rolling resistance and its relation to operating conditions: A literature review". In: *Proceedings of the Institution of Mechanical Engineers, Part D: Journal of Automobile Engineering* 235.12 (Oct. 1, 2021). Publisher: IMECHE, pp. 2931–2948. ISSN: 0954-4070. DOI: 10.1177/09544070211011089. URL: https://doi.org/10.1177/09544070211011089 (visited on 04/18/2023).

[46] Mats Zackrisson. *Life cycle assessment of long life lithium electrode for electric vehicle batteries*. 2017.

[47] Ghassan Zubi et al. “The lithium-ion battery: State of the art and future perspectives”. In: *Renewable and Sustainable Energy Reviews* 89 (2018), pp. 292–308. ISSN: 1364-0321. DOI: https://doi.org/10.1016/j.rser.2018.03.002. URL: https://www.sciencedirect.com/science/article/pii/S1364032118300728.

A Appendix: A

Apendix A represents an Excel table provided by Pål Revheim, Ssnior advisor technology and business development. The table shows average data for the M1 between every stop both to and from Ranheim. The relevant data used in this thesis are as follows:

- Average velocity
- Distance between stops
- Accumulated distance

Direction	Stop name	Distance [m]	Acc. Distance [m]	Altitude [m]	Height difference [m	Average slope [deg]	Driving time [min]	Acc. driving time [mi	Regulation time [min	Average speed [km/h]
T	Ranheim		0	22	0	0	00:01	00:00	00:00	
T	Ranheim idrettsplass	815	815	6	-16	-1	00:02	00:01	00:00	48,9
T	Anders Søyseths veg	848	1663	8	2	0	00:01	00:03	00:00	25,44
T	Grilstadkleiva	437	2100	9	1	0	00:03	00:04	00:00	26,22
T	Skovgård 1	938	3038	50	41	2	00:02	00:07	00:00	18,76
T	Travbanen	913	3951	54	5	0	00:01	00:09	00:00	27,39
T	Gildheim	838	4789	38	-16	-1	00:01	00:10	00:00	50,28
T	Strindheim 1	299	5088	42	4	1	00:01	00:11	00:00	17,94
T	Dalen Hageby	430	5518	35	-7	-1	00:01	00:12	00:00	25,8
T	Rønningsbakken	585	6103	19	-16	-2	00:02	00:13	00:00	35,1
T	Buran 1	697	6800	11	-9	-1	00:02	00:15	00:00	20,91
T	Solsiden	624	7424	4	-7	-1	00:01	00:17	00:00	18,72
T	Bakkegata	355	7779	5	1	0	00:03	00:18	00:00	21,3
T	Olav Tryggvasons ga	488	8267	7	2	0	00:03	00:21	00:00	9,76
T	Prinsens gate P1	563	8830	10	3	0	00:01	00:24	00:00	11,26
T	Nidarosdomen	564	9394	14	5	0	00:01	00:25	00:00	33,84
T	Studentersamfundet	416	9810	15	1	0	00:01	00:26	00:00	24,96
T	Hesthagen	623	10433	21	7	1	00:02	00:27	00:00	37,38
T	Lerkendal 2	563	10996	23	2	0	00:01	00:29	00:00	16,89
T	Valøyvegen	489	11485	27	4	0	00:02	00:30	00:00	29,34
T	Bratsbergvegen	515	12000	35	8	1	00:01	00:32	00:00	15,45
T	Kroppanbrua	952	12952	32	-3	0	00:05	00:33	00:00	57,12

T	Bratsbergvegen	515	12000	35	8	1	00:01	00:32	00:00		15,45
T	Kroppanbrua	952	12952	32	-3	0	00:05	00:33	00:00		57,12
T	Tonstadkrysset 1	3308	16260	123	91	2	00:01	00:38	00:00		39,696
T	Rostengrenda	627	16887	143	19	2	00:01	00:39	00:00		37,62
T	City Syd	558	17445	147	5	0	00:02	00:40	00:00		33,48
T	Tillerterminalen	338	17783	147	0	0	00:02	00:42	00:00		10,14
T	Martin Linges veg	492	18275	146	-1	0	00:01	00:44	00:00		14,76
T	Peder Morsets veg	517	18792	142	-5	0	00:02	00:45	00:00		31,02
T	Heimdal stasjon	655	19447	141	-1	0	00:02	00:47	00:00		19,65
T	Bekkasinvegen	939	20386	148	7	0	00:01	00:49	00:00		28,17
T	Kattemsenteret	533	20919	147	-1	0	00:02	00:50	00:00		31,98
T	Østre Lund 1	784	21703	154	7	1	00:00	00:52	10:00		23,52
R	Østre Lund 1		0	154	0	0	00:02	00:00	00:00		
R	Kattemsenteret	672	672	147	-7	-1	00:01	00:02	00:00		20,16
R	Bekkasinvegen	683	1355	148	1	0	00:02	00:03	00:00		40,98
R	Heimdal stasjon	1020	2375	141	-7	0	00:02	00:05	00:00		30,6
R	Peder Morsets veg	585	2960	142	1	0	00:01	00:07	00:00		17,55
R	Martin Linges veg	498	3458	146	5	1	00:02	00:08	00:00		29,88
R	Tillerterminalen	587	4045	147	1	0	00:01	00:10	00:00		17,61
R	City Syd	352	4397	147	0	0	00:02	00:11	00:00		21,12
R	Rostengrenda	454	4851	143	-5	-1	00:02	00:13	00:00		13,62
R	Tonstadkrysset 1	634	5485	123	-19	-2	00:04	00:15	00:00		19,02

R	Tonstadkrysset 1	634	5485	123	-19	-2	00:04	00:15	00:00		19,02
R	Sluppen 1	3829	9314	35	-89	-1	00:01	00:19	00:00		57,435
R	Bratsbergvegen	420	9734	35	0	0	00:01	00:20	00:00		25,2
R	Valøyvegen	480	10214	27	-8	-1	00:01	00:21	00:00		28,8
R	Lerkendal 1	286	10500	24	-3	-1	00:02	00:22	00:00		17,16
R	Hesthagen	399	10899	21	-3	0	00:02	00:24	00:00		11,97
R	Studentersamfundet	811	11710	15	-6	0	00:01	00:26	00:00		24,33
R	Nidarosdomen	401	12111	14	-1	0	00:02	00:27	00:00		24,06
R	Prinsens gate P2	570	12681	11	-4	0	00:03	00:29	00:00		17,1
R	Olav Tryggvasons ga	692	13373	7	-4	0	00:01	00:32	00:00		13,84
R	Bakkegata	333	13706	5	-2	0	00:02	00:33	00:00		19,98
R	Solsiden	405	14111	4	-1	0	00:02	00:35	00:00		12,15
R	Buran 2	660	14771	9	5	0	00:01	00:37	00:00		19,8
R	Rønningsbakken	618	15389	19	10	1	00:02	00:38	00:00		37,08
R	Dalen Hageby	673	16062	35	16	1	00:01	00:40	00:00		20,19
R	Strindheim 2	379	16441	41	6	1	00:01	00:41	00:00		22,74
R	Gildheim	319	16760	38	-3	-1	00:02	00:42	00:00		19,14
R	Travbanen	820	17580	54	16	1	00:02	00:44	00:00		24,6
R	Skovgård 2	1044	18624	45	-9	0	00:02	00:46	00:00		31,32
R	Grilstadkleiva	595	19219	9	-36	-3	00:01	00:48	00:00		17,85
R	Anders Søyseths veg	591	19810	8	-1	0	00:02	00:49	00:00		35,46
R	Ranheim idrettsplass	873	20683	6	-2	0	00:02	00:51	00:00		26,19
R	Ranheim	722	21405	22	16	1	00:00	00:53	10:00		21,66

B Appendix: B

Appendix B is the MATLAB code used to calculate the energy consumption of the M1. Elevation profiles are gatherd from høydedata.no and utilized at the start of the script. The energy calculations has been made for the round trip and both of the one way trips alone. Lines 56-125 cover the creation of velocity array, made from the number found in appendix A

```
1  clc; clear all; close all;
2
3  data_1 = readtable("elevationProfile.csv");
4  data_2 = readtable("elevationProfile(1).csv");
5  data_3 = readtable("elevationProfile(2).csv");
6  data_4 = readtable("elevationProfile(3).csv");
7  data_5 = readtable("elevationProfile(4).csv");
8  data_6 = readtable("elevationProfile(5).csv");
9
10
11 dette_er_riktig_1 = table2array(data_1(1:1988, 3)).';
12 dette_er_riktig_6 = table2array(data_6(1:1612, 3)).';
13
14 hoydeprofil_1 = dette_er_riktig_1(1:10:end);
15 hoydeprofil_2 = table2array(data_2(1:296, 3)).';
16 hoydeprofil_3 = table2array(data_3(1:594, 3)).';
17 hoydeprofil_4 = table2array(data_4(1:651, 3)).';
18 hoydeprofil_5 = table2array(data_5(1:245, 3)).';
19 hoydeprofil_6 = dette_er_riktig_6(1:10:end);
20
21 ranheim_ostre_lund = [hoydeprofil_1, hoydeprofil_2, hoydeprofil_3
       , hoydeprofil_4, hoydeprofil_5, hoydeprofil_6];
22 ostre_lund_ranheim = flip(ranheim_ostre_lund);
23 hele_driten = [ranheim_ostre_lund, ostre_lund_ranheim];
24 litt_bedre = hele_driten(1:10:end);
25 bedre = hele_driten(1:100:end);
26
27 x_akse = linspace(0,43.1,4294);
28
29 plot(x_akse,hele_driten)
30 xlabel('Distance [km]')
31 ylabel('Altitude [MASL]')
32 plot(ranheim_ostre_lund)
33 plot(ostre_lund_ranheim)
34
35 for i = 1:(length(hele_driten)-1)
36     greader(i) = atan((hele_driten(i+1) - hele_driten(i)) / 10);
37 end
38
39 for i = 1:(length(ranheim_ostre_lund) - 1)
```

```
40      greader_1(i) = atan((ranheim_ostre_lund(i+1) -
            ranheim_ostre_lund(i)) / 10);
41  end
42
43  for i = 1:(length(ostre_lund_ranheim) - 1)
44      greader_2(i) = atan((ostre_lund_ranheim(i+1) -
            ostre_lund_ranheim(i)) / 10);
45  end
46
47  %Konstanter
48
49  G = 9.81;
50  Frontalareal = 10;
51  Luftetthet = 1.225;
52  Rulle_motstand_coeficient = 0.015;
53  Air_drag_coeficient = 0.7;
54  regenetiv_bremsing = 0.5;
55
56  %Fart
57  a = ones(1,82).*48.9.*(5/18);
58  b = ones(1,86).*25.44.*(5/18);
59  c = ones(1,45).*26.22.*(5/18);
60  d = ones(1,95).*18.76.*(5/18);
61  e = ones(1,92).*27.39.*(5/18);
62  f = ones(1,85).*50.28.*(5/18);
63  g = ones(1,31).*17.94.*(5/18);
64  h = ones(1,44).*25.8.*(5/18);
65  i = ones(1,60).*35.1.*(5/18);
66  j = ones(1,71).*20.91.*(5/18);
67  k = ones(1,63).*18.72.*(5/18);
68  l = ones(1,37).*21.3.*(5/18);
69  m = ones(1,50).*9.76.*(5/18);
70  n = ones(1,57).*11.26.*(5/18);
71  o = ones(1,57).*33.84.*(5/18);
72  p = ones(1,43).*24.96.*(5/18);
73  q = ones(1,63).*37.38.*(5/18);
74  r = ones(1,57).*16.89.*(5/18);
75  s = ones(1,50).*29.34.*(5/18);
76  t = ones(1,53).*15.45.*(5/18);
77  u = ones(1,96).*57.12.*(5/18);
78  v = ones(1,332).*39.69.*(5/18);
79  w = ones(1,64).*37.62.*(5/18);
80  x = ones(1,57).*33.48.*(5/18);
81  y = ones(1,35).*10.14.*(5/18);
82  z = ones(1,50).*14.76.*(5/18);
83  aa = ones(1,53).*31.02.*(5/18);
84  bb = ones(1,67).*19.65.*(5/18);
```

```
cc = ones(1,95).*28.17.*(5/18);
dd = ones(1,54).*31.98.*(5/18);
ee = ones(1,79).*23.52.*(5/18);

xa = ones(1,68).*20.16.*(5/18);
xb = ones(1,69).*40.98.*(5/18);
xc = ones(1,104).*30.6.*(5/18);
xd = ones(1,61).*17.55.*(5/18);
xe = ones(1,52).*29.88.*(5/18);
xf = ones(1,61).*17.61.*(5/18);
xg = ones(1,37).*21.12.*(5/18);
xh = ones(1,47).*13.62.*(5/18);
xi = ones(1,65).*19.02.*(5/18);
xj = ones(1,385).*57.435.*(5/18);
xk = ones(1,44).*25.2.*(5/18);
xl = ones(1,50).*28.8.*(5/18);
xm = ones(1,31).*17.16.*(5/18);
xn = ones(1,42).*11.97.*(5/18);
xo = ones(1,83).*24.33.*(5/18);
xp = ones(1,42).*24.06.*(5/18);
xq = ones(1,59).*17.1.*(5/18);
xr = ones(1,71).*13.84.*(5/18);
xs = ones(1,34).*19.98.*(5/18);
xt = ones(1,42).*12.15.*(5/18);
xu = ones(1,67).*19.8.*(5/18);
xv = ones(1,63).*37.08.*(5/18);
xw = ones(1,68).*20.19.*(5/18);
xx = ones(1,39).*22.74.*(5/18);
xy = ones(1,33).*19.14.*(5/18);
xz = ones(1,83).*24.6.*(5/18);
xaa = ones(1,106).*31.32.*(5/18);
xbb = ones(1,61).*17.85.*(5/18);
xcc = ones(1,60).*35.46.*(5/18);
xdd = ones(1,88).*26.19.*(5/18);
xee = ones(1,73).*21.66.*(5/18);



HastighetRO = [a b c d e f g h i j k l m o p q r s t u v w x y z
   aa bb cc dd ee]*1.4;
HastighetOR = [xa xb xc xd xe xf xg xh xi xj xk xl xm xo xp xq xr
    xs xt xu xv xw xx xy xz xaa xbb xcc xdd xee]*1.4;
Hastighet = [HastighetRO HastighetOR];

%Innputs
vekt = [24000 24000 + 80*50 24000 + 80*80 24000 + 80*159];
vekt2 = 24000 + 80*50;
```

```
130 vekt3 = 24000 + 80*100;
131 vekt4 = 24000 + 80*159;
132 Distanse_Mellom_Stopp = 10;
133 Gjennomsnittelig_Slope = greader;
134 Gjennomsnittelig_hastighet = 28.06 * (5/18);
135 akselerasjon = 0.9;
136 vekten = linspace(24000,36720,160);
137 vektene = [20000:500:50000];
138
139
140
141
142 %Kreftene
143
144 for i = 1:length(Hastighet)
145     for ii = 1:length(vekt)
146         Total_kraft(i,ii) =(vekt(ii)* G .* sin(greader(i)) ) + (
               vekt(ii)* G * Rulle_motstand_coeficient * cos(greader(i
               ))) + (0.5 * Luftetthet * Frontalareal * Hastighet(i)
               .^(2) * Air_drag_coeficient);
147     end
148 end
149
150 Total_kraft = Total_kraft';
151
152
153 %Arbeid
154 for i = 1:length(vekt)
155     for ii = 1:(length(Total_kraft))
156         Arbeid(i,ii) = Total_kraft(i,ii) .* Distanse_Mellom_Stopp
               ;
157         if Arbeid(i,ii) < 0
158             Arbeid(i,ii) = Arbeid(i,ii)*regenetiv_bremsing;
159         end
160         if Arbeid(i,ii) > 0
161             Arbeid(i,ii) = Arbeid(i,ii)/0.9;
162         end
163     end
164 end
165
166
167
168
169
170 for i = 1:length(Arbeid)
171     if isnan(Arbeid(:,i))
172         Arbeid(:,i) = 0;
```

```
    end
end


%Energiforbruk

tot_energi1 = sum(Arbeid(1,:)) * 2.7777 * 10^(-7)
tot_energi2 = sum(Arbeid(2,:)) * 2.7777 * 10^(-7)
tot_energi3 = sum(Arbeid(3,:)) * 2.7777 * 10^(-7)
tot_energi4 = sum(Arbeid(4,:)) * 2.7777 * 10^(-7)



% Ranheim -  stre  Lund
for i = 1:length(HastighetRO)
    for ii = 1:length(vekt)
        Total_kraftRO(i,ii) =(vekt(ii)* G .* sin(greader_1(i)) )
           + (vekt(ii)* G * Rulle_motstand_coeficient * cos(
           greader_1(i))) + (0.5 * Luftetthet * Frontalareal *
           HastighetRO(i).^(2) * Air_drag_coeficient);
    end
end



Total_kraftRO = Total_kraftRO';

for i = 1:length(vekt)
    for ii = 1:(length(Total_kraftRO))
        ArbeidRO(i,ii) = Total_kraftRO(i,ii) .*
           Distanse_Mellom_Stopp;
        if ArbeidRO(i,ii) < 0
            ArbeidRO(i,ii) = ArbeidRO(i,ii)*regenetiv_bremsing;
        end
        if ArbeidRO(i,ii) > 0
            ArbeidRO(i,ii) = ArbeidRO(i,ii)/0.9;
        end
    end
end



for i = 1:length(ArbeidRO)
    if isnan(ArbeidRO(:,i))
        ArbeidRO(:,i) = 0;
    end
end
```

```
216
217 %   stre   Lund - Ranheim
218 for i = 1:length(HastighetOR)
219     for ii = 1:length(vekt)
220         Total_kraftOR(i,ii) =(vekt(ii)* G .* sin(greader_2(i)) )
               + (vekt(ii)* G * Rulle_motstand_coeficient * cos(
               greader_2(i))) + (0.5 * Luftetthet * Frontalareal *
               HastighetOR(i).^(2) * Air_drag_coeficient);
221     end
222 end
223
224
225 Total_kraftOR = Total_kraftOR';
226
227 for i = 1:length(vekt)
228     for ii = 1:(length(Total_kraftOR))
229         ArbeidOR(i,ii) = Total_kraftOR(i,ii) .*
               Distanse_Mellom_Stopp;
230         if ArbeidOR(i,ii) < 0
231             ArbeidOR(i,ii) = ArbeidOR(i,ii)*regenetiv_bremsing;
232         end
233         if ArbeidOR(i,ii) > 0
234             ArbeidOR(i,ii) = ArbeidOR(i,ii)/0.9;
235         end
236     end
237 end
238
239 for i = 1:length(ArbeidOR)
240     if isnan(ArbeidOR(:,i))
241         ArbeidOR(:,i) = 0;
242     end
243 end
244
245
246
247
248 eforbruk0 = Arbeid(1,:);
249 eforbruk50 = Arbeid(2,:);
250 eforbruk100 = Arbeid(3,:);
251 eforbruk150 = Arbeid(4,:);
252
253
254 Arbeid1 = Arbeid(1,:)* 2.7777 * 10^(-7);
255 Arbeid2 = Arbeid(2,:)* 2.7777 * 10^(-7);
256 Arbeid3 = Arbeid(3,:)* 2.7777 * 10^(-7);
257 Arbeid4 = Arbeid(4,:)* 2.7777 * 10^(-7);
258 Arbeid1 = Arbeid1 + (77/17168);
```

```
Arbeid2 = Arbeid2 + (77/17168);
Arbeid3 = Arbeid3 + (77/17168);
Arbeid4 = Arbeid4 + (77/17168);

Arbeid1RO = ArbeidRO(1,:)* 2.7777 * 10^(-7);
Arbeid2RO = ArbeidRO(2,:)* 2.7777 * 10^(-7);
Arbeid3RO = ArbeidRO(3,:)* 2.7777 * 10^(-7);
Arbeid4RO = ArbeidRO(4,:)* 2.7777 * 10^(-7);
Arbeid1RO = Arbeid1RO + (143/32190);
Arbeid2RO = Arbeid2RO + (143/32190);
Arbeid3RO = Arbeid3RO + (143/32190);
Arbeid4RO = Arbeid4RO + (143/32190);

Arbeid1OR = ArbeidOR(1,:)* 2.7777 * 10^(-7);
Arbeid2OR = ArbeidOR(2,:)* 2.7777 * 10^(-7);
Arbeid3OR = ArbeidOR(3,:)* 2.7777 * 10^(-7);
Arbeid4OR = ArbeidOR(4,:)* 2.7777 * 10^(-7);
Arbeid1OR = Arbeid1OR + (583/128760);
Arbeid2OR = Arbeid2OR + (583/128760);
Arbeid3OR = Arbeid3OR + (583/128760);
Arbeid4OR = Arbeid4OR + (583/128760);

Arbeid = (Arbeid * 2.7777 * 10^(-7)) + (77/17168);
Energiforbruk = sum(Arbeid,2);
Energiforbruk = Energiforbruk.';

ArbeidRO = (ArbeidRO * 2.7777 * 10^(-7))+ (143/32190);
tot_energiRO = sum(ArbeidRO,2);


ArbeidOR = (ArbeidOR * 2.7777 * 10^(-7)) + (583/128760);
tot_energiOR = sum(ArbeidOR,2);


%Energi for rundturen
for i=1:length(Arbeid1)
    Energi_0load(i) = sum(Arbeid1(1:i));
end

for i=1:length(Arbeid2)
    Energi_50load(i) = sum(Arbeid2(1:i));
end

for i=1:length(Arbeid3)
    Energi_100load(i) = sum(Arbeid3(1:i));
end

```

```
306 for i=1:length(Arbeid4)
307     Energi_159load(i) = sum(Arbeid4(1:i));
308 end
309
310
311 %Energi Ranheim -  stre  Lund
312 for i=1:length(Arbeid1RO)
313     Energi_0loadRO(i) = sum(Arbeid1RO(1:i));
314 end
315
316 for i=1:length(Arbeid2RO)
317     Energi_50loadRO(i) = sum(Arbeid2RO(1:i));
318 end
319
320 for i=1:length(Arbeid3RO)
321     Energi_100loadRO(i) = sum(Arbeid3RO(1:i));
322 end
323
324 for i=1:length(Arbeid4RO)
325     Energi_159loadRO(i) = sum(Arbeid4RO(1:i));
326 end
327
328
329 %Energi  stre  Lund - Ranheim
330 for i=1:length(Arbeid1OR)
331     Energi_0loadOR(i) = sum(Arbeid1OR(1:i));
332 end
333
334 for i=1:length(Arbeid2OR)
335     Energi_50loadOR(i) = sum(Arbeid2OR(1:i));
336 end
337
338 for i=1:length(Arbeid3OR)
339     Energi_100loadOR(i) = sum(Arbeid3OR(1:i));
340 end
341
342 for i=1:length(Arbeid4OR)
343     Energi_159loadOR(i) = sum(Arbeid4OR(1:i));
344 end
345
346
347
348 %Plot 4 forskjellige loads
349
350 x_aksen = linspace(0,159,160);
351 x_aksene = linspace(0,43.1,4292);
352
```

```
353 plot(x_aksene,Energi_0load)
354 xlabel('Distance [km]')
355 ylabel('Energy demand [kWh]')
356 hold on
357 plot(x_aksene,Energi_50load)
358 plot(x_aksene,Energi_100load)
359 plot(x_aksene,Energi_159load)
360 hold off
361
362 legend('0 passengers','50 passengers', '100 passengers', '159
       passengers')
363
364 %Plot Barchart over de tre beregningene
365
366 energy1 = [100*Energiforbruk(4)/Energiforbruk(4);100*tot_energiRO
       (4)/Energiforbruk(4);100*tot_energiOR(4)/Energiforbruk(4)];
367 names = {'Total Energy';'Ranheim- stre  Lund';' stre  Lund-
       Ranheim'};
368 %values =
       {'0%';'10%';'20%';'30%';'40%';'50%';'60%';'70%';'80%';'90%';'100%'};

369 values = {'0%';'20%';'40%';'60%';'80%';'100%';'60%';'70%';'80%';'
       90%';'100%'};
370
371
372 chart = bar(energy1)
373 set(gca,'xticklabel',names)
374 set(gca,'yticklabel',values)
375
376 %Plot Ranheim -  stre  Lund,  stre  Lund - Ranheim
377
378 subplot(2, 1, 1)
379 x_akse2 = linspace(0, 21, 2146);
380 plot(x_akse2, Energi_0loadRO)
381 xlabel('Distance [km]')
382 ylabel('Energy demand [kWh]')
383 hold on
384 plot(x_akse2, Energi_50loadRO)
385 hold on
386 plot(x_akse2, Energi_100loadRO)
387 hold on
388 plot(x_akse2, Energi_159loadRO)
389 hold off
390 legend('0 passengers','50 passengers', '100 passengers', '159
       passengers')
391
392
```

```
393 subplot(2, 1, 2)
394 x_akse2 = linspace(0, 22, 2146);
395 plot(x_akse2, Energi_0loadOR)
396 xlabel('Distance [km]')
397 ylabel('Energy demand [kWh]')
398 hold on
399 plot(x_akse2, Energi_50loadOR)
400 hold on
401 plot(x_akse2, Energi_100loadOR)
402 hold on
403 plot(x_akse2, Energi_159loadOR)
404 hold off
```

C Appendix: C

Extensive results for the LCA analysis inlcuding all the impact categories in the baseline method from SimaPro. The first table is the numbers for the LFP battery, while the second and third is for NMC(111) and NCA respectively.

Impact category	Unit	Total	Anode, graphite, for	Carbon black {GLO}| market	Electricity, medium	Copper collector foil,	Aluminium, primary, smelt,	Plastics LFP	Electrolyte LFP	Cathode LFP
Abiotic depletion	kg Sb eq	0,0021	8,77E-6	2,86E-7	1,26E-5	0,00192	x	3,35E-7	5,54E-5	0,000105
Abiotic depletion (fossil fuels)	MJ	228	19,3	1,76	124	16,7	11	1,44	15,8	38,4
Global warming (GWP100a)	kg CO2 eq	22,5	1,07	0,0431	13,9	1,46	1,06	0,0479	1,16	3,81
Ozone layer depletion (ODP)	kg CFC-11 eq	7,69E-7	7,4E-8	2,29E-8	6,67E-8	2,44E-7	1,68E-9	3,28E-8	9,93E-8	2,28E-7
Human toxicity	kg 1,4-DB eq	87,2	1,52	0,0157	4,8	71,7	0,391	0,0218	3,59	5,14
Fresh water aquatic ecotox.	kg 1,4-DB eq	51,1	1,31	0,00894	3,85	40,7	0,0581	0,0146	1,2	4
Marine aquatic ecotoxicity	kg 1,4-DB eq	9,56E4	2,21E3	15,3	2,18E4	4,74E4	2,86E3	32,1	1,33E4	7,99E3
Terrestrial ecotoxicity	kg 1,4-DB eq	0,0806	0,00156	3,01E-5	0,0224	0,0443	0,000487	4E-5	0,00342	0,0083
Photochemical oxidation	kg C2H4 eq	0,00763	0,000334	1,01E-5	0,00229	0,00279	0,000397	1,05E-5	0,000592	0,0012
Acidification	kg SO2 eq	0,182	0,00492	0,000247	0,0618	0,0726	0,00643	0,00017	0,00773	0,0278
Eutrophication	kg PO4--- eq	0,0528	0,00324	2,84E-5	0,0135	0,0219	0,000337	4,19E-5	0,0022	0,0115

Impact category /	Unit	Total	Cathode, NMC111, for	Anode, graphite, for Li-ion	Carbon black {GLO} market	Electricity, medium voltage	Copper collector foil, for Li-ion	Aluminum, primary, smelt,	Electrolyte NMC	Plastics NMC
Abiotic depletion	kg Sb eq	0,00282	0,00101	8,23E-6	2,43E-7	1,03E-5	0,00176	x	2,92E-5	2,94E-7
Abiotic depletion (fossil fuels)	MJ	263	108	18,1	1,49	100	15,3	9,73	8,41	1,29
Global warming (GWP100a)	kg CO2 eq	23,8	8,58	1,01	0,0366	11,3	1,34	0,945	0,614	0,0427
Ozone layer depletion (ODP)	kg CFC-11 eq	1,32E-6	8,73E-7	6,97E-8	1,94E-8	5,42E-8	2,23E-7	1,49E-9	5,23E-8	2,67E-8
Human toxicity	kg 1,4-DB eq	89,6	16,2	1,43	0,0133	3,9	65,8	0,347	1,9	0,0192
Fresh water aquatic ecotox.	kg 1,4-DB eq	55,6	13,2	1,23	0,00759	3,13	37,3	0,0516	0,635	0,013
Marine aquatic ecotoxicity	kg 1,4-DB eq	9,15E4	1,87E4	2,07E3	13	1,77E4	4,35E4	2,54E3	6,99E3	28,4
Terrestrial ecotoxicity	kg 1,4-DB eq	0,136	0,0729	0,00147	2,55E-5	0,0182	0,0407	0,000432	0,0018	3,5E-5
Photochemical oxidation	kg C2H4 eq	0,00891	0,0035	0,000314	8,55E-6	0,00186	0,00256	0,000353	0,000313	9,33E-6
Acidification	kg SO2 eq	0,218	0,0861	0,00463	0,000209	0,0502	0,0666	0,00571	0,00407	0,000152
Eutrophication	kg PO4--- eq	0,0519	0,0162	0,00305	2,42E-5	0,011	0,0201	0,0003	0,00116	3,73E-5

Impact category	Unit	Total	Cathode, NCA, for	Anode, graphite,	Electricity, medium	Carbon black	Copper collector	Aluminum, primary,	Plastics NCA	Electrolyte NCA
Abiotic depletion	kg Sb eq	0,00247	0,000784	8,21E-6	8,99E-6	1,94E-7	0,00164	x	2,78E-7	2,66E-5
Abiotic depletion (fossil fuels)	MJ	223	83,9	18,1	88	1,19	14,3	8,94	1,24	7,59
Global warming (GWP100a)	kg CO2 eq	20,3	6,66	1	9,88	0,0293	1,25	0,868	0,0408	0,557
Ozone layer depletion (ODP)	kg CFC-11 eq	1,09E-6	6,76E-7	6,96E-8	4,75E-8	1,56E-8	2,08E-7	1,37E-9	2,34E-8	4,77E-8
Human toxicity	kg 1,4-DB eq	80,8	12,5	1,43	3,42	0,0107	61,3	0,319	0,0181	1,72
Fresh water aquatic ecotox.	kg 1,4-DB eq	49,6	10,2	1,22	2,74	0,00607	34,8	0,0474	0,0123	0,579
Marine aquatic ecotoxicity	kg 1,4-DB eq	8,14E4	1,45E4	2,07E3	1,55E4	10,4	4,05E4	2,33E3	27	6,4E3
Terrestrial ecotoxicity	kg 1,4-DB eq	0,114	0,0563	0,00146	0,016	2,04E-5	0,0379	0,000397	3,31E-5	0,00165
Photochemical oxidation	kg C2H4 eq	0,00766	0,0027	0,000313	0,00163	6,84E-6	0,00239	0,000324	9,02E-6	0,000284
Acidification	kg SO2 eq	0,187	0,0666	0,00462	0,0439	0,000168	0,0621	0,00524	0,000145	0,00371
Eutrophication	kg PO4--- eq	0,0453	0,0125	0,00304	0,00963	1,93E-5	0,0187	0,000275	3,55E-5	0,00106